universität wien

DISSERTATION

Titel der Dissertation

„ Genetic requirements for SUN-1 phosphorylation in *C. elegans* meiosis “

Verfasser

Mag.rer.nat. Thomas Machacek

angestrebter akademischer Grad

Doktor der Naturwissenschaften (Dr. rer. nat.)

Wien, 2015

Studienkennzahl lt. Studienblatt:	A 091 490
Dissertationsgebiet lt. Studienblatt:	Dr.-Studium der Naturwissenschaften UniStG Molekulare Biologie
Betreuerin / Betreuer:	Dr. rer. nat. Verena Jantsch-Plunger

Table of Contents

1. Abstracts

Faithful chromosome segregation during meiosis I requires coordination of various cellular processes, including induction of DNA double-strand breaks (DSBs), paring of homologous chromosomes, stable association by synapsis and DNA DSB repair via homologous recombination. In this work, the nematode worm *C. elegans* is used as a model system to identify factors of the cellular DNA damage response that are proficient to activate the master regulatory kinase CHK-2 in prophase I. For this, we established the aged *him-19* deficient worm strain as a tool to study meiotic DNA damage signaling. The aged *him-19* deficient strain provides a genetic background which is characterized by, amongst others, impaired homologous pairing, absent polarization of transition zone chromatin, failure to recruit pairing center proteins, restricted synapsis, impaired DSB induction and defective bivalent formation. Artificial DNA lesions by gamma radiation were shown to partially restore the phenotype of aged *him-19* worms, for instance the checkpoint kinase CHK-2 dependent phosphorylation of the inner nuclear membrane protein SUN-1 and SUN-1 aggregate formation. Using phosphorylation of SUN-1 as a read-out of CHK-2 activation, we could show that DNA damage activates CHK-2 in aged *him-19* germline cells dependent on the sensor kinases ATM-1 and ATL-1 as well as the checkpoint kinase CHK-1. Mutation of the p53 homologue *cep-1* decreased phosphorylation of SUN-1 after irradiation in the *him-19* genetic background. In addition, redundant pathways must act in parallel to activate CHK-2 at prophase I, as both meiotic DSBs and chromosome axes were required for robust SUN-1 phosphorylation. Furthermore, strongly reduced SUN-1 S8-Pi phosphorylation levels could be demonstrated in *htp-3* and *him-3; mre-11* mutant germlines. While we have to speculate on the sequential order of how DNA damage activates the respective kinases, novel signaling pathways involving components of the DNA damage response resulting in modifications of the inner nuclear membrane could be shown in context of the *C. elegans* germline.

Zuverlässige Segregation der Chromosomen während der Meiosis I erfordert die Koordination verschiedener zellulären Prozessen, dies inkludiert die Induktion von DNA Doppelstrangbrüchen, Paarung homologer Chromosomen und Etablierung einer stabilen Synapse und die hochregulierte DNA Doppelstrangbruch-Reparatur mit Hilfe homologer Rekombination. In dieser Arbeit wird der Fadenwurmwurm *C. elegans* als Modellsystem benutzt um Faktoren zu identifizieren, die bei der Weitergabe von Signalen die bei meiotischen DNA Doppelstrangbrüchen entstehen beteiligt sind und in weiterer Folge die „Checkpointkinase" CHK-2 im Stadium der Prophase der ersten meiotischen Teilung aktivieren können. Diese Frage wurde mit Hilfe der Mutante *him-19* im gealterten Wurm beantwortet. In diesem genetischen Hintergrund ist die DNA Doppelstrangbruch Induktion und homologe Paarung defekt. Weiters fehlt die Polarisierung des Chromatins im Leptotene / Zygotene Stadium, weiters fehlt die Rekrutierung der „pairingcenter" Proteine und die Synapse der Bivalenten ist eingeschränkt. All dies führt zu defekter Bildung meiotischer Bivalente. In dieser Arbeit zeige ich, dass künstliche DNA Brüche durch Gammastrahlung gewisse Aspekte der Chromosomen Mobilisierung in *him-19* Mutanten wiederhergestellt werden können. Dies inkludiert die Polarisierung des Chromatins im Leptotene / Zygotene Stadium und Phosphorylierung von SUN-1, einen Protein der inneren Kernmembran. Diese Chrakteristika können, abhängig von der „Checkpointkinase" CHK-2, durch Gammastrahlung induziert werden. Ich verwende die Wiederherstellen der SUN-1 Phosphorylierung zur Identifikation von Proteinen, die meiotischen DNA Schaden in der Prophase 1 signalisieren können. Ich zeige, dass CHK-2 Aktivierung in gealterten *him-19* Keimbahnzellen nach künstlicher Doppelstrangbruchinduktion abhängig ist von den Sensor-Kinasen ATM-1 und ATL-1 und der „Checkpointkinase" CHK-1. In *him-19 cep-1* (das *C. elegans* homologe Gen von p53) deffizienten Würmern konnte ich eine verringerte Phosphorylierung von SUN-1 beobachtet werden. Darüber hinaus zeigen meine Ergebnisse, dass Aktivierung von CHK-2 im Wildtyp in der Prophase I von redundanten Signalwegen abhängig ist. Robuste Phosphorylierung von SUN-1 ist abhängig von der Ausbildung meiotischen Chromosomenachsen, sowie aktiver DNA-Doppelstrangbruch-Signalkaskaden. Zusätzlich konnte ich stark verringerte SUN-1 S8-Pi Phosphorylierung in *htp-3* und *him-3; mre-11* Wurmstämmen zeigen.

Während wir über die Abfolge der Aktivierung der jeweiligen meiotischen DNA Doppelstrangbruch Signalwege, die zu einer Aktivierung von CHK-2 führen, spekulieren

müssen, zeigt diese Arbeit, dass Komponenten der DNA-Bruch-Signalkaskaden an der postranslationellen Modifizierung der meiotischen Kernhülle im Wurm beteiligt sind.

2. Introduction

Sexual reproduction is a principal process in generating the vast majority of macroscopic organisms, including plants and animals, and holds numerous evolutionary advantages over nonsexual reproduction, one would be, amongst other things, the more rapid adaption to changing natural environments and the prevention of accumulating deleterious mutations (Bernstein et al. 1985; Wilkins and Holliday 2009). Although there is no general agreement in the field of evolutionary biology on the questions of how sex in eukaryotes arose, current scientific opinion points to the process of homologous DNA repair as the basis for the complex cellular process of sexual reproduction (Marcon and Moens 2005). The term meiosis describes a specialized cell division program, halving the number of chromosomes. This is achieved by one round of DNA replication followed by two consecutive rounds of divisions, meiosis I and meiosis II respectively. Meiosis I, also termed reductional division, segregates each individual homologous chromosome pair. This is followed by meiosis II, termed equational division, where the sister chromatids are subsequently segregated. Correct segregation of chromosomes and thereby faithful transmission of genetic information to the offspring is a core process in biology. Dependent on the organism, defects in chromosome segregation result in aneuploidy leading to congenital birth defects and reproductive failure (Petronczki et al. 2003).

It is reported that aneuploidies account for at least 10% of human pregnancies, a percentage that increases with the age of the women (Hassold and Hunt 2001). Meiotic errors almost always originate from the oocyte, near the end of the reproductive period of the mother, trisomies and monosomies comprise about 50% of human pregnancies. Even though being a topic of multiple studies, the underlying molecular mechanisms leading to aneuploidies in humans have not been exhaustibly understood. Recent studies in humans and multiple model organisms have shown the complexity of meiotic errors, indicating that not a single factor is responsible for the age-related increase in meiotic mistakes in the human female. More likely, the interplay between meiotic factors and endogenous and exogenous contributions results in the occurrence of aneuploidies in this highly conserved process (Nagaoka et al. 2012). For instance, in prophase I multiple landmark events ensure fidelity of chromosome propagation in oocytes. Homologous chromosomes have to find and pair with

their correct partner and the synaptonemal complex (SC) has to polymerize between homologous partners in order to stabilize homologous pairing. In addition, Spo11-dependent meiotic recombination leads to the formation of meiotic chiasmata, a physical link holding the two homologous chromosomes bound together after the dissolution of the SC, a step crucial for the establishment of visible chromosome bivalents in diakinesis of prophase I (Petronczki et al. 2003). Meiotic recombination initiates by the formation of Spo11 mediated DNA breaks and subsequent digestion of the 5' ends generated by the DSB (Keeney et al. 1997). The resulting 3' single-stranded DNA tails are coated by the recombinase Rad51 and the meiosis-specific recombinase Dmc1 who catalyze invasion of the opposite chromatid by the formed nucleoprotein filament (Sauvageau et al. 2005). DNA synthesis primed by the invading 3' ssDNA tails displaces the complementary strand, which in turn can anneal to the ssDNA formed on the chromatin harboring the initial DSB. This cross-exchange results in a tetrahedral structure termed Holliday junction (Krejci et al. 2012). After DNA replication, sister chromatids are joined together by the cohesin complex, proteins that are also implicated in the formation of the loop-axis structure of meiotic chromatin (Blat et al. 2002; Oliveira and Nasmyth 2010). Sister chromosome cohesion facilitates cosegregation of sister chromatids during the first meiotic division and permits bi-orientation of sister chromatids at the second meiotic division. In most eukaryotic organism, this is achieved through incorporation of the meiosis-specific protein Rec8 in cohesin complexes and subsequent cleavage of REC-8 at the second meiotic division, thereby releasing the physical association of the homologous chromosomes (Pasierbek et al. 2001). Multiple key factors contributing to the fidelity of chromosomal transmission have been identified and characterized in the last years.

2.1. *Caenorhabditis elegans* as the model organism of choice for the study of meiotic processes

The nematode *Caenorhabditis elegans* (further referred to as *C. elegans*) is a prominent model organism in the study of meiosis. The species originates from the Greek *Caeno* ("recent"), *rhabditis* ("rod-like") and *elegans*, Latin for "elegant". This 1 mm long worm was first characterized by Sydney Brenner in 1974, as he recognized the usefulness of this animal as a biological model (Brenner 1974). In nature, *C. elegans* lives in temperate soil

environments, predominantly as self-fertilizing hermaphrodite worms. As a particularity, the male sex arises spontaneously from X chromosomal non-disjunction events with a frequency of about 1 in 500.

Advantages of *C. elegans* include fast generational time of about three days, a fully sequenced genome, large brood size consisting of up to 300 offspring and a transparent body simplifying microscopic dissection (Brenner 1974). Facilitating laboratory tasks, *C. elegans* can be long-time stored by freezing. Furthermore, the worms can enter a specialized *dauer* stage in response to starvation and overcrowding (Golden and Riddle 1984). Knockdown of proteins by feeding of RNAi-transcribing bacteria and a complete cell lineage map are examples for the various genetic tools that are available to enable the work on this worm. Published and characterized mutant strains can be accessed via the centralized *C. elegans* mutant library located at the Caenorhabditis Genetics Center, University of Minnesota. Furthermore, the National Bioresource Project is an institution aimed to collect nematode bioresources available in addition to the generation of novel mutant lines. In particular, *C. elegans* is an excellent model system to study meiotic processes.

2.2. The nematode gonad

In addition to 959 somatic cells, the *C. elegans* hermaphrodite body harbors two big gonad arms. As can be seen in Figure Introduction 1, both gonadal arms anastomose into a shared vulva organ, located at approximately the middle of the adult worm body. Due to the hermaphrodite sex of the worms, *C. elegans* hermaphrodites do have to produce both male and female gametes. *C. elegans* achieve that task by first producing sperm cells that are then stored in the spermatheca and are able to fertilize about 300 oocytes over the egg-laying period of the adult worm (for more information see Chapter 2.2.1., spermatogenesis). The sperm cells stored in the spermatheca are the limiting factor with respect to brood size, as offspring numbers can be elevated through cross-fertilization of the hermaphrodite with a male *C. elegans* worm.

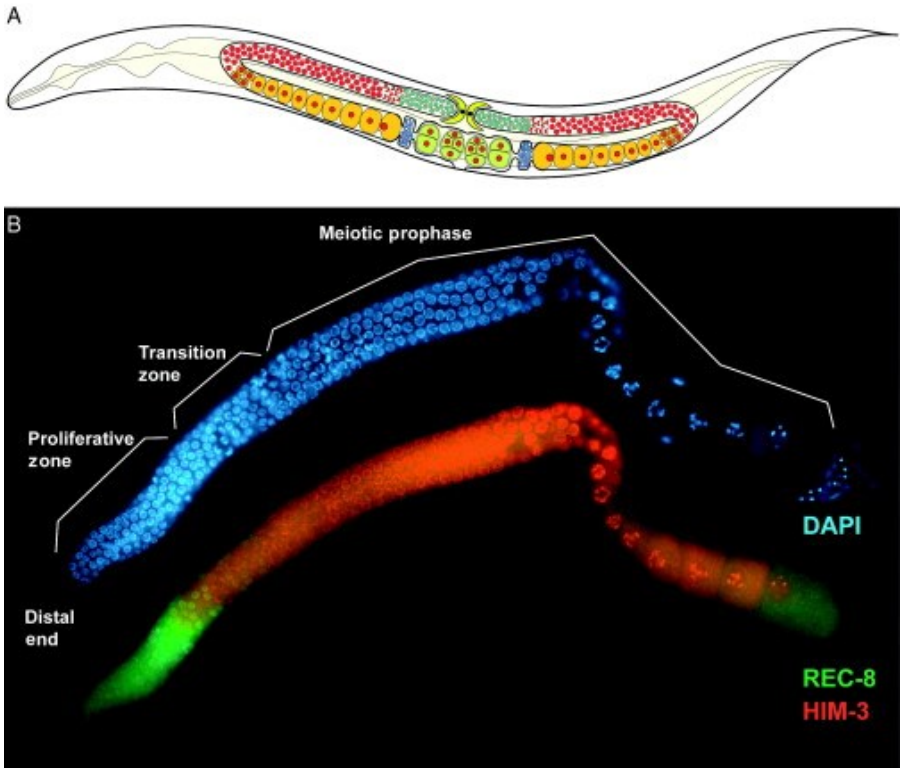

Figure Introduction 1: Overview of the *C. elegans* gonad. (A) Anatomy of the *C. elegans* gonad (B) Cytological preparation of the worm germline. Markers: DAPI (DNA, blue), anti-REC8 (REC-8 meiosis-specific cohesion protein, green), HIM-3 (lateral element protein HIM-3, red), picture taken from (Hansen and Schedl 2006).

Facilitating the study of meiotic processes in *C. elegans*, each gonad arm consists of a gradient of meiotic cells, contained in a syncytium and ordered in a temporal and spatial manner. At the distal end of each gonad arm, the distal tip cell (DTC) serves as stem cell niche and predecessor for cells entering the mitotic zone where cells proliferate before entering meiosis (Kimble and White 1981). The distance from each germ cell to the DTC determines if a germ cell enters meiotic prophase or keeps proliferating. Decisive in this process are the levels of GLP-1 notch signaling, which are responsible to promote the self-renewal and are activated by proximity to the DTC. In contrast, germ cells further away from the DTC have high activity levels of GLD-1 and GLD-2 RNA regulatory pathways promoting entry into the meiotic program (Hansen and Schedl 2013).

In the strict sense, meiosis I, the reductional division, starts in the last cell rows of the mitotic zone, as its most proximal nuclei are initiate expression of meiotic genes (MacQueen et al.

2002; Crittenden et al. 2006). Next, cells enter the transition zone (TZ) were nuclei are in a cell cycle stage corresponding to the leptotene and zygotene stages of prophase I (Pazdernik and Schedl 2013). In leptotene, individual chromosomes, consisting of two sister chromatids, condense and the lateral elements of the SC, HIM-3 and its paralogues HTP-1, HTP-2 and also HTP-3 are loaded onto the chromatin, though no specific antibody for HTP-2 and HTP-3 are available due to high sequence similarity with the other HIM-3 paralogues (see Chapter 2.3.2. (Couteau and Zetka 2005; Colaiacovo 2006).

In zygotene, also termed zygonema (Greek for "paired threads"), homologous chromosomes pair and align. In addition, chromatin gets clustered to one side of the nucleus and one end of each chromosome colocalizes with the nuclear membrane and chromosome end mobilization takes place (Woglar et al. 2013). Chromosome ends move over a crescent shaped surface of the nucleus and show a high tendency to come together into local clusters, reminiscent of the meiotic bouquet, a configuration observed across many species where chromosomes concentrate into a limited area of the nucleus (Chikashige et al. 2006; Tomita and Cooper 2006; Loidl et al. 2012). Furthermore, the central elements of the SC start to polymerize between homologous chromosomes. In the *C. elegans* gonad, leptotene and zygotene appear as a single zone, the transition zone. Nuclei in the TZ can be easily discerned; chromatin at this zone is highly polarized to one side of the nucleus and is visible as a characteristic half-moon like shape. The TZ is followed by the protracted pachytene (Greek for "thick threads") were chromatin, released from its clustered conformation, is visible as parallel stretches spanning the nucleus. In this zone, the SC fully polymerizes and exchange of information between the non-sister chromatids via homologous recombination repair results in the formation of chiasmata, stable physical links between homologous chromosome (for review see (Lemmens and Tijsterman 2011). Upon exit from pachytene, the SC disassembles and further condensation of chromatin can be observed. Proximal to the pachytene zone cells enter the diplotene (Greek for "two threads") and diakinesis (Greek for "moving through") stages of prophase I. At diakinesis, nuclei appear highly enlarged and six distinct DAPI positive structures can be observed. These correspond to five pairs of autosomes and one pair of X-chromosomes held together by the chiasma. Below, major hallmarks and features of meiosis in the context of the nematode gonad are presented.

2.2.1. Spermatogenesis

Due to the hermaphrodite nature of *C. elegans*, both hermaphrodites and males have to engage in the process of spermatogenesis. Similar in the male and the hermaphrodite germ line, spermatogenesis is initiates through the L4 larval stage. In contrast to male individuals, hermaphrodites cease spermatogenesis and switch to producing oocytes when reaching the adult stage. Spermatids accumulate in the proximal end of the gonad arm until the first mature oocyte pushes the spermatids into a specialized organ, the spermatheca. Adult hermaphrodite worms then use the stored sperm in the spermatheca to self-fertilize. Male sperm received via mating can be used as an alternative mode of fertilization. In this situation, sperm received via mating is used preferentially to sperm produced by the hermaphrodite (Shakes et al. 2009).

2.3. Synapsis and the Synaptonemal complex

As discussed above, homologous chromosome pairs have to synapse during meiosis I, a feat achieved by the SC, a zipper-like structure that can be observed via electron microscopy and fluorescent cytology and is ubiquitously present from yeast to humans (Zickler 1977; Zickler and Kleckner 1999). For years, *C. elegans* has proven to be a powerful model system to study the intricate process of synapsis (Goldstein 1984).

A brief summary of the SC will be given in the following paragraphs. The SC forms a tripartite structure that includes proteins that align along each chromosomal axis forming the lateral elements and additional proteins, termed central or transverse elements that polymerize between the axes of each homologous chromosome forming a stable bridge. Furthermore, axis-associated components were shown to have an essential role in the formation of the SC (von Wettstein et al. 1984; Colaiacovo 2006).

2.3.1. Core Synaptonemal complex components

REC-8 loads onto chromosomes independently from other SC components but is required for the assembly of the *C. elegans* axial component HIM-3 and the central elements (MacQueen et al. 2002; Colaiacovo et al. 2003). The *C. elegans* orthologue of the meiotic specific cohesion protein REC-8 was first described in 2001. REC-8 protein forms short filaments at

the TZ that spread continuously over the length of the chromosome until linear localization can be observed at the pachytene stage (Pasierbek et al. 2001). The lateral element protein HIM-3 is a homologue of the S. cerevisiae HORMA domain protein HOP1. In the context of the nematode gonad, HIM-3 protein foci associated with chromatin are visible upon onset of meiosis at the TZ. HIM-3 protein then spreads continuously over the length of the chromosome until it acquires a linear staining pattern between paired homologous chromosomes at early pachytene and stays associated with chromatin until anaphase I. HIM-3 localization is dependent on the cohesin REC-8 but independent on the central region elements SYP-1 and SYP-2 (Zetka et al. 1999). HIM-3 was shown to be dispensable for the initiation of recombination (Couteau et al. 2004).

In *C. elegans* the coiled-coil proteins SYP-1, SYP-2, SYP-3, and SYP-4, most recently identified in a yeast two-hybrid assay, form the central region of the SC and are visible as small foci at leptotene. Until mid pachytene, those foci polymerize to linear structures that can be seen at the interface between paired and aligned homologous chromosomes (MacQueen et al. 2002; Colaiacovo et al. 2003; Smolikov et al. 2009). Localization of the central region proteins is interdependent; SYP-1 can self-interact, can interact with SYP-2 and 3 and is required for the correct loading of the other transversal element proteins between homologous chromosomes. Immuno EM studies allowed the postulation of the following model: The C-terminus of SYP-3 locates closest to chromosome axes and the rest of the SYP proteins are rather positioned in the central region of the SC (Schild-Prufert et al. 2011). Moreover, normal axis morphogenesis, involving HIM-3 and REC-8 protein function, is essential for the polymerization of the central elements of the SC (Couteau et al. 2004). The transverse filament proteins start to depolymerize at diplotene when homologous chromosomes stay physically connected via the meiotic chiasma. Remarkably, the SC was shown to disassemble asymmetrically, central element proteins disassemble along one arm of every pair of homologous chromosomes. This process, influenced by the site of the meiotic crossover, is critical for the correct release of cohesion and subsequent chromosomal segregation (Nabeshima et al. 2005).

Studies on mutant strains of the central element proteins revealed that homology recognition during early prophase is not affected in such mutant genotypes, thereby showing that pairing is a synapsis-independent mechanism (Colaiacovo 2006). However, the

SC is crucial for the stabilization of pairing interactions in later stages of prophase I (MacQueen et al. 2002). Another prominent phenotype displayed by central element mutants is an elongated polarized morphology of the meiotic chromatin. SYP-1, SYP-2, SYP-3 and SYP-4 mutant strains fail to exit this stage with polarized chromatin configuration, characteristic for TZ nuclei in a wild-type genetic background, until late pachytene (Colaiacovo 2006; Smolikov et al. 2009).

2.3.2. SC-associated components

ZHP-3

In *S. cerevisiae*, the protein Zip3 was shown to mark DNA double strand breaks (DSB) sites that are destined to become crossovers and to recruit the central elements of the SC, Zip2 and Zip1 respectively (Chua and Roeder 1998). Its nematode homologue ZHP-3 ("Zip3 homologous protein") was shown to be essential for the formation of the meiotic chiasma and consecutive bivalent formation worms. In a *zhp-3* mutant background, significant persistent of RAD-51 foci can be observed and DNA DSBs are repaired not via the homologue but via alternative repair mechanism such as sister-chromatid mediated repair or gene conversion. In contrast to the yeast Zip3 protein function, wild-type SC formation can be observed in a *zhp-3* mutant gonad. Furthermore, homologue pairing and DSB induction via SPO-11 are not affected in a ZHP-3 negative genetic background (Jantsch et al. 2004).

HTP-1,2,3

The three *h*im *t*hree *p*aralogues HTP-1, 2, and 3 encode HORMA domain proteins that share varying sequence similarly to the meiotic factor HIM-3. HTP-1 and HTP-2 are not required for axis morphogenesis but play a role in regulating central region formation in early prophase. *htp-1* mutant gonads show extensive nonhomologous synapsis between chromosomes at pachytene, whereas *htp-1; htp-2*(RNAi) worms do show extensive loading of SYP-1 onto chromosome cores, despite absence of synapsis, similar to a pattern observed in the synapsis mutant *syp-3*. Those results indicate a key role for those proteins in central element formation (Couteau et al. 2005; Martinez-Perez and Villeneuve 2005). The chromosomal axis component HTP-3 couples DSB formation with SC formation and homologous pairing. HTP-3 protein is recruited to premeiotic chromatin and subsequently localizes to unsynapsed chromosome axes upon entry into the meiotic prophase, forming a DNA complex with the

DSB repair factors MRE-11 and RAD-50 and the axial element HIM-3. Loss of HTP-3 abolishes DSB and crossover formation, localization of meiotic axis proteins, homologous synapsis and sister chromatid cohesion. HTP-1, HTP-2 and HTP-3 localization was shown to be independent of HIM-3, whereas HTP-1, HTP-2 and HIM-3 localization, along with HIM-3-dependent homolog alignment, cross-over and SC formation, is disrupted in HTP-3 deficient germlines (Goodyer et al. 2008). Intriguingly, sister chromatid cohesion mediated by the meiotic kleisins REC-8 and its two paralogues, COH-3 and COH-4, was shown to be essential for the assembly of the axial element proteins HTP-1, HTP-2, HTP-3 and HIM-3 (Severson et al. 2009).

2.3.3. Pairing center regions and pairing center proteins

Various organisms do possess special chromosomal regions that are implicated in establishing homologous pairing, including maize and the fruit fly *drosophila melanogaster* (Maguire 1986; Sherizen et al. 2005). Similarly, pairing centers, located near one end of each chromosome, were shown to be responsible for DSB-independent pairing in C. elegans and implicated in the initiation of synapsis and in promoting crossover recombination in *C. elegans* meiosis (Rosenbluth and Baillie 1981; Rose et al. 1984; McKim et al. 1988; Herman and Kari 1989; Villeneuve 1994). A special group of zinc-finger proteins, HIM-8, ZIM-1, ZIM-2 and ZIM-3, termed pairing center proteins, specifically bind to repetitive sequences at the pairing center region of each chromosome and associate with the nuclear membrane during meiotic prophase I. Furthermore, higher levels of homologous pairing were reached during early prophase in the pairing center regions of chromosomes emphasizing the role of pairing center regions and PC proteins in this process. Paring center proteins are not required for axis morphogenesis, however, mutant gonads for individual pairing center proteins show persistent, transition-zone-like polarization of meiotic chromosomes throughout the pachytene region (MacQueen et al. 2005; Phillips and Dernburg 2006). Recently, polo kinases PLK-1 and PLK-2 were shown to be recruited to the pairing center by the pairing center proteins (Harper et al. 2011; Labella et al. 2011). Furthermore, recruitment of the autosomal pairing center proteins to the chromosomal ends was shown to be mediated by the kinase CHK-2 (Phillips et al. 2006).

2.3.4. Polo kinases

Polo kinases are well studied key regulators in the formation of cytoskeletal structures during mitosis from yeast to higher eukaryotic organism. Polo kinases contain a conserved carboxyl-terminal Polo-box domain that has been implicated in binding to phosphorylated target proteins (Archambault and Glover 2009). Remarkably, Polo like kinases were also shown to be involved in meiotic processes. CDC5, the homologue of Polo kinases in budding yeast, has been linked to crossover formation and pachytene exit (Sourirajan and Lichten 2008). The *C. elegans* genome encodes four known homologues of polo like kinases, PLK-1, 2, 3 and 4, respectively. Corporative functions of polo kinases have been shown in the worm. PLK-1 and PLK-2 have been implicated in regulating cell polarity in embryos (Nishi et al. 2008). Recent results demonstrate that pairing center proteins are essential to recruit PLK-2 to the nuclear envelope in early meiotic prophase I resulting in an defect in homologous pairing, Furthermore, PLK-2 was shown to be implicated in modifying the nuclear envelope protein SUN-1 (Harper et al. 2011; Labella et al. 2011).

2.4. SUN-1 and the meiotic nuclear envelope

Matefin/SUN-1 (referred to as SUN-1) is an inner nuclear envelope transmembrane protein, expressed in the germline of adult hermaphrodites and embryos, required to transmit cytoplasmatic forces from the cytoskeleton to meiotic chromatin (Fridkin et al. 2004; Penkner et al. 2007). As mentioned above, formation of the meiotic chromosome bouquet is a hallmark of meiosis; polarized chromosomal arrangement is a highly conserved feature of meiotic chromatin among eukaryotes. Described first during the late 19th century, the meiotic bouquet defines the *'positioning of one or both ends of the thread-like meiotic prophase chromosomes at a limited sector of the nuclear periphery'* (Scherthan 2001). In *C. elegans* meiosis, the meiotic bouquet stage is represented by leptotene/zygotene chromatin polarization, also termed the meiotic TZ. Chromosome ends are recruited to the inner nuclear envelope via the pairing center proteins bound to the pairing center region on each chromosome. The N-terminal nucleoplasmatic domain of SUN-1 is believed to interact, either directly or indirectly, with chromatin. The SUN-1 C-terminal domain faces the perinuclear space binding to the KASH domain of the outer membrane protein ZYG-12. This evolutionary highly conserved interaction of SUN/KASH-domain proteins effectively forms a

bridge spanning from the inner nuclear space to the cytoskeleton (Penkner et al. 2007; Minn et al. 2009; Morimoto et al. 2012). The ZYG-12 protein was shown to mediate chromosomal movement by cytosolic forces in a dynein dependent fashion (Sato et al. 2009). This bridge acts thereby analogous to a stirring machine and was demonstrated to promote homologous pairing and prevent nonhomologous synapsis (Penkner et al. 2007). Thus, the visible polarization of chromatin at the leptotene/zygotene stage of meiosis corresponds to an ongoing movement and homology licensing process mediated by the SUN/KASH bridge. Accordingly to this model, disruption of SUN/KASH domain interaction prevents chromosome end movement and chromatin polarization in the meiotic TZ (Penkner et al. 2007; Baudrimont et al. 2010).

Meiotic SUN-1 protein undergoes a highly dynamic cellular redistribution during prophase I. SUN-1 protein forms highly mobile aggregates at chromosome end attachments at the onset of the TZ. Protein aggregates disassemble simultaneously with the redispersal of chromatin in mid-prophase until uniform distribution of SUN-1 protein over the nuclear envelope can be observed in late prophase I nuclei (Penkner et al. 2007). SUN-1 was shown to colocalize with pairing center proteins HIM-8 and ZIM-3. In addition, ZIM-1 and ZIM-3 could be co-precipitated with SUN-1 protein. Notably, SUN-1 aggregates colocalizing with the X-chromosomal pairing center protein HIM-8 disassemble significantly later than aggregates connected to the autosomes via ZIM-1, 2 and 3 (Penkner et al. 2009).

Generation of the fusion protein SUN-1::GFP allowed *in vivo* visualization of aggregate movement, which measures chromosome end mobility, via time-lapse microscopy. In doing so it was shown that SUN-1 protein forms mobile protein aggregates at the inner nuclear membrane and SUN-1 displacement tracks, generated by computer-assisted tracking of specific SUN-1 signals, were spread over a restricted zone of the nuclear envelope. It was hypothesized that SUN-1 aggregates help to establish a limited nuclear domain where individual chromosome ends are able to coalesce, assess homology and initiate synapsis (Penkner et al. 2009; Baudrimont et al. 2010).

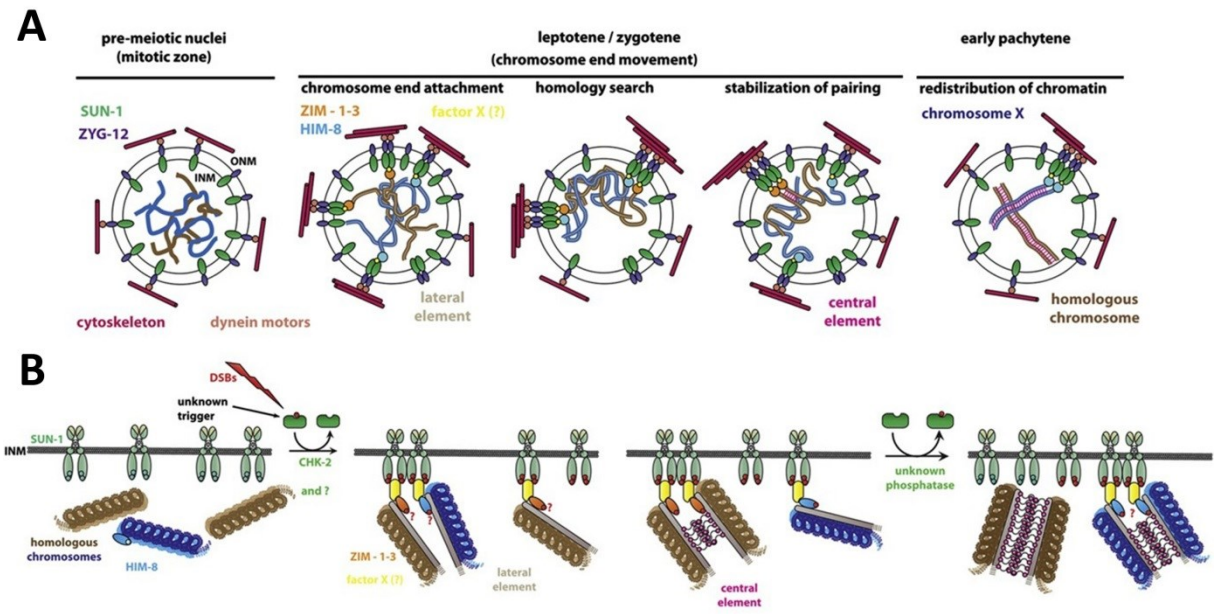

Figure Introduction 2: (A) A model of SUN-1-mediated homologous chromosome pairing. Homologous chromosomes are depicted in blue (chromosome X) and brown (autosome). SUN-1 protein (green ellipses) binds to the outer-nuclear membrane protein ZYG-12 (violet ellipses) and forms a proteinaceous bridge across the NE providing a link between motile, cytoplasm forces (cytoskeleton in dark pink) and the chromosome ends in the nucleoplasm. (B) SUN-1 and Chromosome end attachment. Upon entry into meiosis, paring center-binding proteins (orange and blue ellipses) associate with the respective chromosome ends in a CHK-2-dependent manner. At the inner nuclear membrane, chromosome ends attach to SUN-1 (N-terminus, phosphorylated in a CHK-2-dependent manner). The SC polymerizes after successful homology assessment (magenta lines and dots). The autosomal pairing center-binding proteins ZIM-1,2,3 are lost from chromosome ends, consecutively with disappearance of the connected SUN-1 aggregates after dephosphorylation of SUN-1 in early pachytene. Notably, HIM-8 protein remains bound to the X chromosome pairing center until mid-pachytene. Picture taken from (Baudrimont et al. 2010).

SUN-1 redispersal is dependent on the establishment of the meiotic axis as well as on the formation of the SC. For example, the axis component HIM-3 is essential for the formation of motile SUN-1 aggregates; aggregate formation is strongly impaired in *him-3* gonads. Similar, mutation of the axis component HTP-3 strongly reduces aggregate formation (Labella et al.

2011). In contrast, in synapsis defective mutant strains chromatin remains in a highly polarized conformation until late pachytene stages. Mutants of the serine/threonine kinase CHK-2, required for homologous alignment and DSB formation (see below), abolish SUN-1 aggregate formation (Penkner et al. 2009).

2.4.1. SUN-1 modifications

The N-terminus of SUN-1, facing the nucleoplasm, was shown to be phosphorylated at multiple serines at prophase I (Penkner et al. 2009). Mass spectroscopy analysis of immunoprecipitated SUN-1 protein discovered six phosphorylated serines (Ser8, Ser12, Ser24, Ser43, Ser58, and Ser62) and one phosphorylated serine or threonine (Ser35 or Thr36). Characterization of the phosphorylations was supported by the availability of antibodies raised against SUN-1 protein phosphorylated at S8, S12, S24, and S43 respectively. Thereby it was demonstrated that the entire population of SUN-1 contained both in the nuclear envelope rim and the SUN-1 aggregates at chromosome ends is phosphorylated at S8, S24, and S43 right upon entering leptotene/zygotene stages concurrent with the polarization of chromatin. Entering pachytene, SUN-1 S8, S24, and S43 phosphorylation becomes gradually weaker, concomitantly with the disappearance of SUN-1 aggregates and redispersion of the polarized meiotic chromatin throughout the nucleus. Late pachytene nuclei stained against phosphorylated SUN-1 S8, S24, and S43 display only very faint rim-like signal of the nuclear membrane. The phosphorylation site at SUN-1 S12 displays a more restricted phosphorylation pattern over the course of the meiotic prophase. An antibody recognizing this modification highlights exclusively the fraction of SUN-1 protein in the mobile aggregate complexes colocalizing with chromosomal ends. Remarkably, leptotene/zygotene phosphorylation of SUN-1 aggregates at S12 is influenced weather the attached chromosome bound to the respective SUN-1 aggregate is an autosome or an allosome and the sex of the *C. elegans* worm. In hermaphrodites, SUN-1 S12 phosphorylation is limited to the SUN-1 aggregate that colocalizes with HIM-8 at the cell rows following the meiotic TZ. Conversely, in male *C. elegans* meiosis only aggregates that incorporate autosomes phosphorylate SUN-1 at S12, SUN-1 protein colocalizing with attachment site of the constitutive lone X chromosome is devoid of this particular phosphorylation mark (Woglar et al. 2013). All assessed SUN-1 phosphorylation marks

display a decrease in signal strength after SUN-1 aggregates disperse, this suggests that SUN-1 is either dephosphorylated by a phosphatase at the aggregates and the dephosphorylated protein redistributes evenly through the inner nuclear membrane or dilution of the SUN-1 phosphorylation signal via *de novo* synthesis of unphosphorylated SUN-1 protein (Penkner et al. 2009). Furthermore, it was shown that SUN-1 is kept in a phosphorylated state until chromosome axes are fully synapsed and DNA damage repair and crossover formation have progressed (Woglar et al. 2013).

All known phosphorylation sites of SUN-1 are dependent on the checkpoint kinase CHK-2 but independent of the sensor kinases ATM-1 and ATR-1, and the checkpoint proteins HUS-1, CEP-1 and PCH-2 (Penkner et al. 2009). In addition, DNA DSB induction via the SPO-11 protein is not required for phosphorylating SUN-1. The polo kinase PLK-2 is essential for phosphorylating SUN-1 S12 and to form SUN-1 aggregates, although the closely related polo kinase PLK-1 is believed to be able to partly substitute for PLK-2 in phosphorylating SUN-1 S12 (Harper et al. 2011; Labella et al. 2011).

An interesting question is the biological relevance of SUN-1 phosphorylations in context of nematode meiosis. This was addressed by SUN-1 phosphosite substitution mutants that were generated via the MosSCI single-copy insertion system and analysed in a *sun-1(ok1282)* deletion background. This system allows for the integration of a single copy of the transgene of interest into a defined chromosomal site, thereby ensuring stable transmission and expression of the transgene (Frokjaer-Jensen et al. 2008). A *C. elegans* strain expressing SUN-1 protein with all its phosphor-targets exchanged to the non-phosphoryable amino acid alanine, designated SUN-1(allA), did show strongly delayed synapsis in early pachytene nuclei and an increase in observable RAD-51 foci in mid-pachytene, an indication delayed or defective DNA DSB repair. Offspring viability compared to the wild type was significantly decreased in *sun-1(allA)* mutants after subjecting the worms to ionizing radiation. However, homologous pairing and viability of the brood under non-challenging conditions was not affected by substituting SUN-1 protein with the unphopshoryable SUN-1(allA) transgene (Woglar et al. 2013).

Defective synapsis was shown to result in elongation of the time window of mobile SUN-1 aggregates and prolonged chromatin polarization in a wild-type SUN-1 background (Woglar et al. 2013). Gonads expressing the SUN-1(allA) transgene did suppress the observed

elongation of polarization and aggregate formation in synapsis defective mutant strains. Woglar et al. conclude that SUN-1 phosphorylations are required to sustain aggregate persistence and chromosome mobility beyond the TZ until complete synapsis is achieved (Woglar et al. 2013). SUN-1 phosphorylation is required to efficiently recruit polo kinase PLK-2 to the pairing centers of the autosomes at the TZ and to retain PLK-2 after the zygotene stage of meiosis until meiotic tasks such as synapsis have been completed. Taken together with the observation that SUN-1 S12 phosphorylation is dependent on PLK-2, Woglar et al. propose the existence of a '*self-reinforcing feedback loop between PLK-2 localization and SUN-1 phosphorylation at chromosomal attachment sites*' retaining meiotic SUN-1 aggregates in a phosphorylated and thereby mobile conformation in the presence of unfinished meiotic tasks (Woglar et al. 2013). In summary, mutations of the SUN-1 phosphorylation sites convey only minor meiotic defects however they seem to play an important role under "challenging conditions", such as asynapsis or extensive DNA damage, suggesting that SUN-1 protein phosphorylation is part of a surveillance mechanism that sustains chromosome mobility until vital meiotic tasks essential for the formation of the obligate crossover are completed.

2.5. HIM-19, a regulator of early meiotic events

him-19 was identified in a screen for meiotic mutants based on high incidence of males using Pxol-1::gfp as a reporter for X chromosomal nondisjunction (Kelly et al. 2000). *him-19* shows many characteristics of a regulator of early meiotic functions, affecting multiple processes in prophase I (Tang et al. 2010). Single nucleotide polymorphism (SNP) mapping localized the mutation to the putative ORF Y95B8A.11, that is transcribed in two differentially spliced mRNA transcripts, a shorter (413 amino acids containing 11 exon) and longer (433 amino acids containing 10 exons) protein variant. Apart from the close relative nematode worms *Caenorhabditis briggsae* and *Caenorhabditis remanei*, no other homologue of *him-19* was found in other model organism. Two different *him-19* mutant alleles have been isolated. *him-19(jf6),* generated by chemical mutagenesis, harbors a point mutation interfering with the splice acceptor site at the intron 6-exon 7 junction, the resulting splicing defect prevents transcription of full-length HIM-19 mRNA (Tang et al. 2010). The allele *him-19(tm3538)* was generated at the National Bioresource Project via radiation-induced mutagenesis

(Department of Physiology, Tokyo Women's Medical University School of Medicine, Shinjuku-ku, Tokyo). Although different *him-19* splicing variants could be detected in the *jf6* mutant, it was shown that no full length HIM-19 protein can be expressed. *him-19(tm3538)* bears a 294bp deletion that removes exon 6. It is phenotypically similar to the *jf6* allele and fails to complement the *jf6* allele (Tang et al. 2010).

Intriguingly, defects in *him-19* worms aggravate with the age of the hermaphrodite mother. This cannot be attributed to maternal mRNA contribution as *him-19(jf6)* and *him-19(tm3538)* mutants can be maintained as a homozygous mutant strain on the plate over many successive generations where each generation recapitulates the worsening of *him-19* dependent processes. In addition, transgene mediated cosuppression of *him-19* phenocopied the age-dependent phenotype seen in *him-19(jf6)* and *him-19(tm3538)* worms (Tang et al. 2010).

In accordance to the model of HIM-19 as a regulator of early meiotic events, mutations in *him-19* result in defects in multiple meiotic processes such as homologue recognition, DSB induction, chromosome end mobilization and SC formation. In *him-19* gonads, mitotic divisions are not disturbed and nuclei, when entering leptotene/zygotene stages, express known meiotic markers such as HTP-3. Hence, entry into meiosis seems not affected in *him-19* mutant worms (Tang et al. 2010). Furthermore, the SC complex protein SYP-1 is expressed in *him-19* deficient early meiotic nuclei, but polymerization of the SC is restricted compared to the wild type. Extended synapsis in *him-19* can be seen in later pachytene cells where SYP-1 stretches form between nonhomologous chromosomes (Tang et al. 2010). In *him-19* worms, the pairing center protein ZIM-3 is not loaded onto the pairing center regions near the chromosome ends and SPO-11 dependent initiation of meiotic recombination is defective, resulting in an absence of RAD-51 foci in late zygotene and early pachytene stage nuclei. Chromosomes pair with a nonhomologous partner in the *him-19* mutant, levels of pairing assessed by FISH do not rise significantly above those in mitotic cells (Tang et al. 2010).

Interestingly, artificially induced DSBs via gamma radiation were shown to partly restore meiotic features in the *him-19* mutant. TZ nuclei reestablish chromatin polarization, the pairing center protein ZIM-3 gets recruited to the chromosome ends and enhanced SYP-1 polymerization can be observed. In contrast, levels of homologous chromosome pairing

were not increased (Tang et al. 2010). Hence, the *him-19* mutant reveals a cryptic DSB dependent SC polymerization mechanism in *C. elegans*.

2.6. Coordinating meiotic recombination, pairing, and synapsis

Coordination of cell cycle processes during meiosis is essential for the formation of viable gametes and generation of offspring, in particular during the extended meiotic prophase I. At this stage, essential processes such as active chromosome movement, establishment of homologous paring, induction of DNA double-strand breaks, synapsis and DNA repair have to be coordinated. DNA-damage checkpoint proteins have proven to be at the center of surveying and controlling cell cycle functions and other processes during meiosis in many organisms.

One striking conclusion of comparative meiotic studies in various model systems was that central meiotic processes, such as homologous pairing, synapsis, and recombination, are coordinated differently dependent on the subject species. Homologous pairing and the formation of a stable physical connection in the meiotic chiasma can be established via both DSB-dependent and DSB-independent mechanisms. In budding yeast, the flowering plant *Arabidopsis thaliana* and mice, DNA DSB induction by the endonuclease SPO-11 is required for homologous chromosomes to pair and synapse. In contrast, homologous chromosome pairing and synapsis in the fruit fly Drosophila melanogaster and the nematode *C. elegans* is not dependent on the timely initiation of meiotic DSBs (Page and Hawley 2003). While the coordination between DSB induction, synapsis and crossover formation is still under investigation, current publications demonstrate that this topic is a multifaceted challenge.

2.6.1. Sensing DNA DSBs

In the majority of species, detection of DSBs is achieved by the related and highly conserved proteins ATM (ataxia telangiectasia mutated) and ATR (ATM and Rad3-related) (Lovejoy and Cortez 2009). The sensor kinases detect different DNA lesions, unprocessed DSBs are sensed by ATM, which binds to DNA ends with the help of the MRN complex MRE11/RAD50/NBS1 complex (Lee and Paull 2005). On the other hand, ATR protein was shown to bind to processed DNA lesions in the presence of RPA (replication protein A) bound to the single-

stranded DNA. This process is shown to be mediated in the budding yeast and other model organism by the activator protein ATRIP (ATR-interacting protein) (Harrison and Haber 2006; MacQueen and Hochwagen 2011).

In *C. elegans*, ATM-1 and ATL-1 (ataxia telangiectasia mutated-like) are the corresponding PI-3 kinase homologues (see below). Interestingly, a homologue of ATRIP has not yet been identified in *C. elegans* (Lee et al. 2010). The 9-1-1 protein complex, comprising of RAD9, RAD1 and HUS1, or the *C. elegans* homologues HPR-9, MRT-2 and HUS-1, are implicated in recognizing arrested replication forks activating ATR protein leading to cell cycle arrest and apoptosis (Ahmed and Hodgkin 2000; Hofmann et al. 2002). Activated ATM and ATR kinases were shown to phosphorylate various downstream substrates to induce the cellular DNA-damage response, for instance the checkpoint mediator kinases CHK1 and CHK2 (MacQueen et al. 2011). Publications indicate that, at least to a certain degree, the two PI-3 kinases ATM and ATR have overlapping cellular functions and can substitute for each other. Overexpression of a dominant-negative kinase defective variant of ATR blocks ATM checkpoint activation after radiation exposure and overexpression of ATR was shown to compensate for the lack of ATM dependent signaling in an ATM-deficient cell line from a patient with *Ataxia telangiectasia* (Cliby et al. 1998; Wright et al. 1998).

2.6.2. SPO-11

SPO-11, related to a subunit of the archaebacterial topoisomerase VI, induces DNA double strand breaks at early meiotic stages of *C. elegans* meiosis, likely via a highly conserved topoisomerase-like transesterase mechanism (Dernburg et al. 1998). SPO-11 is required to initiate meiotic recombination in *C. elegans*, *spo-11* deficient worms show 12 univalent signals at diakinesis stage nuclei and strain viability is strongly decreased, as expected for a meiotic segregation mutant. However, homologous chromosomes synapse independent of the induction of recombination, normal levels of SC polymerization were visible in a *spo-11* mutant background. Remarkably, radiation-induced breaks were shown to restore crossover und subsequent bivalent formation in this genotype (Dernburg et al. 1998). Lack of a reliable antibody against the protein implies that SPO-11 function can be only indirectly assessed through the appearance of RAD-51 foci.

2.6.3. ATL-1

Although *C. elegans* ATL-1 is an essential gene, rescue by maternal mRNA permits analysis of *atl-1* loss-of-function. In *C. elegans*, ATL-1 was shown to function in the S-phase checkpoint during mitosis, important to avoid fork collapse during replication fork pausing (Garcia-Muse and Boulton 2005). In this pathway, ATL-1 signals upstream of rad-5/clk-2, the nematode orthologue of the *S. cerevisiae* telomere length-regulating protein Tel2p. Notably, both mutants exhibit mitotic catastrophe and an excess of RPA-1 and RAD-51 covered DSBs in the mitotic zone of the *C. elegans* germline. Furthermore, ATL-1, together with ATM-1, has a role in the checkpoint in response to artificial DSBs leading to induction of either cell cycle arrest or apoptosis via the CEP-1/EGL-1 pathway (Garcia-Muse et al. 2005). The replication protein orthologue RPA-1 bound to ssDNA is essential for the recruitment of ATL-1 to stalled replication forks, *mre-11*, *atm-1*, *rad-5/clk-2*, *hus-1* and DSB repair genes were shown to be dispensable for ATL-1 recruitment to breaks originating from stalled replication forks. In contrast, strand resection via MRE-11 is a prerequisite for RPA-1 association and subsequent ATL-1 recruitment to meiotic DSBs. Therefore, it was proposed that DNA end processing via MRE-11 induces ATL-1 recruitment and activation at DSBs but is dispensable in the signaling response to replication fork stalling (Garcia-Muse et al. 2005). ATL-1 deficient worm gonads display elevated levels of DNA breaks visible via RPA-1 and RAD-51 foci formation while SC formation and crossover recombination are not affected (Garcia-Muse et al. 2005).

2.6.4. ATM-1

Mutation of human ATM leads to the autosomal recessive disorder Ataxia-telangiectasia, a rare disease characterized by a predisposition to developing cancer (Lavin 2008). Many functions of ATM protein are conserved between humans and nematodes. ATM gets activated via autophosphorylation before the protein localizes to DSBs through interaction with the MRN complex (Bakkenist and Kastan 2003; Falck et al. 2005). Its *C. elegans* homologue, ATM-1, was shown to be implicated in the DNA damage response and DNA DSB repair (Lemmens et al. 2011). Similar to other model organism, ATM-1 responds mainly to DSB after exposure to DSB inducing chemical agents and gamma radiation, and to a lower extend to UV-C induced DNA lesions (Stergiou et al. 2007). *C. elegans atm-1* mutant strains are viable and do display a fully functioning S-phase checkpoint (Garcia-Muse et al. 2005).

Notably, the *atm-1* worm line shows all characteristics of a mutator strain as recent publications describe genomic instability, leading to reduced viability, HIM phenotype and sterility, as an inherited phenotype in *atm-1* (Jones et al. 2012).

2.6.5. Checkpoint kinases CHK-1 and CHK-2

DNA damage checkpoint pathways comprise of sensors to detect DNA errors and damage and proteins to transduce the respective signal to downstream effector proteins, thereby facilitating amplification of the checkpoint signal. The phosphatidylinositol 3-kinase-related protein kinases ATM and ATR sense and react to various DNA lesions (see above) and signal by phosphorylating several downstream targets, including the kinases CHK1 and CHK2 (Smith et al. 2010; MacQueen et al. 2011). Homologues of both proteins have been identified in *C. elegans* and were shown to have crucial functions during meiosis. In many organisms, persistent activation of ATM and ATR by unrepaired DSBs activates the recombination checkpoint (also termed pachytene checkpoint) and leads to a suspension of meiotic progression, analogous to the mitotic DNA-damage checkpoint response. This response halts the cell cycle and provides additional time to complete DNA repair tasks before resuming meiotic divisions. In addition, the pachytene checkpoint also provides an opportunity to eliminate meiotic cells that are unable repair DNA DSBs. In contrast to budding yeast that arrests the cell cycle in response to unrepaired DSBs, higher organisms have the ability to cull meiotic cells through apoptosis (Roeder and Bailis 2000). While the recombination checkpoint was shown to mainly rely on the sensor kinase ATR and to a lesser extent on ATM, downstream signaling in response to persistent unrepaired DSBs between organisms is multifaceted and an ongoing topic of scientific investigation.

For instance, cell cycle arrest in flies and yeast is mediated by CHK2 homologues, while CHK1 is dispensable for this process (Hochwagen and Amon 2006; Wu et al. 2010). In contrast, in the *C. elegans* germline the recombination checkpoint, activating p53 and promoting apoptosis, is signaled via CHK-1 (Gartner et al. 2000; Boulton et al. 2002). In the worm, the *chk-1* gene encodes a CHK1-like serine threonine protein kinase and was first described in a screen for proteins involved in the DNA damage response pathway (Boulton et al. 2002). It has been shown in the fission yeast *Schizosaccharomyces pombe* that CHK-1 is phosphorylated and activated under pro-apoptotic conditions, leading to a delay in cell-cycle

progression through inhibition of the cell cycle regulators CDC25 or to induction of apoptosis in damaged cells dependent on the tumor suppressor p53 (Furnari et al. 1999). Accordingly, knockdown of CHK-1 in *C. elegans* abrogates IR-induced increase in apoptosis (Jaramillo-Lambert et al. 2010).

A central role in regulating meiotic processes was shown for CHK-2, a member of the Cds1/Chk2 checkpoint kinase family. *C. elegans* CHK-2 is orthologous to human CHK2, CHEK2, a protein that has been linked with a variant of human Li-Fraumeni syndrome when mutated, although this topic is still under clinical investigation (Evans et al. 2008; Ruijs et al. 2009). CHK-2 is expressed in the worm germline and controls multiple meiotic functions, mutations in *chk-2* gene affect homologous pairing between chromosomes during meiotic prophase (MacQueen and Villeneuve 2001; Martinez-Perez et al. 2005). Furthermore, pachytene region nuclei of *chk-2* deficient gonads show disorganized DAPI-stained tracks that are not arranged as parallel threads, consistent with a failure in alignment and synapsis between homologous chromosomes and a substantially restriction and delayed loading of SYP-1 protein (MacQueen et al. 2001; Martinez-Perez et al. 2005). Although the axial component HIM-3 is loaded onto meiotic chromosomes, meiotic prophase nuclei fail to reorganize their chromatin at leptotene/zygotene stages. Hence, no TZ containing nuclei with polarized chromatin can be observed in *chk-2* mutant worms (MacQueen et al. 2001). A possible explanation for the lack in polarization offer publications showing that the recruitment of the autosomal pairing center proteins ZIM-1, ZIM-2, and ZIM-3 to the pairing center regions is dependent on CHK-2. Localization of HIM-8, the pairing center protein binding to the X chromosome, was not affected in *chk-2* mutants (Phillips et al. 2006). During the process of meiosis, RAD-51 protein localized to distinct foci, most abundant in nuclei at late zygotene to early pachytene, dependent on DSB induction via SPO-11 and MRE-11 mediated strand resection. CHK-2 gonads lack rad-51 foci, suggesting a defect in either DSB induction or processing (Alpi et al. 2003). At diakinesis, chromosomes lack chiasmata and are visible as univalents. Comparable to other meiotic segregation mutants, the few embryos from *chk-2* mutant hermaphrodites that obtain a correct set of chromosomes by random segregation can develop into adulthood, confirming that *chk-2* is not essential for embryogenesis. Furthermore, germ cell apoptosis did increase in a dose-dependent manner, confirming that *chk-2* germ-line nuclei activate the DNA damage checkpoint in response to irradiation (MacQueen et al. 2001). As written above, phosphorylation of SUN-1 at its

nuclear N-terminus is dependent on *chk-2* and *plk-1/2*. Therefore, a plausible explanation for the absence of chromosomal polarization in *chk-2* mutants could be provided by a failure to recruit PLK-2 to the pairing centers leading to a lack of chromosome end mobilization (Penkner et al. 2009; Harper et al. 2011; Labella et al. 2011).

2.6.6. PCH-2

PCH-2 encodes a putative ATPase orthologous to budding yeast PCH2 and human TRIP13. The protein is enriched during oogenesis and was shown to be essential for apoptosis in response to asynapsis but dispensable for DNA damage induced apoptosis. Unsynapsed chromosomes elicit the synapsis checkpoint dependent on the pairing center proteins and PLK-2 but independent of SPO-11 protein (Bhalla and Dernburg 2005).

2.6.7. MRE-11

The Mre11 gene encodes a nuclear protein implicated in DNA double-strand break repair, homologous recombination and telomere length maintenance. Mre11 is a member of the MRX/N complex (Mre11, Rad50, and Xrs2/Nbs1).It is required for meiotic DSB formation and for resection in Saccharomyces cerevisiae and has 3' to 5' exonuclease activity and endonuclease activity (Johzuka and Ogawa 1995; Stracker and Petrini 2011). Mutant alleles of Mre11 are sensitive to IR and have moderate defects in processing meiosis specific DSBs including reduced resection of DSBs suggesting that MRE-11 is involved in processing IR-induced DSBs to generate RPA-1 bound ssDNA overhangs (Tsubouchi and Ogawa 1998; Moreau et al. 1999). Studies in *C. elegans* indicate that meiotic DSBs in *C. elegans* are dependent on the MRX/N complex and MRE-11. Furthermore, MRE-11's role in DSB formation and strand resection can be genetically separated in the *mre-11*(*iow1*) mutant strain (Chin and Villeneuve 2001; Hayashi et al. 2007; Yin and Smolikove 2013). In contrast to many other metazoan organisms, *C. elegans mre-11* null mutants are viable and morphologically wild- type, allowing analysis of meiotic processes (Chin et al. 2001). In *mre-11* gonads, meiotic crossovers are not present, oocyte chromosomes lack chiasmata and univalent are visible at diplotene and diakinesis. Accordingly, although *mre-11* hermaphrodites produce a large number of embryos, about 97% of laid eggs do not hatch and *mre-11* worms do show a Him (High incidence of males) phenotype, indicative of a high

frequency of X-chromosome nondisjunction. Although *mre-11* animals produce viable offspring, *mre-11* was shown to be required for maintenance of reproductive capacity, as most offspring from homozygous mre-11 hermaphrodites fails to lay eggs. This deteriorating of the phenotype in the successive generation is an indication of partial maternal rescue in offspring produced by heterozygous mre-11 mutant animals and suggests an essential role of MRE-11 in *C. elegans*, for instance, repair of DSBs generated spontaneously during DNA replication (Chin et al. 2001). Underlining a conserved role of MRE11 in different model systems, *C. elegans mre-11* regulates processing of IR-induced DSBs to generate ssDNA overhangs bound by RPA. As a consequence, *mre-11* mutant gonads display strongly reduced numbers of RPA-1 foci at sites of DSBs and subsequent chromosomal fragmentation following irradiation (Hayashi et al. 2007). *mre-11* deficient germ lines display a functional meiotic G2 DNA damage checkpoint determined by the appearance of radiation-induced apoptotic germ cells (Chin et al. 2001).

2.6.8. COM-1

C. elegans com-1 encodes for an orthologous protein to *Saccharomyces cerevisiae* Sae2p, AtCOM1 in Arabidopsis thaliana and human CTIP. While SPO-11-dependent DNA double-strand breaks are formed and homologous chromosomes pair comparable to the wild type in *com-1* deficient germlines, COM-1 was shown to be essential for completing meiotic recombination (Penkner et al. 2007). *com-1* mutants show defects the repair of meiotic DSBs and display fragmented DNA instead of six bivalents at diakinesis stage of meiosis I. In addition, DNA fragmentation is dependent on DSB break induction by SPO-11. Meiotic DNA DSBs generated by SPO-11 do not induce formation of RAD-51 protein foci in *com-1* mutant germline nuclei, whereas radiation induced DNA lesions are able to recruit the RAD-51 repair protein (Penkner et al. 2007). This suggests that generation of ssDNA tails upon which RAD-51 is able to bind and subsequent repair of the lesions via homologous recombination is dependent on COM-1 protein function. In contrast to *S. cerevisiae* COM-1, *C. elegans* COM-1 is not required for the removal of Spo11 and for the initiation of meiotic DSB repair. It was recently shown that COM-1 plays a critical role in promoting meiotic recombination by counteracting the NHEJ complex Ku in the worm (Lemmens et al. 2013).

2.6.9. The worm p53 homologue cep-1

p53 is a key transcription factor in the response to genotoxic stress in mammals. p53 is a tumor suppressor gene and mutations of p53 can be detected in the majority of human cancers (Vlatkovic et al. 2013). CEP-1 was identified as the *C. elegans* homologue of mammalian p53 and characterization of the protein and most likely acts as a transcription factor in *C. elegans* (Schumacher et al. 2001). It was shown that knockdown of CEP-1 via RNAi or DNA cosuppression inhibited apoptosis in *C. elegans* late-stage pachytene germ cells in response to DNA damage and meiotic recombination failure, while irradiation-independent, physiological apoptosis was not affected (Rutkowski et al. 2011). Notably, CEP-1 protein expression was shown to be restricted to late pachytene nuclei by MPK-1 dependent regulation of a translational repressor of CEP-1, GLD-1. It was speculated that this could constitute a mechanism to restrict CEP-1 activity, and thereby apoptosis, before cells enter late pachytene in order to allow a time window to repair DSBs via meiotic recombination (Rutkowski et al. 2011).

3. Proposed aims

Here, initial aims of this thesis as well as questions that arose in the course of the project are listed, followed by the brief description of the results. Chapters addressing the respective results are denoted.

At the beginning of my thesis two major questions concerning the newly discovered *him-19* gene were ready to be addressed:

1) What are the molecular mechanisms by which *him-19* acts to prevent age dependent deterioration of germcells?
2) Can we use *him-19* as a tool to understand activation of the master regulatory kinase CHK-2? During the course of our studies it became clear that redundant pathways must act in parallel to activate CHK-2. Phosphorylations of SUN-1 can be used as read-out of CHK-2 activation. It was observed that in situations where no meiotic DSBs were induced SUN-1 phosphorylations were still observed however in a *him-3, mre-11* double mutant a fraction of gonads remained devoid of the SUN-1 Pi signal (Penkner et al., 2009). This suggested that both DSBs and chromosome axes were required for SUN-1 phosphorylations. Possibly, these two redundant pathways seem to be inactive in aged *him-19* worms, however introduction of exogenous DSBs accompanied by SUN-1 phosphorylations allowed us to ask what the genetic requirements for CHK-2 activation and thereby leading to SUN-1 phospho modification in dependence of DSBs were.

3.1. Can the *him-19* mutant be used as a tool to study meiotic signaling pathways in *C. elegans*?

DSBs were shown to induce SUN-1 S8 phosphorylation and SUN-1 aggregate formation in *him-19(jf6)* and *him-19(tm3538)* deficient germline nuclei, a process dependent on the checkpoint kinase CHK-2 (Chapter 5.1.). The majority (22 of 26 gonads) of *him-19(tm3538)* germlines restored SUN-1 S8-Pi at the TZ, allowing me to reliably assay the effects of artificial DSBs in various mutant germlines deficient for *him-19*.

3.2. Which additional meiotic cellular processes/hallmarks are restored by DSB induction in the *him-19* genetic background?

In *him-19* germlines, artificial DSBs generated by exposure to gamma radiation resulted in repolarization of leptotene/zygotene chromatin and reloading of the pairing center protein ZIM-3 onto the chromosomal pairing center regions (Chapter 5.1.). Furthermore, levels of SC polymerization, assessed by quantification of the total length of SYP-1 stretches, were shown to be elevated following DSB induction in *him-19* deficient worms (contributions 3.1).

3.3. What are the genetic requirements for SUN-1 phosphorylation in the TZ in aged *him-19* in response to artificial DNA lesions?

Our study shows that gamma radiation activates CHK-2 mediated by highly conserved factors of the cellular DNA damage response. DSB induced SUN-1 phosphorylation at the meiotic TZ could be shown to depend on the sensor kinase ATM-1 (Chapter 5.3.1.). Furthermore, generation of a *him-19(tm3538) atm-1(gk186); atl-1(tm853)* triple mutant worm strain confirmed a role for the closely related sensor kinase ATL-1 in the DNA damage signaling pathway at late pachytene stage germline nuclei (Chapter 5.3.3.). Knockdown of the checkpoint kinase CHK-1 in *him-19* not only led to pronounced defects in *C. elegans* gonad morphology but also abrogated SUN-1 S8 phosphorylation in response to artificial DSBs (Chapter 5.5.). Surprisingly, our results implicated the p53 homologue *cep-1* in CHK-2 dependent SUN-1 phosphorylation events in response to artificial DSBs (Chapter 5.4.).

3.4. Can we characterize the molecular signal, induced by gamma radiation that subsequently activates the checkpoint kinase CHK-2?

The inability to correctly process DNA lesions by recruitment of the DNA strand invasion protein RAD-51 led to elevated levels of SUN-1 phosphorylation in *C. elegans* meiosis, robust SUN-1 S8 phosphorylation can be detected in RAD-51 deficient germlines until nuclei reach the late pachytene stage of *C. elegans* meiosis (Chapter 5.6.1., (Woglar et al. 2013). We also tried to address whether early repair intermediates mediated by the DNA single strand

binding protein complex with RPA would contribute to signaling of DNA lesions in *him-19* upon irradiation (Chapter 5.6.2.).

3.5. Can we find the constituents of the second path of CHK-2 activation acting in parallel to DNA damage signaling in aged *him-19* worms?

Strongly reduced SUN-1 S8-Pi phosphorylation levels could be demonstrated in *him-3(gk149); mre-11(ok179)* double mutant germlines, even though *him-3(gk149)* and *mre-11(ok179)* single mutant worms are competent to activate CHK-2 and phosphorylate SUN-1 protein (Chapter 5.9.). SUN-1 S8-Pi in *him-3(gk149); mre-11(ok179)* could be augmented by induction of DNA DSBs, as gamma radiation increased meiotic SUN-1 phosphorylation levels. Therefore, our results suggest that disruption of the meiotic axis concurrent with the inability to correctly introduce or process meiotic DNA DSBs restricts CHK-2 dependent SUN-1 phosphorylation in *C. elegans* germline cells.

4. Contributions to publications where I am a co-author

Prof. Jantsch and her workgroup performed a screen for *C. elegans* mutants with defects in meiotic segregation. By this means, multiple mutant alleles were isolated, including the SUN-domain mutant *sun-1(jf18*) and the novel meiotic regulator gene *him-19(jf6)*. At the time I joined the laboratory of Prof. Jantsch I was trained by the doctoral student Lois Tang and had the opportunity to participate in the characterization of the novel meiotic protein HIM-19.

My contribution to Tang et al. 2010 included the generation of a feminized *him-19(jf6)* mutant strain and subsequent evaluation of strain viability counted over the reproductive time span and cytological analysis of *spo-11* mediated DNA DSB formation (Tang et al. 2010, Figure 2A, Figure 6B). I could characterize the alternative mutant allele *him-19(tm3538*) and confirmed that *him-19(tm3538)* is phenotypical similar to the *jf6* allele, confirming that *him-19* maps to the chromosomal region Y95B8A.11. Furthermore, *him-19(3538)* showed strongly reduced offspring numbers and univalent formation at diakinesis when brought over a deficiency of the respective chromosomal region containing *him-19* ORF (Tang et al. 2010). I could demonstrate that the age dependent worsening of the meiotic phenotype seen in *him-19* worms includes localization of the pairing center protein ZIM-3, as *him-19(jf6)* 12 hrs post L4 larval stage show reduced levels of ZIM-3 foci formation, intermediary between the wild-type levels and the absence of a specific ZIM-3 signal seen in *him-19(jf6)* 48 hrs post L4 (Tang et al. 2010, Figure4D).

Artificially induced DSBs were shown to restore chromosome clustering in the *him-19* mutant. We were interested in the effect of gamma radiation on two additional phenotypes of *him-19*, restricted synapsis and lack of recruitment of pairing center proteins onto meiotic chromatin. I could establish that gamma radiation enhances SC formation via quantification of the length of SYP-1 covered chromosomal axes 6 hrs post radiation exposure (Tang et al. 2010, Figure 7C). Furthermore, I could demonstrate that gamma irradiation restores loading of the pairing center protein ZIM-3 in *him-19* parallel to the previously observed restoration of clustered chromatin (Tang et al. 2010, Figure 7D).

For the publication Penkner et al. 2009 I could contribute to the characterization of *C. elegans* strains expressing a transgenic SUN-1 protein, fused to a GFP-tag and rendered nonphosphorylatable at either Serine 16 or serine 12 and 16 via base substitution to alanine, denoted as SUN-1 S16A::gfp and SUN-1(S12A,S16A)::gfp, respectively. My work on Penkner

et al. 2009 comprised assessing offspring viability of the of SUN-1 S16A::gfp worm strain (Penkner et al. 2009, Table S1) and cytological evaluation of gonad morphology of SUN-1 S16A::gfp and SUN-1(S12A,S16A)::gfp. Immunostaining of the outer nuclear membrane protein ZYG-12 in SUN-1 S16A::gfp and SUN-1 (S12A,S16A)::gfp revealed that ZYG-12 protein is retained at the outer NE, in contrast to the SUN-domain mutant *sun-1(jf18)*, where ZYG-12 localization is lost from the nuclear membrane (Penkner et al. 2009, Figure S7B).

I could demonstrate that ionizing radiation induces SUN-1::gfp aggregate aged *him-19(jf6)* hermaphrodites. The appearance of mobile SUN-1::gfp aggregates could be correlated to reloading of PC proteins and polarization of TZ chromatin (Penkner et al. 2009, Figure 5A). Furthermore, aggregate formation and loading of PC protein are dependent on the checkpoint kinase CHK-2, irradiation of *chk-2(me64)* worms does not restore SUN-1 S8 phosphorylation and chromatin polarization after ionizing radiation whereas SUN-1 S8 is phosphorylated at Serine 8 in response to DSB induction in aged *him-19* gonads (Penkner et al. 2009, Figure 5B). These results support the assumption that the characteristic clustering of chromatin at leptotene/zygotene is a direct result of an active motion of meiotic chromosomes attached to the nuclear periphery.

4.1. Mutations in *C. elegans him-19* show meiotic defects that worsen with age

In this publication, the authors could identify *him-19 as* a novel meiotic factor in *C. elegans* meiosis by a screen for meiotic missegregation mutants based on high incidence of males. *him-19* was shown to have diverse functions in the nematode germline, particularly in prophase of meiosis I. Tang et al. did recover the splicing-defective *him-19(jf6)* mutant allele, worms homozygous for *him-19(jf6)* which display reduced levels of homologous pairing and defective bivalent formation in diakinesis stage nuclei. Polymerization of the SC was shown to be spatially restricted SC forms between nonhomologous chromosomes. Additionally, DSB induction is impaired in *him-19* gonads, assessed by delayed formation of RAD-51 repair protein foci. Taken together, the results of the publication Tang et al. 2010 indicate a central function of HIM-19 in early meiotic processes such as homology recognition and formation of meiotic DNA DSBs. Furthermore, meiotic defects in the *him-19(jf6)* germline worsen with increasing age of the adult hermaphrodites and defects were shown to be more severe in female meiosis than in male meiosis.

4.2. Meiotic chromosome homology search involves modifications of the nuclear envelope protein Matefin/SUN-1

In Penkner et al. 2009 the authors describe the changing properties of the nuclear envelope (NE) protein SUN-1 during meiosis. At leptotene/zygotene stages of meiosis, SUN-1 forms mobile protein aggregates at sites where chromosomal ends attach to the NE. Chromosomes are actively moved via the SUN/KASH domain proteins SUN-1 and ZYG-12, which form a bridge connecting the cytoplasm and nucleoplasm and mediate cytoplasmatic forces essential for the establishment of homologous pairing. In this publication we could describe SUN-1 phosphorylation at multiple serines at the meiotic TZ during the time window of chromosome homology search. We were able to detect multiple phosphorylated residues (S8, S12, S24, S35/T36, S43, S58 and S62) at the nuclear N-terminus of SUN-1 by mass spectroscopy. The appearance of the phosphorylation marks correlates with visible polarization of meiotic chromatin and could be shown to be dependent on the function of the checkpoint kinase CHK-2 whereas studied modifications were independent of SPO-11 and the checkpoint proteins ATM-1/ATL-1. We could establish that DSB induction via gamma radiation restored SUN-1 phosphorylation together with chromatin polarization in the meiotic mutant *him-19*. Additionally, the chromosome axis component HIM-3 is required for efficient aggregate formation. Dephosphorylation of SUN-1 is concomitant with the redistribution of paired chromosomes during pachytene; asynapsis was shown to prolong the zone of phosphorylated SUN-1, concomitantly with an extended polarization of meiotic chromatin.

5. Results

5.1. Artificial DNA-DSBs induce chromatin polarization and SUN-1 phosphorylation and recruitment of the pairing center proteins ZIM-3 in aged *him-19* worms

We demonstrated that *him-19* mutant gonads lack both meiotic SUN-1 phosphorylation and SUN-1 aggregates formation (Figure 1, Table 1, Contributions Chapter 4.2., (Penkner et al. 2009)). In addition, no polarization of TZ chromatin could be observed in *him-19(tm3538)* gonads. In this regard, the defects of the aged *him-19* mutant hermaphrodite resemble those of the checkpoint mutant *chk-2* (Figure 1, Table 1). Gonads deficient for CHK-2 protein analogously lack SUN-1 phosphorylation and DNA polarization and produce dead eggs due to chromosomal missegregation (MacQueen et al. 2001). Notably, both *chk-2* and aged *him-19* mutant backgrounds are deficient in *spo-11* dependent DSB formation (MacQueen et al. 2001; Tang et al. 2010). However, Spo-11 mediated DSBs are evidently not essential in the activation of CHK-2 and subsequent phosphorylation of SUN-1, as SPO-11 deficient worms were shown to phosphorylate SUN-1 in a wild-type manner (Penkner et al. 2009). Previous work on a *spo-11* mutant in *C. elegans* demonstrated that radiation-induced DSB restore bivalent formation, therefore, artificial DNA breaks can substitute for *spo-11* induced DNA DSBs and can be processed into meiotic crossovers (Dernburg et al. 1998). We were interested whether artificial induction of DNA DSBs by gamma irradiation can replace endogenous, *spo-11* mediated DSB formation and activate downstream target proteins. We used SUN-1 phosphorylations as readout to assess activation of the checkpoint kinase CHK-2 upon induction of artificial DSBs in aged *him-19* mutants.

Remarkably, introduction of artificial DSBs via gamma radiation partially restored meiotic SUN-1 S8 phosphorylation and SUN-1 aggregate formation in aged *him-19(tm3538)* and *him-19(jf6)* worms (Figure 1, Table 1, see Contributions 3.2, (Penkner et al. 2009)). Furthermore, our results revealed that germline chromatin morphology in the *him-19* background was sensitive to DSB induction in that polarization of DNA to one side of the nucleus at the meiotic TZ was reestablished 120 min after irradiation (Figure 1, see Contributions 3.1, (Tang et al. 2010)).

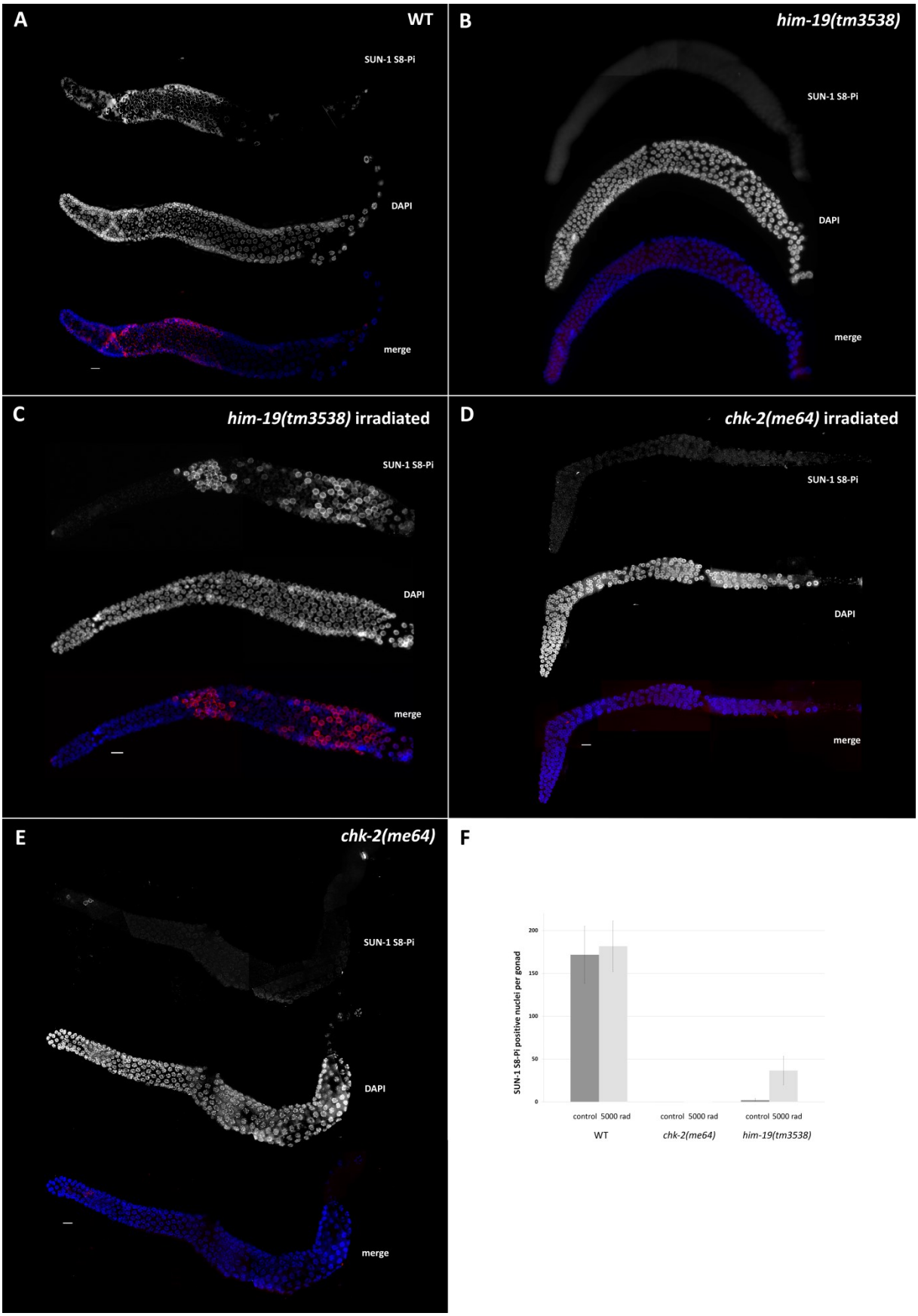

Figure 1: SUN-1 phosphorylation patterns in wild-type (WT), aged *him-19* and *chk-2 C. elegans* germlines. (A) Meiotic SUN-1 phosphorylation in 2 day post L4 wild-

type gonads. (B-C) Irradiation partially restores SUN-1 S8-Pi in *him-19(tm3538)* worms, concurrent with formation SUN-1 aggregate and chromosomal clustering at leptotene/zygotene. (D-E) Restoration of SUN-1 S8-Pi is dependent on the checkpoint kinase CHK-2, artificial DSBs do not restore SUN-1 S8-Pi in *chk-2(me64)* germline cells. Scale bars represent 10 µm. (F) Quantification of SUN-1 S8 phosphorylation levels in the wild type (N2), irradiated and control *him-19(tm3538)* and *chk-2(me64)* germlines 2 days post L4. Diagram represents average number of SUN-1 S8-Pi positive nuclei per gonad.

In the wild type, polarization of germline chromatin has been correlated with an ongoing, active pairing process (MacQueen et al. 2001; Couteau et al. 2004; Couteau et al. 2005; Penkner et al. 2007; Baudrimont et al. 2010). Failure to cluster leptotene/zygotene chromatin was observed in various meiotic such as *chk-2*, *sun-1, htp-1* and *him-3* (Figure 1 (MacQueen et al. 2001; Couteau et al. 2004; Couteau et al. 2005; Martinez-Perez et al. 2005; Penkner et al. 2007). Analogous to the phenotype of the *chk-2* mutant, aged *him-19*-deficient gonads fail to recruit the pairing center protein ZIM-3 onto the pairing center regions, specifically to the right end of chromosome I and the left end of chromosome IV (Figure 2, see contributions 3.1, (MacQueen et al. 2001; MacQueen et al. 2005; Tang et al. 2010). As clustering of TZ chromatin was evoked by DSB induction in the *him-19* genetic background, we were interested to monitor ZIM-3 localization upon irradiation. Surprisingly, irradiation experiments in the *him-19* background revealed that artificially induced DSBs promoted reloading of pairing center proteins onto the chromosomal ends at leptotene/zygotene stage nuclei in aged *him-19(jf6)* worms (Figure 2). Additionally, our cytological studies showed that ZIM-3 foci colocalized with the simultaneously induced SUN-1 aggregates (Figure 2). Pairing center proteins are implicated in the recruitment of the chromosomal ends to the nuclear membrane, therefore this finding suggest a mechanistic link between chromosomal clustering, loading of the pairing center proteins and SUN-1 aggregate formation (Penkner et al. 2009; Tsai and McKee 2011). Recruitment of the chromosomal ends to the nuclear membrane mediated by the pairing center proteins und subsequent transmission of cytosolic motion via mobile SUN-1 aggregates is appearing alongside with visible chromatin polarization in the nematode germline. Notably, restoration ZIM-3 localization is dependent on CHK-2 protein function, as irradiation does not restore in

ZIM-3 localization in *chk-2(me64)* (data not shown). In contrast to aged *him-19*, meiotic SUN-1 phosphorylation, aggregate formation and chromatin polarization, cannot be restored by irradiation in *chk-2* deficient worms, demonstrating that DNA damage induced phosphorylation events are signaled via the CDS1/CHK2 checkpoint kinase family member CHK-2 and substantiate the essential role of CHK-2 in *C. elegans* meiosis (Figure 1, (MacQueen et al. 2001; Penkner et al. 2009).

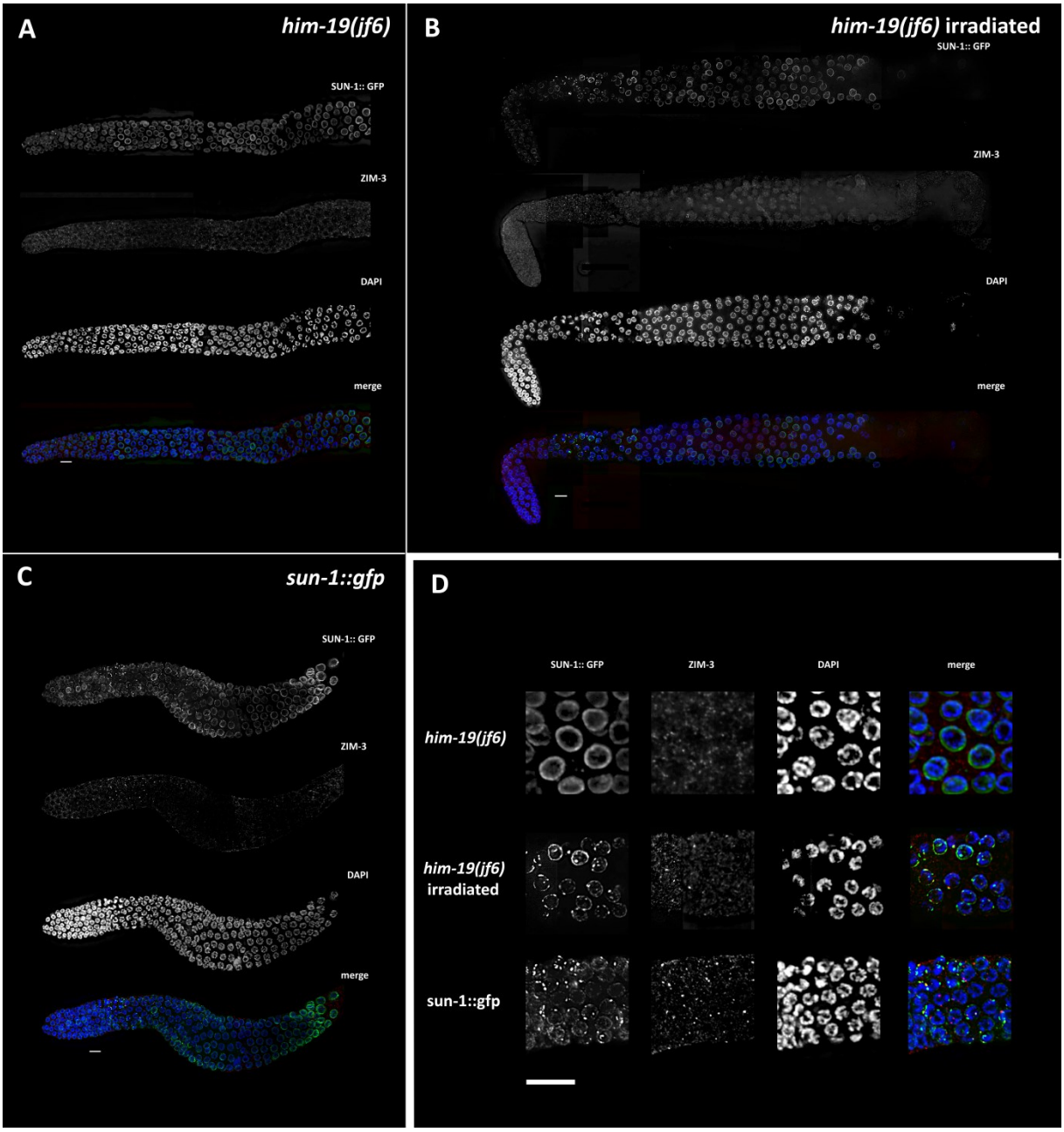

Figure 2: (A-C) SUN-1::gfp (green) and ZIM-3 (red) protein localization in wild-type *SUN-1::gfp*, aged *him-19(jf6); SUN-1::gfp* worms and *him-19(jf6); SUN-1::gfp* 2h

post irradiation. In wild-type TZ, two ZIM-3 foci, corresponding to the paired chromosome I and chromosome IV chromosomal ends can be detected until early pachytene. In the *him-19(jf6); SUN-1::gfp* worm strain, no distinct ZIM-3 foci can be detected and SUN-1::gfp protein remains evenly distributed on the inner nuclear membrane. Scale bars represent 10 µm, rectangles represent magnified area. (D) Enlarged leptotene/zygotene nuclei of aged *him-19(jf6)* worms and irradiated *him-19(jf6); SUN-1::gfp*. Scale bars represent 10 µm.

	control			irradiated		
	Average number of SUN-1 S8 positive cells per gonad	SD	n	Average number of SUN-1 S8 positive cells per gonad	SD	n
N2 (Bristol)	171,56	33,47	18	181,56	29,54	18
him-19(tm3538)	1,73	2,05	15	36,52	16,52	21
chk-2(me64)	0,00	0,00	13	0,00	0,00	14
atm-1(gk186); atl-1(tm853)	161,57	24,68	7	nd	nd	nd
him-19(tm3538),atm-1(gk186)	2,15	1,95	13	12,54	5,83	13
him-19(tm3538); atl-1(tm853)	115,50	30,10	10	147,40	32,92	10
him-19(tm3538), atm-1(gk186); atl-1(tm853)	1,57	1,65	14	3,50	3,16	14
cep-1(gk138)	171,83	16,76	6	nd	nd	nd
him-19(tm3538), cep-1(gk138)	3,74	3,54	19	11,88	10,61	34
him-19(tm3538), rrf-3(pk1426)	0,60	0,89	5	31,71	14,90	7
him-19(tm3538), rrf-3(pk1426), chk-1 RNAi irradiated	0,50	0,84	6	0,50	0,80	12
dpy-13(e184), rad-51(lg8701)	146,83	25,80	6	146,00	12,57	6
him-19(tm3538); rad-51(lg8701), dpy-13	3,62	3,57	13	73,16	20,36	19
mre-11(ok179)	176,20	20,29	5	nd	nd	nd
him-19(tm3538); mre-11(ok179)	1,50	2,00	8	25,56	16,19	9
him-19(tm3538); unc-32(e189), com-1(t1626)	0,50	0,84	6	23,33	9,58	6
him-19(tm3538); brc-2(tm1086)	30,33	17,05	6	nd	nd	nd
him-3(gk149); mre-11(ok179)	13,80	6,87	20	53,33	19,86	21
him-3(gk149); mre-11(ok179) 4 days old	21,94	22,44	18	nd	nd	nd
him-3(gk149); mre-11(ok179) SYP-1 RNAi	15,27	6,45	15	nd	nd	nd
htp-3(tm3655)	76,71	41,80	17	93,54	43,21	13
htp-3(tm3655) 4 days	75,23	54,66	13	nd	nd	nd
htp-3(y428) ccIs4251 2 days	79,77	47,01	13	nd	nd	nd
ieDf2	159,20	23,77	10	nd	nd	nd
ieDf2, mre-11(ok179)	143,20	33,13	10	nd	nd	nd
ieDf2, htp-3(tm3655)	77,20	31,45	18	nd	nd	nd
him-19(tm3538); com-1(t1626)	0.50	0,84	6	23,33	9,58	6

Table 1: Quantification of SUN-1 phosphorylation patterns at the meiotic TZ in various meiotic mutant strains. Table shows average number of SUN-1 S8-Pi positive nuclei in irradiated and control worms 2 days post L4 (unless stated otherwise). SD represents standard deviation, n denotes number of analysed worm germlines.

5.1.1. Dynamics of the DNA damage response in aged *him-19* worms

To learn more about the dynamics of DNA damage signaling in the *C. elegans* germline, we were interested in the kinetics of the observed restoration of SUN-1 S8-Pi. Analysis of SUN-1 S8 phosphorylation dynamics in the aged *him-19(jf6)* background following radiation treatment showed robust restoration of leptotene/zygotene SUN-1 phosphorylation at the meiotic TZ 120 min post irradiation with 5000 rad, with first nuclei displaying SUN-1 S8 phosphorylation and SUN-1 aggregate formation appearing approximately 30 min after exposure to gamma radiation (Table 2). *him-19(tm3538*) gonads showed no increase in SUN-1 phosphorylation when analysed 15 min after exposure to gamma radiation (data not shown).A lower radiation dosage of 830 rad showed maximum restoration of SUN-1 S8-Pi at 2 hrs post irradiation in *him-19(tm3538)* worms. Notably, decreasing radiation dosage from 5000 rad to 830 rad resulted in a decreased and protracted appearance of SUN-1 S8-Pi, first SUN-1 S8-Pi positive cells could be observed 60 min post irradiation (data not shown) robust SUN-1 S8 phosphorylation detectable 120 min after DSB induction (Table 2). After reaching maximum at 120 min, SUN-1 S8-Pi signal strength progressively decreases. 6 hrs post irradiation, SUN-1 phosphorylation levels again reach *him-19* control levels. These results suggest that gamma radiation induced DNA damage signaling leading to phosphorylation of SUN-1 and repolarization of germ cell chromatin is rapid and a transient response and increases with the extent of genomic damage.

	Average number of SUN-1 S8 positive cells per gonad	SD	n
N2 (Bristol) control	171,56	33,47	18
N2 (Bristol) irradiated, 5000rad, 120min	181,56	29,54	18
him-19(tm3538) control	1,73	2,05	15
him-19(tm3538) irradiated, 5000rad, 30min	6,33	3,50	6
him-19(tm3538) irradiated, 5000rad, 60min	11,67	3,67	6
him-19(tm3538) irradiated, 5000rad, 120min	36,52	16,52	21
him-19(tm3538) irradiated, 5000rad, 240min	1,83	1,94	6
him-19(tm3538) irradiated (830 rad)	10,50	4,84	8

Table 2: Quantification of SUN-1 S8 phosphorylation dynamics in the wild type (N2), irradiated and control *him-19(tm3538)* mutant worms 2 days post L4. Worms were dissected at various time points after exposure to gamma radiation. SD represents standard deviation, n denotes number of analysed worm germlines.

5.2. Pairing Dynamics in the meiotic transition zone

Previous studies in the organism *C. elegans* describe pairing of homologous chromosomes in meiosis (MacQueen et al. 2002; MacQueen et al. 2005; Nabeshima et al. 2011; Zhang et al. 2012). In addition, studies have shown that active chromosomal movement is essential for the establishment of homologous pairing in *C. elegans* meiosis (Penkner et al. 2007; Hiraoka and Dernburg 2009). Typically, pairing of homologous chromosomes is assayed by dividing the nematode gonad into six equal sections. We wanted to get a better understanding of the dynamics of active chromosomal movement on the establishment of homologous pairing.

Therefore, we analysed homologous pairing in wild-type meiosis with temporal high resolution focusing on early meiotic nuclei. The first cell row displaying polarized chromatin conformation served as point of reference to determine the start of the meiotic TZ. In this experiment we used a probe recognizing the pairing center end of chromosome I. As can be seen in Table 3, analysis of chromosome paring in each individual cell row reveals that

homologous pairing is a fast and non-linear process, with a high percentage of homologous pairing established rapidly within the first few cell rows after beginning of the TZ.

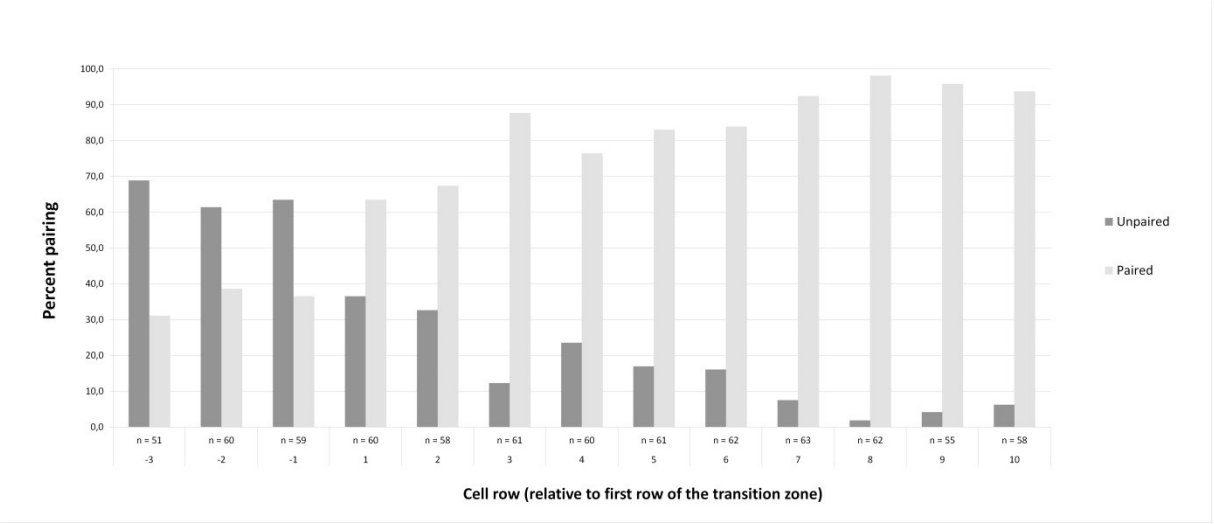

Table 3: Pairing dynamics of the pairing center region of the X chromosome. n denotes number of analysed germline nuclei for each individual cell row, numeric characters their position relative to the first row of polarized TZ nuclei.

5.3. The role of the serine/threonine protein kinase ATM-1 and ATL-1 in DNA damage signaling in the nematode germline

The *C. elegans* genome encodes for two phosphatidylinositol 3-kinase related proteins, including the ATM homologue *atm-1* and the C. elegans ATR, *atl-1 (Garcia-Muse et al. 2005)*. Both proteins were shown to be dispensable for SUN-1 phosphorylation at the meiotic TZ, as *atm-1(gk186)* and *atl-1(tm853)* mutant gonads phosphorylate SUN-1 at S8 in a wild-type manner (data not shown). Likewise, combining both mutant alleles in an *atm-1(gk186)*; *atl-1(tm853)* double mutant worm strain permits phosphorylation of SUN-1 S8 at the TZ, formation of SUN-1 aggregates and clustering of TZ chromatin (Figure 3, Table 1, (Penkner et al. 2009)). In order to study putative involvement of the two kinases ATM-1 and ATL-1 in the activation of CHK-2 in response to DNA damage, we crossed mutant alleles of both kinases into the aged *him-19(tm3538)* genetic background strain to generate a *him-19(tm3538) atm-1(gk186)* and *him-19(tm3538); atl-1(tm853)* double mutant worm strain. By comparing SUN-

1 S8-P levels to those observed in irradiated, aged *him-19(tm3538)* single mutant worms, we could assess the role of the *C. elegans* ATM/ATR homologues in CHK-2-dependent meiotic SUN-1 phosphorylation and SUN-1 aggregate formation in response to artificial DSBs.

5.3.1. ATM-1 is essential for DNA damage induced phosphorylation of SUN-1 in the meiotic TZ in aged *him-19* mutants

2 day post L4-larvalstage *him-19(tm3538) atm-1(gk186)* worms showed an absence of meiotic SUN-1 S8 phosphorylation, SUN-1 aggregate formation and chromatin polarization (Figure 3, Table 1). Remarkably, aged *him-19(tm3538) atm-1(gk186)* did not restore anti-SUN-1 S8-Pi staining at the TZ after subjecting the gonads to 5000 rad gamma radiation. Concurrent to this observation, no restitution of chromatin polarization could be observed in irradiated *him-19(tm3538) atm-1(gk186)* double-mutant gonads (Figure 3, Table 1). Hence, the *him-19* mutant background reveals a central function for the PI3/PI4-kinase ATM-1 in CHK-2 dependent SUN-1 phosphorylation events at leptotene/zygotene of meiosis I. Our results indicate that this dependence on ATM-1 is released in nuclei at the mid-pachytene region. Irradiated *him-19(tm3538) atm-1(gk186)* gonads were competent to phosphorylate SUN-1 S8 in nuclei in the late pachytene region (Figure 3).

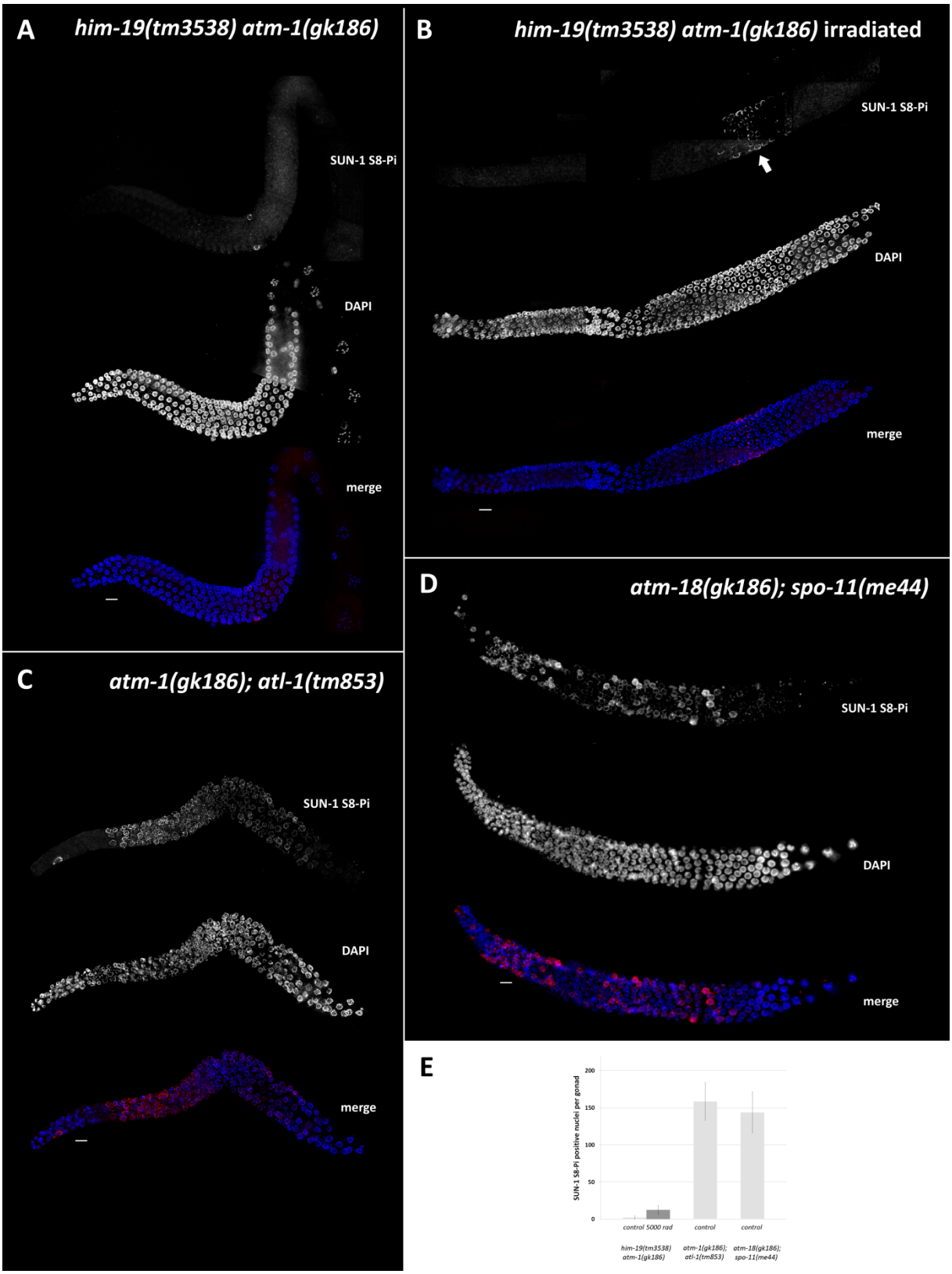

Figure 3: (A) Aged *him-19(tm3538) atm-1(gk186)* gonads show absence of meiotic SUN-1 S8-Pi (red), SUN-1 aggregate formation and chromatin polarization. (B) DNA damage signaling in the TZ is dependent on ATM-1, artificial DSB induction via gamma radiation does not restore SUN-1 S8 phosphorylation, SUN-1

aggregation and DNA clustering in the TZ of *him-19(tm3538) atm-1(gk186)* double-mutants. Notably, SUN-1 S8-Pi restitution can be detected in irradiated late pachytene region nuclei (arrows). (C) An *atm-1(gk186)*; *atl-1(tm853)* double mutant worm strain permits phosphorylation of SUN-1 S8 (red) at leptotene/zygotene, formation of SUN-1 aggregates and clustering of TZ chromatin. (D) Analysis of CHK-2 dependent Sun-1 phosphorylation events in a genetic background deficient for meiotic DNA DSB induction and the DNA damage sensor ATM-1. *atm-1(gk186); spo-11(me44)* double mutants phosphorylate SUN-1 S8 (red) at the TZ concurrent with formation of SUN-1 aggregates and polarization of meiotic chromatin. Scale bars represent 10 µm. (E) Quantification of SUN-1 S8 phosphorylation levels in irradiated and control *him-19(tm3538) atm-1(gk186)*, *atm-1(gk186); atl-1(tm853)* and *atm-18(gk186); spo-11(me44)* germlines. Diagram represents average number of SUN-1 S8-Pi positive nuclei per gonad.

One hallmark of aged *him-19* mutants is the lack of SPO-11 dependent initiation of meiotic recombination, resulting in the absence of RAD-51 foci in zygotene and early pachytene region nuclei (see contributions Chapter 4.2., (Tang et al. 2010)). We generated an *atm-1(gk186); spo-11(me44)* double mutant strain to investigate CHK-2 dependent SUN-1 phosphorylation in a germline lacking SPO-11 induced DSBs in addition to defective DNA damage signaling of radiation induced DSBs. As anticipated, *atm-1(gk186); spo-11(me44)* double mutants phosphorylate SUN-1 at leptotene/zygotene concurrent with formation of SUN-1 aggregates and clustering of meiotic chromatin (Figure 3). These results support a model in which HIM-19 activates CHK-2 via two distinct pathways, one emanating from DNA lesions, either generated by SPO-11 or artificial, gamma radiation induced DSBs, and a second signaling pathway independent of the DNA damage signaling. This DNA damage independent CHK-2 activation could potentially also stem from CHK-2 self-activation by local concentration of the kinase.

5.3.2. ATL-1 is dispensable for DNA damage dependent activation of CHK-2 at the meiotic TZ

atl-1, encoding for the second serine/threonine protein kinase in *C. elegans*, showed a diverging phenotype to *atm-1* regarding SUN-1 phosphorylation and chromatin polymerization in the *him-19* background. In aged *him-19(tm3538); atl-1(tm853)* double mutant worms, SUN-1 protein was phosphorylated timely at the onset of the meiotic TZ even without introduction of artificial DNA DSBs by means of gamma radiation (Figure 4, Table 1). Similarly, SUN-1 formed aggregates and polarization of TZ chromatin could be observed in control *him-19(tm3538); atl-1(tm853)* gonads. Notably, gamma radiation did not alter the SUN-1 phosphorylation pattern in this genotype (Figure 4, Table 1). These results suggest constitutive activation of CHK-2 dependent phosphorylation events in aged *him-19(tm3538); atl-1(tm853)* gonads. Mitotic catastrophe events and defects in the S-phase checkpoint, reported to occur in ATL-1 deficient gonads, represent a likely cause for the dominant CHK-2 activation phenotype seen in a homozygous *atl-1(tm853)* deletion background. (Garcia-Muse et al. 2005). Mitotic defects, resulting in persistent DNA lesions that are likely carried over into the meiotic zone and are able to substitute for radiation induced DSB, are similarly seen in other mutant backgrounds (for more information, see Chapter 5.7.).

5.3.3. ATM-1 and ATL-1 perform distinct DSB damage signaling functions in aged *him-19* meiosis

We generated the triple mutant, *him-19(tm3538) atm-1(gk186); atl-1(tm853),* to study a potential interaction between the two kinases in the context of the *C. elegans* meiosis. As shown in Figure 4, comparable to the *him-19(tm3538)* mutant background, aged *him-19(tm3538) atm-1(gk186); atl-1(tm853)* triple mutant worms show absence of SUN-1 phosphorylation, aggregate formation and chromatin polarization at the meiotic TZ (Figure 4, Table 1). Next, we were interested in the ability of this respective mutant background to activate CHK-2 and phosphorylate SUN-1 over the course of meiosis I. Strikingly, irradiated *him-19(tm3538) atm-1(gk186); atl-1(tm853)* triple mutant gonads lacked SUN-1 phosphorylation, only few and sporadic nuclei at the late pachytene region displaying phosphorylation of SUN-1 S8 could be seen 2 hrs after DSB induction in worms 2 days post

L4- larval stage. Throughout the germline recruitment of the repair protein RAD-51 was not affected, we did observe extensive RAD-51 focus formation irradiated, aged *him-19(tm3538) atm-1(gk186); atl-1(tm853)* worms 2 hrs after irradiation (Figure 4, Table 1).

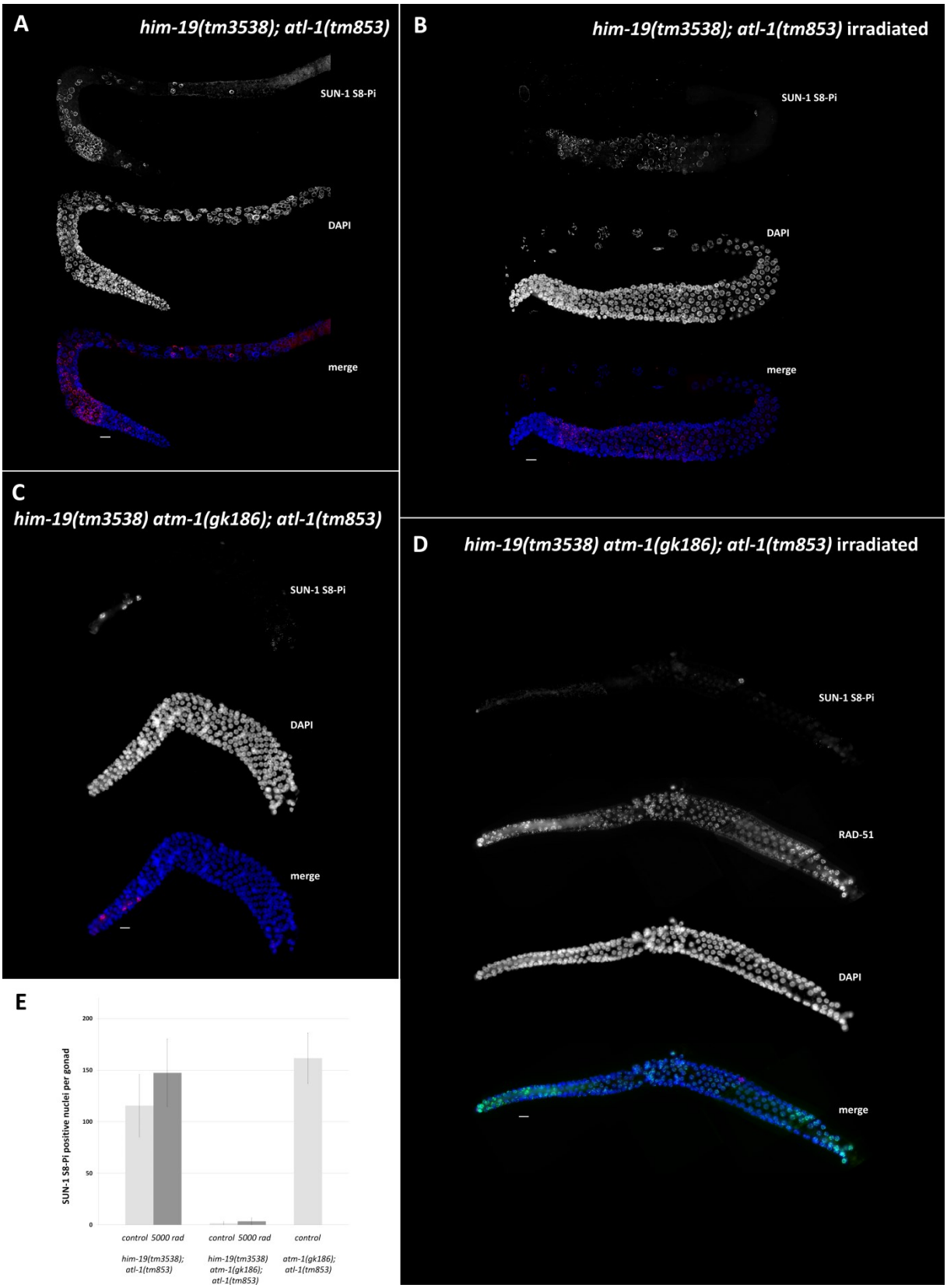

Figure 4: (A) SUN-1 is phosphorylated at S8 (red) in aged *him-19(tm3538); atl-1(tm853)* double mutant worms even without introduction of artificial DNA DSBs. (B) SUN-1 phosphorylation is not altered by subjecting the worms to 5000 rad gamma radiation. (C) Aged *him-19(tm3538) atm-1(gk186); atl-1(tm853)* deficient

worms show lack of SUN-1 phosphorylation at S8 in non-irradiated control worms. This triple mutant genotype demonstrates the central role of the two *C. elegans* sensor kinases ATM-1 and ATL-1 in the meiotic DNA damage response, as *him-19(tm3538) atm-1(gk186); atl-1(tm853)* gonads lack restoration of DNA clustering and phosphorylation of Sun-1 S8 after exposure to gamma radiation (D). Under this condition, the DNA damage repair protein RAD-51 (green) is recruited extensively to DNA lesions 120 min post irradiation in *C. elegans him-19(tm3538), atm-1(gk186); atl-1(tm853)* germline cells. Scale bars represent 10 µm. (E) Quantification of SUN-1 S8 phosphorylation levels in irradiated and control *him-19(tm3538); atl-1(tm853)*, *him-19(tm3538) atm-1(gk186); atl-1(tm853*) and *atm-1(gk186); atl-1(tm853*) germlines. Diagram represents average number of SUN-1 S8-Pi positive nuclei per gonad.

This result facilitates the interpretation of the meiotic phenotypes observed in aged *him-19(tm3538) atm-1(gk186)* and *him-19(tm3538); atl-1(tm853)* worms. CHK-2 activation and subsequent SUN-1 S8 phosphorylation at the meiotic TZ observed in the *him-19(tm3538)*; *atl-1(tm853)* mutant background even without introduction of artificial DSBs is consequently dependent on ATM-1 protein function. Furthermore, aged *him-19(tm3538) atm-1(gk186)* are competent to phosphorylate SUN-1 at the late-pachytene region (Figure 3). As this phosphorylation of SUN-1 is absent in the triple mutant *him-19(tm3538) atm-1(gk186); atl-1(tm853)*, our results suggest that DNA lesions activate CHK-2 at late pachytene dependent on ATL-1 protein function.

5.4. DNA damage dependent activation of CHK-2 in aged *him-19* mutants is reduced in mutants of the p53 homologue CEP-1

CEP-1, the published homologue of the mammalian p53 tumor suppressor protein in the nematode *Caenorhabditis elegans*, is required for DNA damage-induced apoptosis and normal meiotic chromosome segregation in the germline (see Chapter 2.6.8., (Derry et al. 2001). The p53 protein functions as a transcription factor, its target genes include constituents of the DNA damage response pathway (for review see (Menon and Povirk 2014), (Zheng et al. 2013)). Hence, we were interested in the role of CEP-1 in the DNA

damage response in the meiotic TZ, resulting in subsequent activation of CHK-2. First, we analysed CHK-2 dependent SUN-1 phosphorylation events in a CEP-1 deficient genetic background. As shown in Figure 5, early meiotic events such as meiotic SUN-1 phosphorylation and SUN-1 aggregate formation were not impaired in a *cep-1(gk138)* deletion background.

Next, we were interested in the effects of *cep-1* depletion in aged *him-19* mutants. We generated a *him-19(tm3538) cep-1(gk138)* double mutant worm strain by recombination of the two deletion alleles and analysed their ability to restore CHK-2 dependent meiotic SUN-1 phosphorylation. Similar to the *him-19* single mutant background, aged *him-19(tm3538) cep-1(gk138)* gonads showed absence of leptotene/zygotene SUN-1 phosphorylation in non-irradiated germline nuclei (Figure 5, Table 1). In contrast to *him-19* single mutants, we could detect homogenous onset of weak phosphorylation of SUN-1 S8 in nuclei in the late pachytene region in aged *him-19(tm3538) cep-1(gk138)*, coinciding with weak polarization of late pachytene chromatin (Figure 5, Arrow). Notable, aged *him-19(tm3538) cep-1(gk138) C. elegans* worms displayed traits of genetic instability, for instance a high incidence of broken genetic balancers. As we were interested in the role of the p53 homologue CEP-1 in DNA damage signaling in the nematode germline, we irradiated 2 day old *him-19(tm3538) cep-1(gk138)* homozygous worms with 5000 rad. Although introduction of artificial DNA DSBs restored CHK-2 dependent SUN-1 phosphorylation in the meiotic TZ in the *him-19(tm3538) cep-1(gk138)* double mutants, several analysed gonads were devoid of SUN-1 phosphorylation and the average total number of SUN-1 S8-Pi (11.88 ± 10.61 [SD, n=34]) was significantly decreased compared to *him-19(tm3538)* single mutant worms (36.52 ± 16.52 [SD, n=21], $p < 0.05$) (Figure 5, Table 1). Detection of the repair factor RAD-51 in irradiated gonads revealed extensive formation of chromatin associated RAD-51 foci. Hence, early meiotic repair events are not affected in the aged *him-19(tm3538) cep-1(gk138)* double mutant germline. This experiment reveals the nematode p53 homologue CEP-1 as a factor in the meiotic signal cascade from the DNA break to downstream effector proteins, initiating chromatin clustering and induction of SUN-1 phosphorylation and aggregate formation.

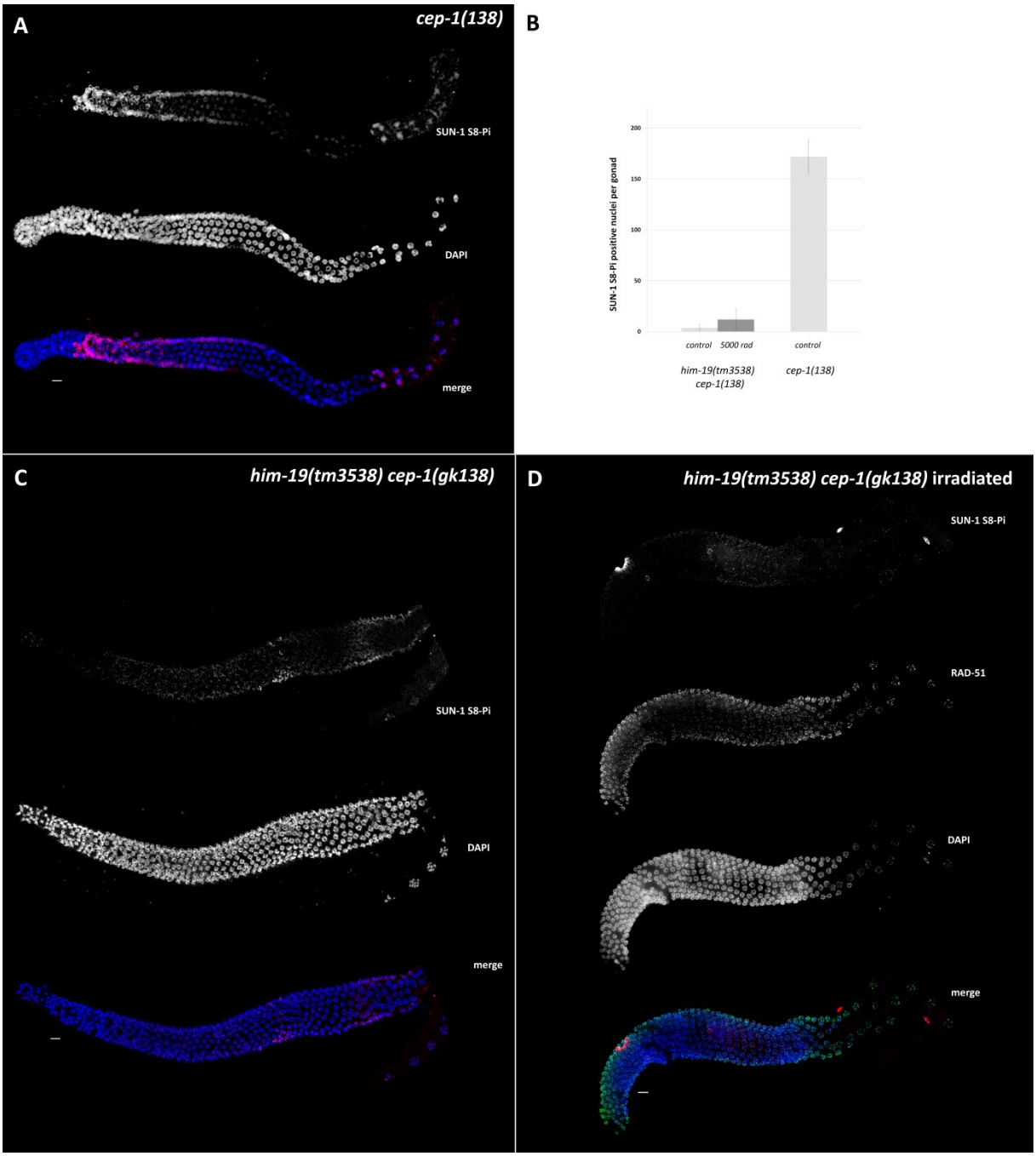

Figure 5: (A) Meiotic SUN-1 S8 phosphorylation (red) and SUN-1 aggregate formation are not compromised in 2 day-post L4 *cep-1(gk138)* deletion worms. (B) Quantification of SUN-1 S8 phosphorylation levels in irradiated and control *him-19(tm3538) cep-1(gk138);* germlines. Diagram represents average number of SUN-1 S8-Pi positive nuclei per gonad. (c) Aged *him-19(tm3538) cep-1(gk138)* double mutants gonads show absence of SUN-1 phosphorylation at the TZ in non-irradiated control worms (D) Artificial DNA DSBs do show decreased SUN-1 phosphorylation at the meiotic TZ in analysed *him-19(tm3538) cep-1(gk138)* double mutants compared to the *him-19(tm3538)* single mutant. The repair

protein RAD-51 (green) is recruited to irradiated germline cells in the *him-19(tm3538) cep-1(gk138)* background. Scale bars represent 10 µm.

5.5. Depletion of CHK-1 prevents damage dependent phosphorylation of SUN-1

C. elegans chk-1 encodes a CHK1-like serine threonine protein kinase that was first described in a screen for proteins involved in the DNA damage response pathway (see Chapter 2.6.5.) (Boulton et al. 2002). Null mutation and high-efficacy RNAi against *chk-1* are reported to result to embryonic lethality phenotype, whereas milder *chk-1* RNAi permits normal development to adulthood (reported by Williams 2011). We performed depletion of CHK-1 by feeding and soaking protocols in wild-type and aged *him-19* mutants. Reliability of the CHK-1 gene knockdown was assessed by scoring the hatch rate of laid eggs and in our experiment, knock-down of CHK-1 was more efficient in worms deficient for RRF-3. RRF-3, a homologue of RNA-directed RNA polymerase, is reported to inhibit somatic RNAi in *C. elegans* (Simmer et al. 2002). As a consequence, *rrf-3* worms are hypersensitive to somatic and exogenous RNAi while meiotic processes, such as SUN-1 phosphorylation dynamics, are not affected (data not shown). We therefore decided to generate a *him-19(tm3538); rrf-3(pk1426)* double mutant strain to assess SUN-1 phosphorylation dynamics in a CHK-1 depleted situation.

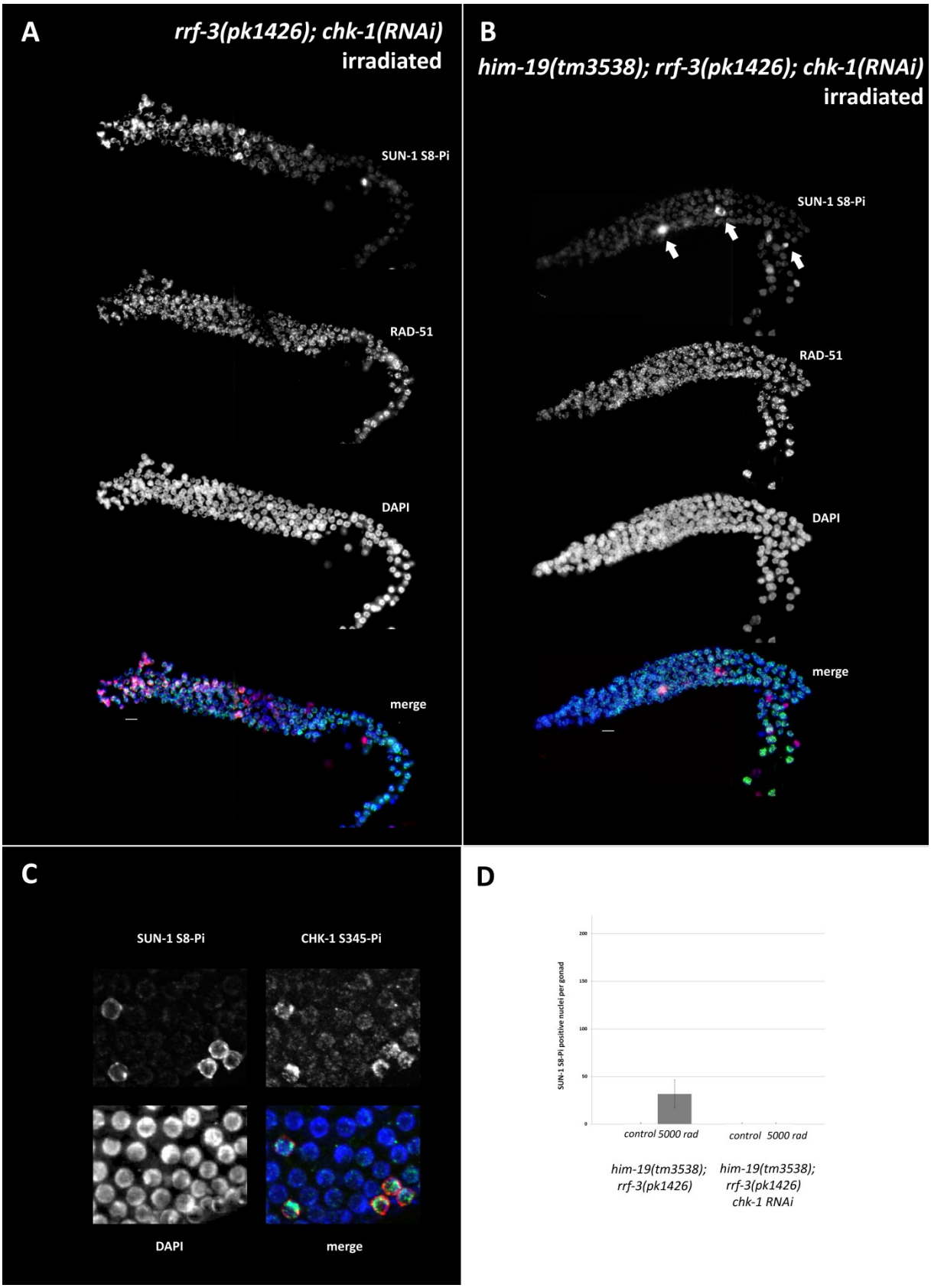

Figure 6: *chk-1* RNAi knockdown prevents damage dependent phosphorylation of SUN-1 S8 (red) in aged *him-19*. (A) Irradiated *rrf-3(pk1426),* chk-1(RNAi) hermaphrodites phosphorylate SUN-1 at S8 (red) and show morphological defects

including decreased size of the germline. In contrast, irradiated, aged *him-19(tm3538); rrf-3(pk1426); chk-1(RNAi)* worms do not restore SUN-1 S8-Pi and chromatin polarization 120 min after subjecting the worm to 5000 rad (B). RAD-51 protein (green) is able to load onto DNA DSBs in irradiated *rrf-3(pk1426); chk-1(RNAi)* and *him-19(tm3538); rrf-3(pk1426); chk-1(RNAi)* worms. Notably, the antibody recognizing SUN-1 S8-Pi depicts unspecific signals in immunofluorescence stainings in the analysed *chk-1(RNAi)* knockdown worms. These SUN-1 S8Pi signals do not represent phosphorylated SUN-1 protein located around the nucleus of germline cells (arrows). Scale bars represent 10 µm. (C) Co-immunofluorescence staining of irradiated *him-19(tm3538)* worms with antibodies recognizing phosphorylated SUN-1 S8-Pi and phosphorylated CHK-1 at Ser345. (D) Quantification of SUN-1 S8 phosphorylation levels in irradiated and control *him-19(tm3538); rrf-3(pk1426)* and *him-19(tm3538); rrf-3(pk1426); chk-1(RNAi)* germlines. Diagram represents average number of SUN-1 S8-Pi positive nuclei per gonad.

Efficient knockdown of CHK-1 protein, assessed by high percentage of dead eggs in the progeny, was achieved by soaking L4-larval stage worms (for conditions of CHK-1 knockdown see Materials and Methods, Chapter 6.8.). In our hands, *chk-1(RNAi*) knockdown led to high mortality rate of soaked worms, less than 25% of treated worms survived the soaking step and reached adult stage. The respective high mortality rate is a result and specific phenotype of the *chk-1* knockdown, as worms readily survived soaking in dH_2O. Dissection of *rrf-3(pk1426)*; *chk-1(RNAi*) and *him-19(tm3538); rrf-3(pk1426); chk-1(RNAi*) worms was difficult due to morphological changes of the gonad caused by the *chk-1* RNAi treatment. Approximately half of the worms surviving *chk-1(RNAi*) soaking either lacked a detectable gonad or harbored diminutive gonads that could not be released onto a microscope slide (data not shown). Successfully dissected *chk-1(RNAi*) gonads were drastically shorter and contained a reduced numbers of meiotic nuclei compared to wild-type *C. elegans*. In addition, gonads proved to be extensively fragile when released from the adult nematode body. Previous reports suggest an essential role of CHK-1 in early gonad development, compatible to our findings that treatment of *C. elegans* larval stages leads to morphological dysplasia or absence of the nematode gonad organ (Kamath et al. 2001; Lehner et al. 2006).

High mortality rates in the CHK-1 RNAi treated worms emphasize the essential function of this checkpoint protein in *C. elegans* development. Therefore my sample size of non-irradiated control *rrf-3(pk1426)*; *chk-1(RNAi*) and *him-19(tm3538); rrf-3(pk1426); chk-1(RNAi*) gonads is rather small and I subjected all worms to irradiation. SUN-1 protein is phosphorylated and forms aggregates at the meiotic TZ in *rrf-3(pk1426)*; *chk-1(RNAi*) control gonads, concurrent with observable leptotene/zygotene clustering of meiotic chromatin (data not shown, Table 1). Notably, a shortened mitotic zone or an overall absence of a defined mitotic zone could be detected in *rrf-3(pk1426)*; *chk-1(RNAi*) control gonads, suggesting a role for CHK-1 in control of mitotic proliferation in the nematode germline. Comparable to the *him-19* single mutant, aged *him-19(tm3538); rrf-3(pk1426); chk-1(RNAi*) gonads did not phosphorylate SUN-1 protein during the course of meiosis and chromatin remained in a non-polarized configuration. Comparable to *rrf-3(pk1426)*; *chk-1(RNAi*) gonads, the morphology of the germline was distorted, prohibiting identification of mitotic nuclei at the distal part of the gonads organ (data not shown).

Next, we were interested in the role of CHK-1 in DNA damage signaling in the germline. SUN-1 protein was phosphorylated in irradiated *rrf-3(pk1426); chk-1(RNAi*) knockdown gonads, Polarized, transition zone-like nuclei could be distinguished in the distal parts of the dissected gonads (Figure 6). Remarkably, aged *him-19; rrf-3(pk1426); chk-1(RNAi*) worms did not show meiotic SUN-1 phosphorylation 2 hrs after subjecting the worms to 5000 rad gamma radiation. As shown in Figure 6 and Table 1, irradiated *him-19; rrf-3(pk1426); chk-1(RNAi*) gonads are devoid of phosphorylated SUN-1 protein throughout meiosis. This experiment identifies the checkpoint kinase CHK-1 as an essential protein linking DNA damage to CHK-2 activation during *C. elegans* meiosis in aged *him-19*. As stated above, only incomplete knockdown of CHK-1 was achieved in *him-19(tm3538)* worms expressing wild-type RRF-3. In this situation, heterogeneity of the phenotype due to the incomplete CHK-1 knockdown in *him-19* worms impeded a qualitative analysis. We could identify aged *him-19(tm3538); chk-1(RNAi)* hermaphrodites that did not restore SUN-1 S8-P after irradiation, together with displaying all the morphological defects also visible in the RNAi-sensitized *him-19(tm3538); rrf-3(pk1426); chk-1(RNAi*) strain. However, the majority of irradiated, aged *him-19(tm3538); chk-1(RNAi)* gonads restored SUN-1 S8-Pi comparable to the *him-19(tm3538)* single mutant strain (data not shown), indicating that a penetrant depletion of CHK-1 was crucial. We performed co-immunofluorescence staining of *him-19(tm3538)*

worms with antibodies recognizing phosphorylated SUN-1 S8-Pi and phosphorylated CHK-1 protein, a reported indicator of checkpoint activation in the *C. elegans* germline. DNA damage and unrepaired recombination checkpoint signal results in phosphorylation of the checkpoint kinase CHK-1 at Ser345 (Jaramillo-Lambert et al. 2010). Therefore, restoration of SUN-1 phosphorylation and aggregate formation correlated with phosphorylated, and thereby activated, CHK-1 protein in gamma radiated *him-19(tm3538)* gonads (Figure 6). Meiotic nuclei that displayed phosphorylation of SUN-1 protein and formed SUN-1 aggregates did also show strong signal for an antibody recognizing CHK-1 S345-Pi. Furthermore, a partial co-localization between the two antibody signals was observable in the respective nuclei. S8-P positive SUN-1 aggregates on the nuclear membrane were frequently found in close proximity to the nucleoplasmatic CHK-1 S345-P signal. This result suggests a functional link between DNA damage induced activation of CHK-1 and CHK-2 dependent phosphorylation of SUN-1 protein in the nematode germline and is in accordance with data presented in (Woglar et al. 2013).

These results suggest a central role for the PI3/PI4-kinase ATM-1 in the DNA DSB signaling cascade independent of HIM-19 protein function (see Chapter 5.3.1.). As CHK-1 knockdown abolished DNA damage dependent SUN-1 phosphorylation events in the aged *him-19(tm3538)* genetic background, our results might suggest that ATM-1 and CHK-1 are functioning in the same, *him-19* independent, signaling pathway activating CHK-2 in response to DNA damage. We therefore depleted CHK-1 in an ATM-1 deficient background. Noteworthy, CHK-1 depletion was performed in an *rrf-3* wild-type background and unreliability of the knockdown has therefore to be considered. However, in my experiments I only retrieved *atm-1(gk186); chk-1(RNAi)* gonads that were competent to phosphorylate SUN-1 during the course of meiosis (data not shown). For a comparison, knockdown of CHK-1 in aged *him-19(tm3538)* worms, resulted in the presence of a number of gonads devoid of SUN-1 S8-P, indicating that the knock-down nevertheless worked, but in an inefficient way. This result is compatible to the hypothesis that ATM-1 and CHK-1 are acting in the same DNA damage signal cascade. However, knockdown of CHK-1 has to be performed in an RNAi sensitized *atm-1* worm strain to rule out involvement of CHK-1 in ATM-1 independent activation of CHK-2.

5.6. Experiments to find the molecular signal needed for activating CHK-2 at the TZ

Our results reveal that introduction of artificial DSBs leads to activation of CHK-2 via the PI3/PI4-kinase family members ATM-1 and ATL-1 (see Chapter 5.3.). In this Chapter, I want to characterize the molecular signal that stimulates the signal pathway leading to activation of CHK-2 kinase after induction of artificial DNA DSBs in *C. elegans* meiosis. Potential candidates comprise the intermediates of the different stages of DNA repair, we addressed this question by either crossing a selection of DNA repair mutants into the *him-19* genetic background or by RNAi knockdown of candidate genes.

5.6.1. RAD-51

We analysed CHK-2 activation and subsequent SUN-1 phosphorylation in a RAD-51 deficient genetic background to learn more about the molecular signal required for the activation of CHK-2 after DNA damage induction. *rad-51* encodes two isoforms of a protein orthologous to the bacterial RecA gene and S. cerevisiae RAD-51p and DMC-1 (Rinaldo et al. 1998). In previous studies, RAD-51 was shown to be dispensable for homology recognition and synapsis but required for bivalent formation at diakinesis due to its strand invasion activity (Alpi et al. 2003). In *rad-51(lg8701)* single mutant worms, SUN-1 protein gets timely phosphorylated at the onset of the meiotic TZ and SUN-1 aggregates can be detected in leptotene/zygotene stage nuclei (Figure 7). Remarkably, robust SUN-1 S8 phosphorylation can be detected in nuclei in the late pachytene region of *C. elegans* meiosis. This elongation of SUN-1 phosphorylation in *rad-51(lg8701)* gonads is accompanied by extended chromosomal clustering. These results are in consistent with results obtained in *rad-51(ok2218)*-deletion mutant and published in Woglar et al. 2013. *rad-51(ok2218)* germ cells show early pachytene-like chromatin clustering throughout pachytene and a prolonged zone of SUN-1 aggregates, colocalizing with the X-chromosomal pairing center (Woglar et al. 2013).

Similar to *him-19(tm3538)* gonads, aged *him-19(tm3538); rad-51(lg8701)* double mutant gonads lack SUN-1 phosphorylation and aggregate formation at the meiotic TZ (Figure 7, Table 1). In contrast to aged *him-19(tm3538)* single mutant worms, we detected SUN-1 S8-P positive nuclei in late pachytene region in aged *him-19(tm3538); rad-51(lg8701)* mutants.

Next, we were interested in the implications of a repair defective genetic background on CHK-2-dependent phosphorylation of SUN-1 in aged *him-19*. Aged *him-19(tm3538); rad-51(lg8701)* germline nuclei show robust restoration of SUN-1 phosphorylation 2 hrs after artificial DSB induction via gamma radiation. Artificial DSB induction in *him-19(tm3538); rad-51(lg8701)* gonads resulted in more prominent restoration of SUN-1 phosphorylation compared to *him-19(tm3538)* single mutants, as gonads showed robust levels of SUN-1 S8 phosphorylation at TZ and the pachytene stage of meiosis (Figure 7, Table 1). A conceivable interpretation supported by these results is that the inability to correctly process DNA DSBs in an RAD-51 deficient background leads to hyperphosphorylation of SUN-1 protein, either by activating signal cascades leading to phosphorylation of SUN-1 protein, or by reduced levels of SUN-1 dephosphorylation events.

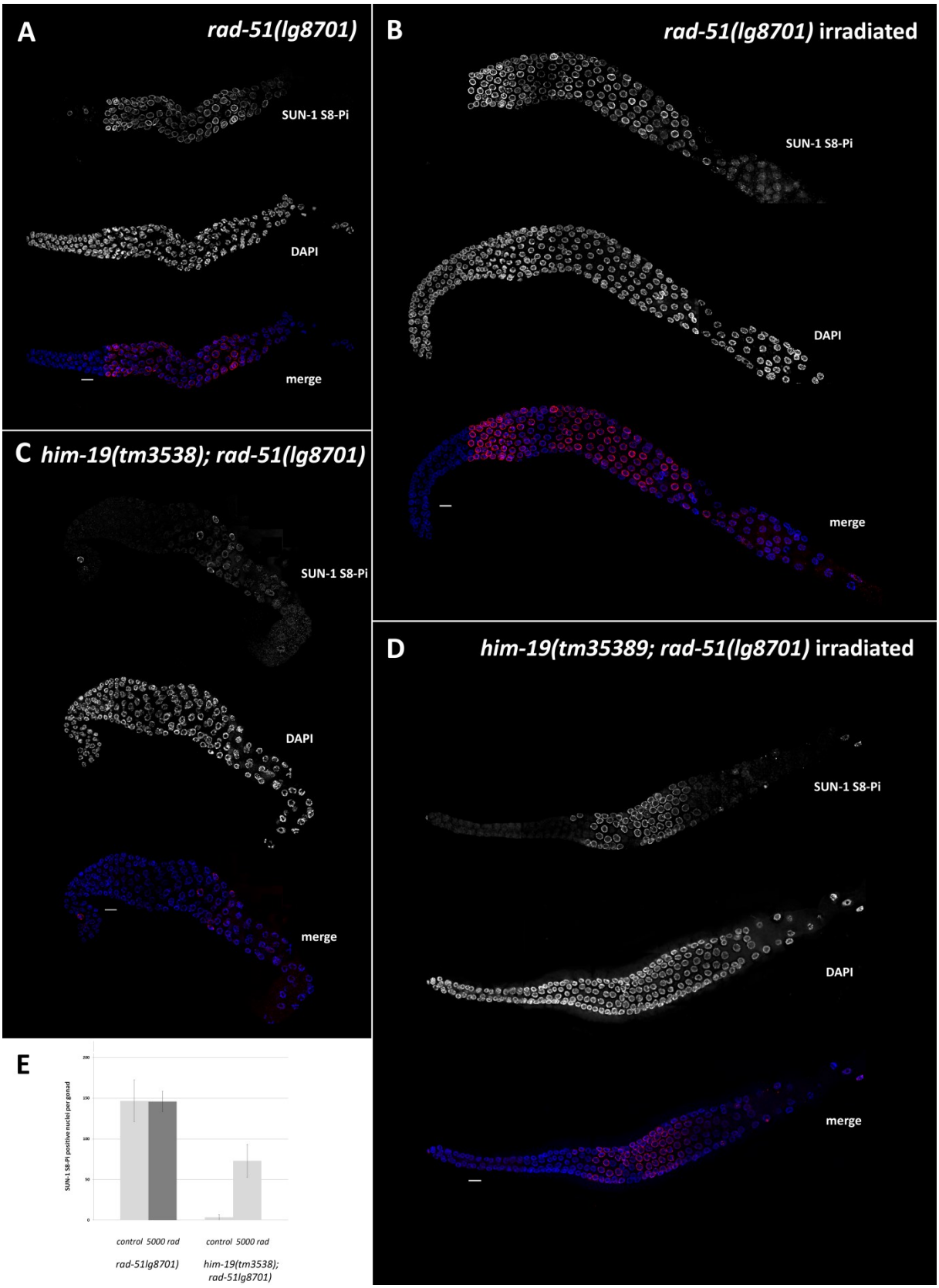

Figure 7: CHK-2-dependent SUN-1 phosphorylation in aged *him-19* in a RAD-51 deficient genetic background. (A) *rad-51(lg8701)* single mutant worms form SUN-1 aggregates at the onset of the meiotic TZ and robust phosphorylation of SUN-1

S8 (red) can be observed in leptotene/zygotene and pachytene region nuclei of meiosis I. (B) Subjecting *rad-51(lg8701)* worms to 5000 rad does not alter the respective SUN-1 phosphorylation pattern. (C) SUN-1 phosphorylation and aggregate formation at the meiotic TZ is absent in aged *him-19(tm3538); rad-51(lg8701)* double mutant gonads. (D) Artificial induction of DSBs by gamma radiation results in robust restoration of SUN-1 S8-Pi in repair-defective *him-19(tm3538); rad-51(lg8701)* germline nuclei. Scale bars represent 10 µm. (E) Quantification of SUN-1 S8 phosphorylation levels in irradiated and control *rad-51(lg8701)* and *him-19(tm3538); rad-51(lg8701)* germlines. Diagram represents average number of SUN-1 S8-Pi positive nuclei per gonad.

5.6.2. The RPA repair complex

As loading of the RPA complex precedes recruitment of RAD-51 protein onto the meiotic break, we next focused on the role of the different RPA protein complex members in the DNA damage response. This protein complex associates with ssDNA and was shown to be implicated in various cellular processes including DNA replication, nucleotide excision repair, DNA damage checkpoint responses and homologous recombination (Fairman et al. 1988; Braun et al. 1997; Lee et al. 1998; Stauffer and Chazin 2004). *rpa-1* encodes the *C. elegans* orthologue of the RPA (replication protein A (RPA)) large subunit. RPA-1 is predicted to function as a DNA-binding protein required for DNA replication, repair, and recombination (Martin et al. 2005). We performed an RNAi based knockdown of RPA-1 to assess whether depletion of the RPA complex has an effect on CHK-2 activation at the meiotic TZ (for reagents used, see chapter Materials and Methods). After RNAi treatment, the worms were sterile and we observed strongly disorganized gonad morphology in RPA-1 knockdown gonads. As no DAPI positive structures were visible in a shortened gonad organ, it was not possible to assess the different stages of *C. elegans* meiosis. No specific signal could be obtained in cytological preparations via immunofluorescence staining utilizing an antibody recognizing SUN-1 S8-Pi. Therefore, respective gonadal remnants could not be assessed for SUN-1 phosphorylation dynamics in RPA-1 RNAi knockdown worms (Data not shown).

To target the RPA complex member RPA-2, we generated a *him-19(tm3538) rpa-2(ok1627)* double mutant worm strain. RPA-2 encodes the nematode homologue of the medium subunit of RPA, RPA-2 was shown to physically interact with RPA-1 in vivo (Martin et al.

2005). Aged *him-19(tm3538) rpa-2(ok1627)* worms displayed reduced broodsize and embryonic lethality. Dissection and cytological evaluation of the gonad organs show disorganized gonad morphology, although DAPI positive bodies representing meiotic nuclei can be distinguished. Immunofluorescence staining of aged *him-19(tm3538) rpa-2(ok1627)* gonads reveals mosaic SUN-1 S8 phosphorylation, even in a control situation without induction of artificial DSBs (Figure 8). Since gonads are disorganized and do not allow identification of the mitotic zone and of the different stages of *C. elegans* meiosis, CHK-2 dependent phosphorylation events could not been analysed in a *him-19(tm3538) rpa-2(ok1627)* genetic background.

rpa-3 encodes a homologue of yet another component of the *C. elegans* RPA complex (Kimberly Van Auken). We performed knockdown of *rpa-3* by RNAi feeding and soaking protocol (see M&M, Chapter 6.8.). Worms treated with RPA-3 knockdown RNAi were phenotypically wild-type, viable and fertile (data not shown). Gonad morphology, SUN-1 aggregate formation and SUN-1 S8 phosphorylation dynamics were not altered. Therefore, our results indicate that RPA-3 knockdown RNAi is either ineffective or RPA-3 protein is not essential in *C. elegans* meiotic events.

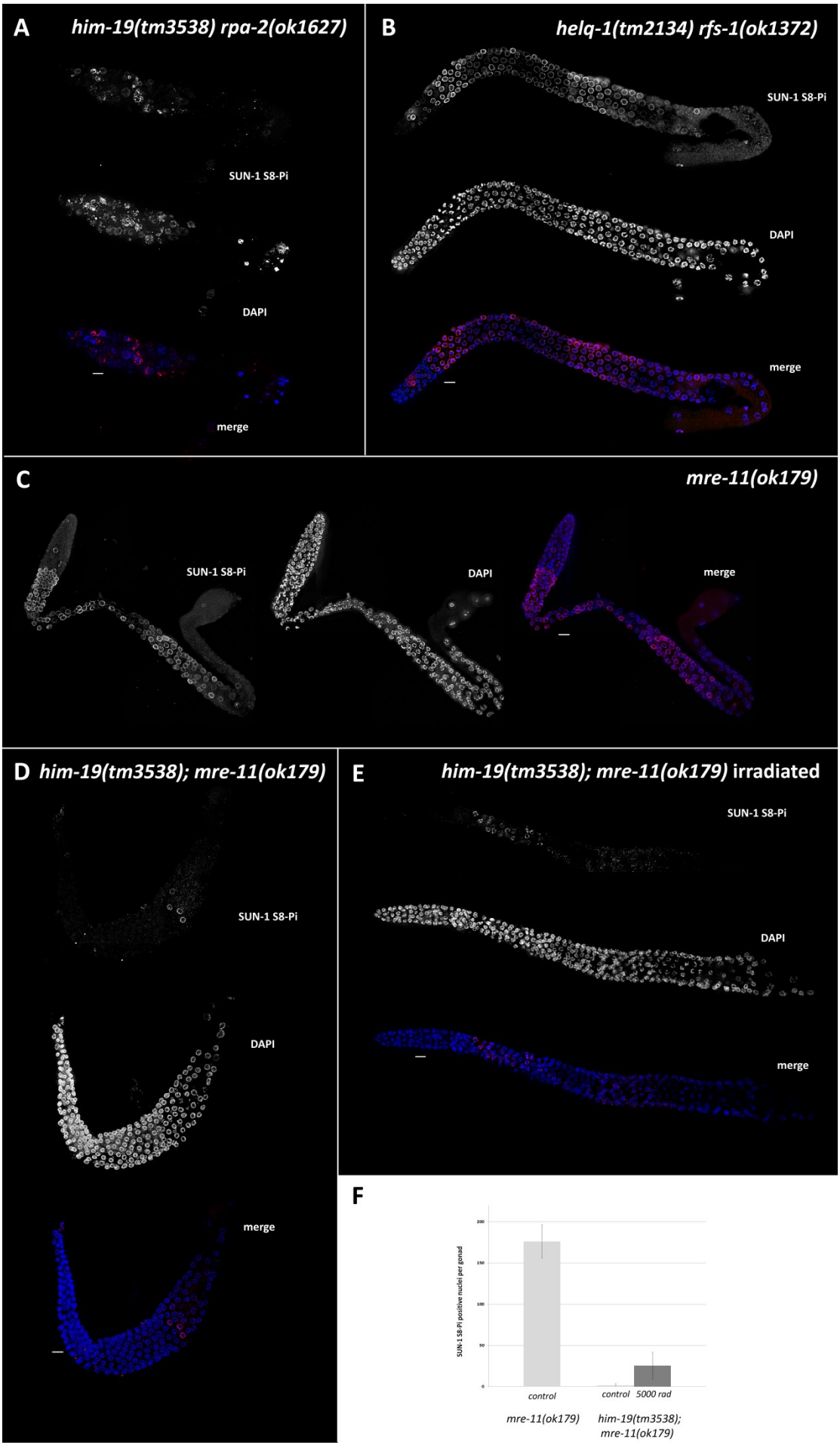
A
him-19(tm3538) rpa-2(ok1627)
SUN-1 S8-Pi
DAPI
merge
B
helq-1(tm2134) rfs-1(ok1372)
SUN-1 S8-Pi
DAPI
merge
C
mre-11(ok179)
SUN-1 S8-Pi
DAPI
merge
D
him-19(tm3538); mre-11(ok179)
SUN-1 S8-Pi
DAPI
merge
E
him-19(tm3538); mre-11(ok179) irradiated
SUN-1 S8-Pi
DAPI
merge
F
SUN-1 S8-Pi positive nuclei per gonad
200
150
100
50
0
control
control
5000 rad
mre-11(ok179)
him-19(tm3538); mre-11(ok179)

Figure 8: (A) Aged *him-19(tm3538) rpa-2(ok1627)* double mutant gonads display pronounced morphological changes concurrent with mosaic SUN-1 S8 phosphorylation (red) in a control situation without induction of artificial DNA lesions. (B) Defects in postsynaptic RAD-51 filament disassembly do not alter SUN-1 phosphorylation dynamics in the *C. elegans* germline, as SUN-1 S8 is phosphorylated similar to the wild type in 2 day old *helq-1(tm2134), rfs-1(ok1372)* worms. (C) *mre-11(ok179)* worms, unable to process meiotic DNA DSBs, are competent to phosphorylate SUN-1 S8 (red) and form SUN-1 aggregates at the meiotic TZ. (D) Similar to *him-19* single mutants, aged *him-19(tm3538); mre-11(ok179)* double mutant gonads do not phosphorylate SUN-1 at leptotene/zygotene nuclei and no polarization of meiotic chromatin is visible via DAPI staining (blue). (E) Irradiated *him-19(tm3538); mre-11(ok179)* hermaphrodites restore SUN-1 S8-Pi together with re-polarization of TZ chromatin 120 min after subjecting the adult worm to 5000 rad. Scale bars represent 10 µm. (F) Quantification of SUN-1 S8 phosphorylation levels *in mre-11(ok179)* and irradiated and control *him-19(tm3538); mre-11(ok179)* germlines. Diagram represents average number of SUN-1 S8-Pi positive nuclei per gonad.

5.6.3. RAD-51 filament disassembly factors *helq-1, rfs-1*

The helicase *helq-1* (also referred to as *hel-308*) and the *rad-51* paralogue *rfs-1* have implicated in mutually promoting postsynaptic RAD-51 filament disassembly. Whereas RAD-51 protein localization was shown unaltered in *helq-1, rfs-1* double mutant *C. elegans* germline cells, RAD-51 protein fails to disassemble from the strand invasion intermediates (Ward et al. 2010). Therefore, this double mutant genotype allows us to investigate whether accumulation of RAD-51 filament covered ssDNA strands has an effect on SUN-1 phosphorylation kinetics. As can be seen in Figure 8, SUN-1 S8 is phosphorylated with wild-type dynamics in the TZ in 2 day old *helq-1(tm2134), rfs-1(ok1372)* worms, concomitant with clustering of meiotic chromatin. Notably, SUN-1 S8-P signal diminishes in early pachytene region nuclei, whereas phosphorylation of SUN-1 S8 increases in later regions of pachytene (Figure 8). We generated a *him-19(tm3538); helq-1(tm2134) rfs-1(ok1372)* triple mutant strain and evaluated the SUN-1 phosphorylation pattern. Non-irradiated, aged *him-19(tm3538); helq-1(tm2134) rfs-1(ok1372)* gonads showed absence of meiotic SUN-1 phosphorylation whereas gamma radiation treatment restored SUN-1 S8-P signal

comparable to aged *him-19* single mutant worms (Table 1, data not shown). Therefore, inability to remove RAD-51 from the resected ssDNA strand does not lead to hyperphosphorylation of SUN-1 protein in response to artificial DNA lesions as seen in a *rad-51* deficient background.

5.6.4. MRE-11

The *C. elegans* repair protein MRE-11 is required for meiotic recombination and involved in the processing of IR-induced DSBs to generate ssDNA overhangs bound by RPA proteins. Similar to *spo-11* worms, depletion of RAD-51 protein in *mre-11* worms results in intact and properly condensed univalents in diakinesis, indicating that MRE-11 protein is needed for induction of meiotic DSBs (Chin et al. 2001; Rinaldo et al. 2002; Hayashi et al. 2007). In *mre-11(ok179)* single mutant gonads SUN-1 S8 is phosphorylated in a timely fashion (Figure 8, Table 1). Hence, a signal emanating from endogenous DNA breaks was not required to activate CHK-2 and phosphorylate SUN-1. This result is in accordance with results obtained in *spo-11* deficient germlines, as *spo-11* germline cells, lacking meiotic DNA DSB formation, phosphorylate SUN-1 protein in a wild-type manner. SUN-1 S8-P overall signal intensity decreases in mid-pachytene region of *mre-11(ok179)* gonads analogous to the wild type (Figure 8).

Next, we were interested if the inability to resect exogenous DNA breaks in *mre-11(ok179)* worms would lead to the inability to respond to DSBs in irradiated *him-19* gonads. We did generate *him-19(tm3538); mre-11(ok179)* double mutant worms and assessed SUN-1 phosphorylation dynamics in response to radiation. Aged *him-19(tm3538); mre-11(ok179)* hermaphrodites produce wild-type numbers of embryos, comparable to *mre-11(ok179)* single mutant worms, laid eggs do not hatch. Cytological evaluation of aged *him-19(tm3538); mre-11(ok179)* gonads demonstrated that SUN-1 protein is not phosphorylated at leptotene/zygotene stage meiotic nuclei and chromatin remains in a nonclustered configuration, comparable to *him-19* single mutant worms (Figure 8, Figure 1). Strand resection mediated by MRE-11 was not essential for radiation-induced activation of CHK-2, although a role for MRE-11 in early prophase cannot be excluded. Analysed irradiated *him-19(tm3538); mre-11(ok179)* gonads showed SUN-1 S8-Pi phopshorylation 2 hours after exposure. Nucleus-by-nucleus assay of the total number of SUN-1 S8-Pi positive cells per

gonad showed average total number of SUN-1 S8-Pi (25,56 ± 16.19 [SD, n=9]) in 2 day post L4. Although this value is slightly decreased compared to *him-19(tm3538)* single mutant worms (36.52 ± 16.52 [SD, n=21], p > 0.1), analysis of our data showed that this reduction is non-significant compared to the wild type (Figure 8, Table 1).

5.6.5. COM-1

We wanted to address if artificial DNA damage can activate CHK-2 dependent phosphorylation of SUN-1 in a *com-1* mutant strain. COM-1 is implicated in resection of meiotic DNA breaks, induced by SPO-11 protein, and subsequent loading of RAD-51 onto the ssDNA tails. In the worm, COM-1 was recently shown to promote meiotic recombination by counteracting the NHEJ complex Ku (Penkner et al. 2007; Lemmens et al. 2013). Aged *him-19(tm3538); com-1(t1626)* double mutant gonads are characterized by an absence of meiotic clustering and SUN-1 S8 phosphorylation at the transition zone (Figure 9). Similar to *him-19* single mutant worms, gamma radiation does partially restore a meiotic transition zone and SUN-1 S8 phosphorylation levels (Figure 9, Table 1). Consequently, COM-1 protein function is not involved in the DNA damage response activing CHK-2 in irradiated aged *him-19* worms.

5.6.6. ieDf2

Our data implies that DNA damage signaling can activate CHK-2 dependent meiotic processes, for instance phosphorylation of SUN-1. Taking into consideration that DNA breaks can induce concurrent recruitment of the pairing center protein ZIM-2 in the him-19 background (Figure 2), we were considering the possibility that the ZIM proteins at the chromosomal paring centers are involved in meiotic signaling processes. In order to assess the role of the pairing centers, we used the worm strain *ieDf2*, which denotes a deletion on chromosome IV, resulting in a deficiency of the pairing center proteins ZIM-1, ZIM-2, ZIM-3, and HIM-8 (Harper et al. 2011). Considering that *ieDf2* worms do phosphorylate SUN-1 at the onset of meiosis (see Table 1), loading of the pairing center proteins to the chromosomal ends cannot constitute the only signal needed to activate downstream processes. In consequence, we analysed ieDf2 in genetic backgrounds with impaired DNA damage signaling and in a meiotic axis mutant background.

We generated the genotype *iedf2; mre-11(ok179)*, deficient for the pairing center proteins in addition to meiotic DNA resection. Likewise, we crossed *ieDF2* into a meiotic axis mutant strain, *htp-3(tm3655)*. SUN-1 phosphorylation levels were determined to assess activation of CHK-2-dependent downstream signaling processes. 2 day post L4 *iedf2; mre-11(ok179)* gonads showed robust meiotic phosphorylation of SUN-1 S8, comparable to the wild type. Similar to *htp-3(tm3655)* single mutant worms, assessed *iedf2; htp-3(tm3655)* mutant gonads did depict a mosaic SUN-1 phosphorylation pattern (see Table 1). These results indicate that the ZIM proteins and/or recruitment of the ZIM proteins to the pairing centers are not involved in CHK-2 dependent meiotic signaling pathways.

5.7. Genetic backgrounds that generate DNA lesions that activate CHK-2 in the meiotic TZ in aged *him-19*

During the course of this thesis I generated multiple double mutant lines to investigate activation of CHK-2 in the aged *him-19* mutant background. In this process I made the observation that several meiotic mutants, when crossed into the *him-19* background, showed CHK-2 activation even without introduction of DSBs by irradiation which came along with SUN-1 S8 phosphorylation and SUN-1 aggregate formation in the meiotic TZ.

For instance, *brc-2*, an orthologue of mammalian BRCA2 protein in *C. elegans*, is required for the maintenance of genomic integrity, mutations in the *brc-2* gene were shown to abrogate RAD-51 foci formation in response to DNA damage and to lead to chromosome fragmentation and decompaction of germline chromatin at diakinesis (Ko et al. 2008). *brc-2(tm1086)*-deletion mutants are competent to phosphorylate SUN-1 at the meiotic transition zone and form SUN-1 aggregates (data not shown). Remarkably, aged *brc-2(tm1086); him-19(tm3538)* double mutant gonads displayed persistent phosphorylation of SUN-1 protein at the meiotic TZ without introducing artificial double-strand breaks by gamma radiation (Figure 9). Furthermore, chromatin clustering in leptotene/zygotene could be observed in non-irradiated *brc-2(tm1086); him-19(tm3538)* nuclei. In this work we reported that *him-19(tm3538) rpa-2(ok1627)* hermaphrodite gonads are morphologically disorganized and meiotic maturation appears unstructured (see Chapter 5.6.2.). However, aged *him-19(tm3538) rpa-2(ok1627)* gonads are competent to phosphorylate SUN-1 48 hrs

post L4 larval stage without preceding induction of artificial DNA DSBs (Figure 8). Similarly, analysis of aged *him-19(tm3538); atl-1(tm853)* double mutant gonads reveals constitutive SUN-1 phosphorylation and chromatin polarization in the meiotic TZ (see Chapter 5.3.2., Figure 4]. The laboratory of Simon Boulton established that ATL-1 deficient hermaphrodites exhibit mitotic catastrophe and defects in the S-phase checkpoint (Garcia-Muse et al. 2005). The aged *him-19(tm3538); atl-1(tm853)* double mutant strain demonstrates that a variety of DNA lesions, in addition to radiation-induced DNA DSBs are competent to activate CHK-2 in the context of the *C. elegans* germline. Hence, CHK-2 activation can be shown to be a general response to DNA damage in *C. elegans* prophase I, irrespective of their origin. Moreover, in the context of the nematode gonad, our results indicate that unrepaired premeiotic DNA lesions observed in different mutant backgrounds are likely carried over into the meiotic zone and are competent to activate CHK-2.

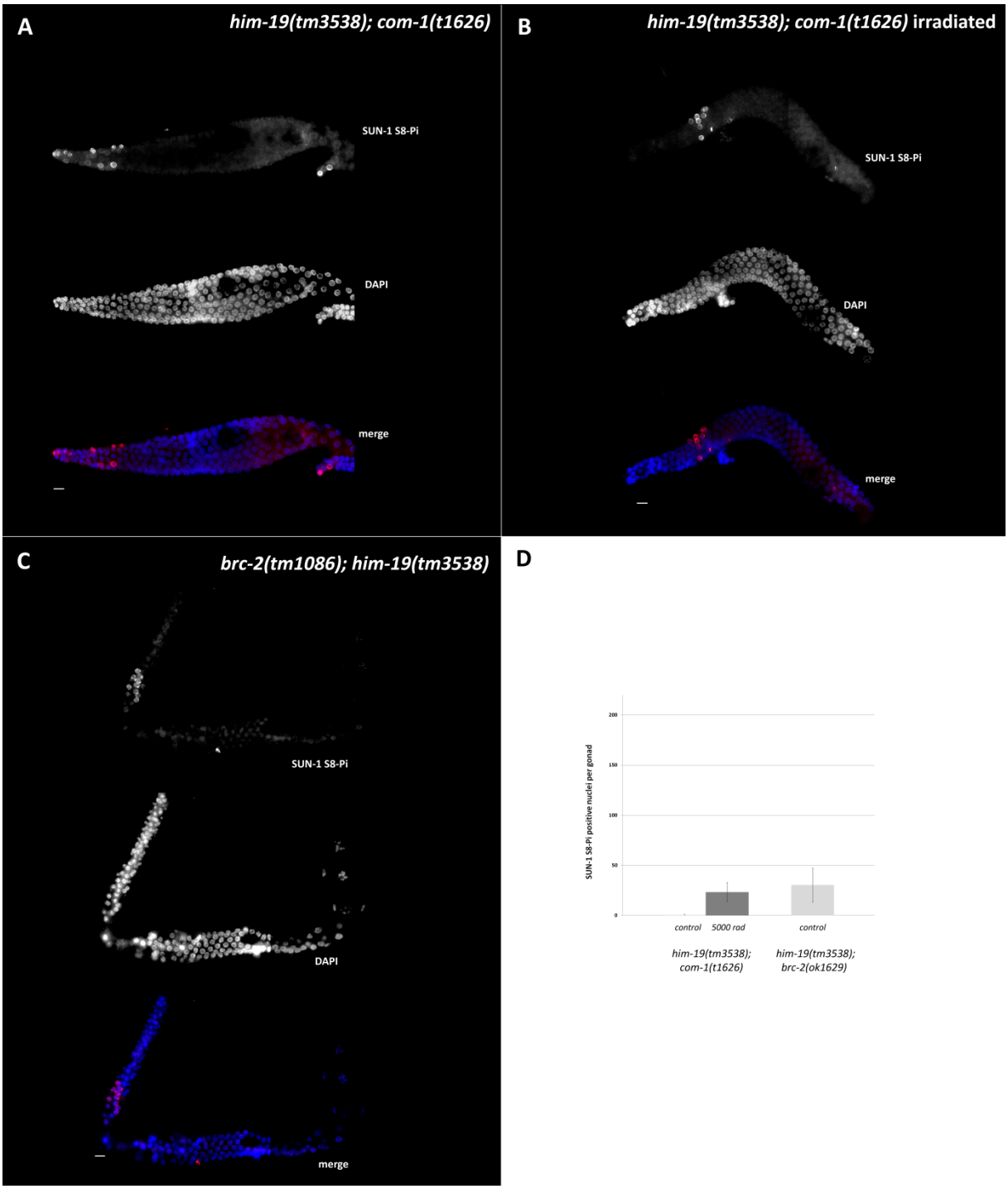

Figure 9: (A-B) Exposure to gamma radiation induces SUN-1 S8 phosphorylation and chromosomal clustering in aged *him-19(tm3538); com-1(t1626)* hermaphrodites. Scale bars represent 10 µm. (C) Persistent phosphorylation of SUN-1 S8 and nuclei displaying chromatin clustering can be observed at the meiotic TZ of control (non-irradiated) *him-19(tm3538); brc-2(tm1086)* double mutant gonads. (D) Quantification of SUN-1 S8 phosphorylation levels in irradiated and *control him-19(tm3538); com-1(t1626)* germlines and in control

***him-19(tm3538); brc-2(tm1086)* gonads. Diagram represents average number of SUN-1 S8-Pi positive nuclei per gonad.**

5.8. Disruption of meiotic chromosome axis concurrent with defective processing of meiotic DNA DSBs restricts SUN-1 S8-Pi in *C. elegans* germline cells

As described in chapter 4.1., phosphorylated SUN-1 protein is absent in aged *him-19* meiotic nuclei. Aged *him-19* mutants are defective in SPO-11 dependent DSB induction as well as recruitment of meiotic, chromatin-associated components such as the pairing center proteins and proteins forming the central element of the SC. The lack of DSBs itself is not sufficient to eliminate SUN-1 phosphorylations (we see SUN-1 phosphorylations in *spo-11*), therefore we raised the question whether CHK-2 dependent SUN-1 phosphorylation events are under the control of parallel signaling cascades, one originating from DNA damage signaling and a second, DSB independent signaling pathway, possibly derived from recruited factors of the meiotic chromosome axis. Both pathways are in an "off state" in aged *him-19* gonads, however DSBs can be induced by irradiation. In order to address this, we generated a double mutant strain to evaluate SUN-1 phosphorylation dynamics in a background disrupting both DNA damage signaling and chromosome axes morphogenesis.

5.8.1. A *him-3; mre-11* double mutant strain show reduction in SUN-1 S8 phosphorylation levels

HIM-3, the homologue of the *S. cerevisiae* HORMA-domain protein Hop1, is required for axis morphogenesis, synapsis, chiasma formation and chromosome segregation (see Introduction Chapter 2.3.1. (Zetka et al. 1999; Couteau et al. 2004). Furthermore, a strain carrying a mutation in *mre-11*, required for DNA repair, induction of meiotic DNA DSBs, meiotic recombination and localization of RAD-51 to foci in late zygotene/early pachytene nuclei, was utilized to abrogate DNA damage signaling (Chin et al. 2001; Alpi et al. 2003; Stracker et al. 2011).

Both *mre-11* and *him-3* single mutant strains are competent to phosphorylate SUN-1 at the meiotic TZ. Immunofluorescence staining of *mre-11(ok179)* deletion mutant gonads at leptotene/zygotene demonstrates wild-type-like phosphorylation with regard to SUN-1 S8, corresponding with concurrent polarization of TZ nuclei (Figure 8). HIM-3 was previously

reported to be required for efficient SUN-1 aggregate formation, *him-3(gk149)*-null mutant gonads only form one mobile SUN-1 aggregate on average (Penkner et al. 2009; Baudrimont et al. 2010). Notable, the single SUN-1 aggregate was shown to colocalize with the X-chromosomal paring center protein HIM-8 (Penkner et al. 2009). These results demonstrate that HIM-3 is required for the loading of the PC proteins to the autosomes at the chromosome end attachments.

Remarkably, the *him-3(gk149); mre-11(ok179)* double-mutant exhibited pronounced restriction of SUN-1 S8 phosphorylation. Only a small number of SUN-1 S8-Pi positive nuclei could be seen in 2 day old *him-3(gk149); mre-11(ok179)* mutant germlines, dispersed in a mosaic pattern at leptotene/zygotene and pachytene. Furthermore, SUN-1 S8-P positive nuclei in the meiotic TZ display weak polarization of TZ chromatin. This is in accordance with the lack of spatial reorganization of chromatin at the onset of the meiotic prophase reported in *him-3(gk149)* germlines. *him-3(gk149); mre-11(ok179)* double mutants showed considerable variation in SUN-1 S8 phospho-modification. 2 day-post-L4 larval stage wild-type control gonads displayed 171.1 ± 35.2 [SD, n=16] SUN-1 S8-P positive cells. This number represents virtually all meiotic nuclei from start of the meiotic TZ to mid-pachytene. In contrast, *him-3(gk149); mre-11(ok179)* double mutant gonads of the same age showed a reduced number of 13.8 ± 6.9 [SD, n=20] SUN-1 S8-P positive cells per gonad (Figure 10, B, Table 1). Despite the fact that both *him-3(gk149)* and *mre-11(ok179)* mutant worms are competent to activate CHK-2 and phosphorylate SUN-1 protein in the single mutant situation, our results indicate that disruption of wild-type meiotic axis morphology concurrent with defective induction/processing of meiotic DNA DSBs restricts SUN-1 phosphorylation in *C. elegans* germline cells. In *him-19* mutant worms, Sun-1 S8 phosphorylation decreasing with the age of the analysed hermaphrodite. Analysed 4 days post L4 *him-3(gk149); mre-11(ok179)* worms show highly variant but comparable levels of SUN-1 S8 phosphorylation compared to 2 day post L4 worms (see Table 1). Therefore, restriction of SUN-1 phosphorylation in *him-3(gk149); mre-11(ok179)* mutants is not dependent on the age of the worm.

Exposure to gamma radiation was shown to induce CHK-2 dependent phosphorylation of SUN-1 in the *him-19* genetic background (see Chapter 5.1.). Hence, we were interested to quantify the effect of gamma radiation induced activation of DNA damage signaling on SUN-

1 S8 phosphorylation levels in the double mutant *him-3(gk149); mre-11(ok179)*. Subjecting 2 day post L4 larval stage worms to 5000 rad radiation elevated the total number of SUN-1 S8-P positive cells per gonad to 53.3 ± 19.9 [SD, n=21]. Considering that SUN-1 phosphorylation events are under the control of CHK-2 checkpoint kinase (see Figure 1, (Penkner et al. 2009), our results indicate that radiation-induced DNA damage signaling is competent to activate CHK-2 leading to phosphorylate SUN-1 in *him-3(gk149); mre-11(ok179)* double mutant worms.

Previous studies identified the lateral element protein HIM-3 as a crucial factor in forming the meiotic chromosome axes, a basis for SC formation. SYP-1 antibody staining mainly identified nuclear aggregates of SYP-1 protein in *him-3(gk149)* mutants, although short stretches of linear SYP-1 signal are discernible in the *gk149* background (Couteau et al. 2004). Although formation of a central SC complex was shown to be dispensable for meiotic SUN-1 phosphorylation in *C. elegans* meiosis (Penkner et al. 2009), we were interested if small linear stretches of SC could activate CHK-2 and were sufficient to induce the limited SUN-1 S8-Pi phosphorylation observed in *him-3(gk149); mre-11(ok179)* double mutants. Therefore, we suppressed SYP-1 protein expression in *him-3(gk149); mre-11(ok179)* worms via specific RNAi knockdown. As can be seen in Figure 10, B, impaired formation of the SC did not alter SUN-1 phosphorylation levels in *him-3(gk149); mre-11(ok179)* germline cells as RNAi treated worms did show comparable phosphorylation levels to those observed in control *him-3(gk149); mre-11(ok179)* gonads (Table 1).

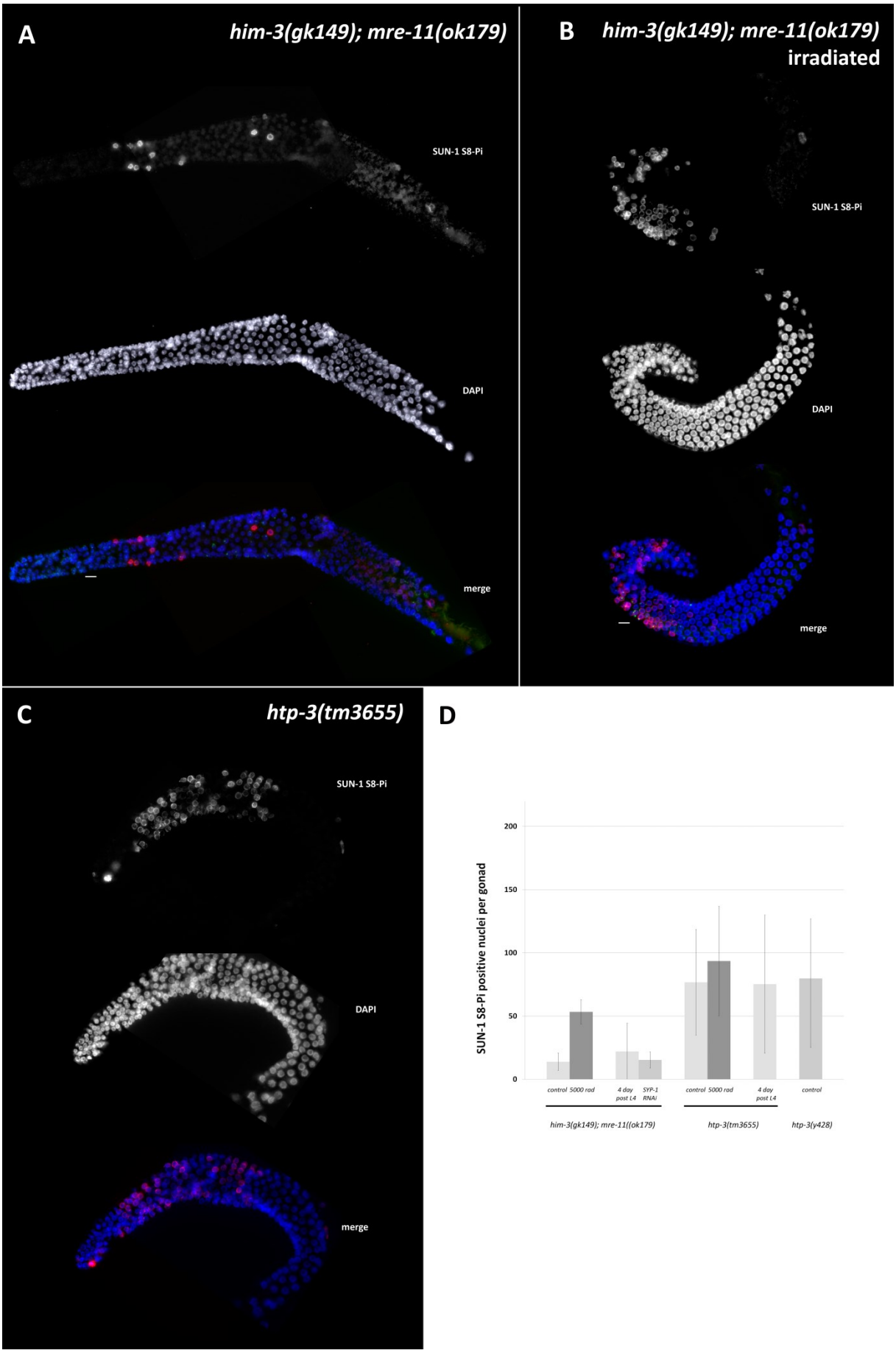
A
him-3(gk149); mre-11(ok179)
SUN-1 S8-Pi
DAPI
merge
B
him-3(gk149); mre-11(ok179)
irradiated
SUN-1 S8-Pi
DAPI
merge
C
htp-3(tm3655)
SUN-1 S8-Pi
DAPI
merge
D
SUN-1 S8-Pi positive nuclei per gonad
200
150
100
50
0
control
5000 rad
4 day post L4
SYP-1 RNAi
control
5000 rad
4 day post L4
control
him-3(gk149); mre-11((ok179)
htp-3(tm3655)
htp-3(y428)

Figure 10: Formation of a proper meiotic axis and DSB formation and DNA end processing affects CHK-2 dependent SUN-1 phosphorylation. (A) *him-3(gk149); mre-11(ok179)* double-mutant worms show reduced SUN-1 S8 phosphorylation. Only a minor fraction of germline nuclei phosphorylate SUN-1 at S8 concurrent with weak polarization of TZ chromatin. (B) Exposure to gamma radiation increases SUN-1 S8 phosphorylation in *him-3(gk149); mre-11(ok179)* gonads. (C) *htp-3(tm3655)* mutant worms display mosaic meiotic SUN-1 S8 phosphorylation. Scale bars represent 10 µm. (D) Quantification of SUN-1 S8 phosphorylation levels in irradiated and control *him-3(gk149); mre-11(ok179)* gonads, 4 day post L4 larval stage *him-3(gk149), mre-11(ok179)* gonads, SYP-1 *RNAi* treated *him-3(gk149); mre-11(ok179)* gonads, irradiated and control *htp-3(tm3655)* gonads, 4 day post L4 *htp-3(tm3655)* gonads and *htp-3(y428)* gonads. When not stated otherwise, SUN-1 phosphorylation levels were counted in adult worms 2 day post L4. Diagram represents average number of SUN-1 S8-Pi positive nuclei per gonad.

5.8.2. HTP-3 mutant strains show reduced levels of SUN-1 S8-Pi

Our results in *him-3; mre-11* double mutants worms indicate a signaling function of the meiotic axis in combination with defects in DSB induction, hence we were interested in SUN-1 phosphorylation in *htp-3* mutant *C. elegans* worms. Loss of HTP-3 leads to defects in both DSB formation and localization of meiotic axis proteins, including HIM-3 (Goodyer et al. 2008). Analogous to *him-3; mre-11* mutants, 2 day post L4 *htp-3(tm3655)* and *htp-3(y428)* worms display mosaic meiotic SUN-1 S8 phosphorylation with variant but overall reduced levels of SUN-1 S8 phosphorylation (Figure 10, Table 1). Interestingly, induction of artificial DNA DSBs via irradiation of *htp-3* mutant germline cells increased the total number of SUN-1 S8-Pi positive cells 2 hours after radiation exposure, similar to the effect seen in aged *him-19* germlines and *him-3; mre-11* mutants. In contrast to *him-19* mutant worms, Sun-1 S8 phosphorylation in the *htp-3* mutant is not decreasing with the age of the analysed hermaphrodite. Analysed 4 days post L4 *htp-3(tm3655)* worms show similar levels of SUN-1 S8 phosphorylation compared to 2 day post L4 worms (see Table 1).

5.9. Aged *him-19* worms correctly express meiotic candidate proteins

Considering that many meiotic features, such as homologous pairing, DSB induction and synapsis are affected in aged, *him-19* deficient worms, we examined mRNA transcript levels of important meiotic proteins using Real-time PCR. In order to avoid contamination of mRNA levels with embryonal mRNA, we prepared total RNA extracts of 2 day old *him-19(tm3538), fem-3(e1996)* and *fem-3(e1996)* worms. *fem-3* encodes a protein that promotes male development in multiple tissues (Ahringer and Kimble 1991). Hence, *fem-3(e1996)* worms do not produce sperm required to produce fertilized eggs. Candidate genes were chosen according to central function in meiosis in respect to the phenotype seen in aged *him-19* worms. mRNA transcript levels of CHK-2, SPO-11, ATM-1, MRE-11, SYP-2 and RAD-51 were evaluated, whereas primer targeting CHK-1 could not be reliably assessed due to low fidelity of the Real-time PCR reaction. In addition, we utilized PGL-1, a predicted RNA-binding protein essential for fertility and present on germ granules in the *C. elegans* gonad, as a control transcript. Enrichment of target mRNAs was calculated using the average ΔCt values. Ct denotes the cycle threshold value and is inversely proportional to the amount of transcript in each probe, whereas ΔCt defines the spread between target and reference values (*him-19(tm3538); fem-3(e1996)* and *fem-3(e1996)*). Finally, ΔΔCt values reference a control transcript, in our case PGL-1, against the obtained ΔCt values to equalize for concentration differences in the input cDNA samples. Evaluation of mRNA transcript levels showed minor variation in expression of the genes CHK-2, CHK-1, SPO-11, ATM-1, MRE-11, SYP-2, RAD-51 in aged *him-19* worms compared to the wild type (Table 4), implying that meiotic errors observed in aged *him-19* hermaphrodites are not are a consequence of mis-expression of the assessed candidate genes.

		Ct	Ct SD	ΔΔCt	ΔΔCt (equalised)
CHK-2	*him-19, fem-3*	38,73	0,57	1,35	1,02
	fem-3	37,38	0,24		
SPO-11	*him-19, fem-3*	35,36	0,09	2,41	1,83
	fem-3	32,95	0,44		
ATM-1	*him-19, fem-3*	36,50	0,23	1,60	1,21
	fem-3	34,90	0,43		
MRE-11	*him-19, fem-3*	33,90	0,53	1,37	1,04
	fem-3	32,53	0,18		
RAD-51	*him-19, fem-3*	32,41	0,60	1,72	1,30
	fem-3	30,69	0,05		
SYP-2	*him-19, fem-3*	35,95	0,28	2,28	1,73
	fem-3	33,67	0,49		
PGL-1	*him-19, fem-3*	29,23	0,18	1,32	1,00
	fem-3	27,91	0,28		

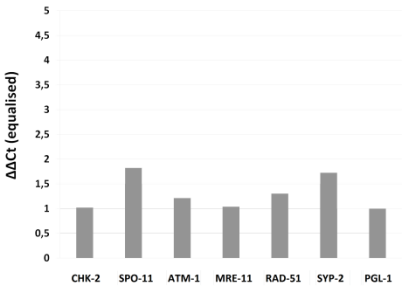

Table 4: Expression of meiotic candidate genes in aged *him-19* worms. Ct denotes the cycle threshold value, ΔCt defines the spread between target and reference value, ΔΔCt values reference a control transcript (PGL-1).

6. Materials and methods

6.1. Immunochemistry

C. elegans gonads were dissected in 1x phosphate-buffered saline (PBS) on a poly-L-lysine covered slide and fixed for 5 min in 1% formaldehyde solution. Samples were covered with a glass coverslip, transferred into liquid nitrogen (−195.8 °C) and kept frozen for 10 min. After a freeze-crack, samples were transferred into Methanol (-20°C) for 1 minute. This step provides additional fixation by dehydration and permeabilizes the nematode gonad by weakening cellular membranes. Slides were washed 3x in 1x PBS-T for 5 min and transferred to a humid chamber. Blocking of unspecific protein-protein interactions was done in in 3% bovine serum albumin (BSA) for 15 min at room temperature. Primary antibody was diluted to the suitable working dilution (see table below) and the primary antibody dilution was incubated at 4°C over night. Samples were afterwards washed 3x with PBS-T for 5 min, followed by secondary antibody incubation at room temperature for 2 h in a dark. Slides were washed 3x in 1 PBS-T for 5 min and mounted with Vectashield (Vector Laboratories®) containing 4',6-diamidin-2-phenylindol (DAPI, 2 µg/ml). DAPI is a fluorescent stain that binds A-T rich DNA regions and is used to visualize DNA molecules.

6.2. Microscopy and Sample Evaluation

Samples were analysed with an Axioskop epifluorescence microscope (Zeiss®) and images were recorded with a cooled charge-coupled device camera (Photometrics®). Three-dimensional stacks (Z-stacks) of images were taken using MetaVue® software (Molecular Devices®). Dependent on gonad morphology, stacks comprised between in 35 and 60 individual pictures (Z-dimension spacing 0.2µm) of 16-bit color depth and 1315x1033 pixels resolution. Images were deconvolved with AutoDeblur software (AutoQuant Imaging®) and projected with Helicon Focus software (Heliconsoft®). If advisable, Z-stacks were processed using ImageJ software suite (available from http://rsb.info.nih.gov, National Institutes of Health, USA).

6.3. Worm strains and culture conditions

C. elegans strains were kept and grown under standard conditions at 20°C (Brenner 1974). N_2 (Bristol) strain was used as a wild-type control. Some strains were provided by the CGC, which is funded by NIH Office of Research Infrastructure Programs (P40 OD010440).

Following strains were used in this study:

N2 (Bristol)

him-19(jf6) (I)

him-19(tm3538) (I)

atm-1(gk186) (I)

msh-5(me23) (IV)/nT1[unc-?(n754) let-?] (IV;V)

dpy-13(e184) rad-51(lg8701) (IV)/nT1[let-?(m435)] (IV;V)

atm-1(gk186) (I); atl-1(tm853) (IV)/nT1 [qIs51] (IV;V)

atl-1(tm853) (IV)/nT1[unc-?(n754) let-? qIs50] (IV;V)

mre-11(ok179) (IV)/nT1[unc-?(n754) let-?] (IV;V)

chk-2(me64), rol-9(sc148)/unc-51(e369), rol-9(sc148) (V)

spo-11(ok79)/nT1[unc-?(n754) let-?] (IV;V)

him-3(gk149) (IV) /nT1 [qIs51] (IV;V); mre-11(ok179) (V) /nT1 [qIs51] (IV;V)

him-19(jf6) (I)

him-19(tm3538) (I)

cep-1(gk138) (I)

ieDf2 (IV)

htp-3(tm3655) (I)

unc-32(e189) com-1(t1626)/qC1 dpy-19(e1259) glp-1(q339) (III)

unc-32(e189) com-1(t1626)/qC1 dpy-19(e1259) glp-1(q339) (III)

him-3(gk149) (IV) /nT1 [qIs51] (IV;V); mre-11(ok179) (V) /nT1 [qIs51] (IV;V).

Following strains were generated in the course of this work:

him-19(tm3538) (I); unc-32(e189) com-1(t1626)/qC1 dpy-19(e1259) glp-1(q339) (III)

him-19(tm3538) (I); mre-11(ok179)/nT1[unc-?(n754) let-?] (IV;V)

him-19(tm3538) (I); msh-5(me23) (IV)/nT1 [qIs51] (IV;V)

him-19(tm3538) (I); helq-1(tm2134),rfs-1(ok1372),lon-1(e185) (III)/helq-1(tm2134),dpy-19(e1259),unc-32(e189) (III)

him-19(tm3538) (I); gen-1(tm2940) (III)

him-19(tm3538) (I); rad-51(lg8701), dpy-13(e184)/nT1 [qIs51] (IV;V)

him-19(tm3538) (I); msh-5(me23) (IV)/nT1[unc-?(n754) let-?] (IV;V)

him-19(tm3538) (I); atl-1(tm853) (IV)/nT1[unc-?(n754) let-? qIs50] (IV;V)

him-19(tm3538) atm-1(gk186) (I); atl-1(tm853) / nT1 [qIs51] (IV;V)

him-19(tm3538) atm-1(gk186)/hT2 (I); +/hT2 [bli-4(e937) let-?(q782) qIs48] (III)

him-19(jf6) (I); htp-1(gk174)/nT1[qIs51] (IV;V)

him-19(tm3538) (I); mtf-1/sun-1(jf18)/nT1 [qIs51] (V,IV)

him-19(tm3538) (I); fem-3/nT1 [qIs51] (IV); +/nT1 (V)

him-19(tm3538), rpa-2(ok1627)/hT2 (I); +/hT2 (III)

cep-1(gk138) him-19(tm3538) / hT2[bli-4(e937) let-?(q782) qIs48] (I)

atm-1(gk186); cdc-7(ok1267) / hT2[bli-4(e937) let-?(q782) qIs48] (I)

him-19(tm3538) / hT2 (I), him-18 (tm2181) unc-32 (e189) /hT2 (III)

him-19(tm3538)/hT2 (I); brc-2(tm1086) (III)/hT2[bli-4(e937) let-?(q782) qIs48] (III)

him-19(tm3538) (I), rrf-3(pk1426) (II)

him-19(tm3538) (I); unc-32(e189) com-1(t1626)/qC1 dpy-19(e1259) glp-1(q339) (III)

hus-1(op244); him-19(tm3538) / hT2 (I); +/hT2[bli-4(e937) let-?(q782) qIs48] (III)

him-19(tm3538) (I), chk-2(me64) rol-9(sc148)/unc-51(e369) rol-9(sc148) (V)

him-19(tm3538) (I), spo-11(me44)/nT1[qIs51] (IV); +/nT1[qIs51] (V)

htp-3(tm3655) (I); iedf2 (IV)

him-19(tm3538) (I); unc-32(e189) com-1(t1626)/qC1 dpy-19(e1259) glp-1(q339) (III)

6.4. Gamma radiation assay

Hermaphrodite worms were irradiated using a radioactive Cs-137 ionizing source. According to the manual of the device, 12 min radiation exposure is quantified as a dosage of 5000rad (50Grey). Accordingly, shorter exposure time was used to achieve lower radiation doses. If not stated otherwise, dissection and subsequent fixation of worm gonads was performed 120 min post-irradiation.

6.5. Whole gonad nucleus-by-nucleus assay of dissected *C. elegans* gonads

Dissected and immunochemically stained *C. elegans* gonads were assayed on the slide under an Axioskop epifluorescence microscope (Zeiss®). In order to assay each individual meiotic nucleus in the dissected gonadal tube, manual focusing of the z-dimension allowed counting of all respective nuclei. Each individual meiotic nucleus displaying SUN-1 S8 phosphorylation signal above background levels was counted as SUN-1 S8-Pi positive. Notably, SUN-1 S8-Pi positive nuclei located at the distal mitotic zone of the gonad tube, displaying specific antibody signal emanating from the NE and the centrosomes, were shown to represent nuclei in the mitotic prometaphase stage or onward and were not counted in this analysis (Penkner et al. 2009). Analogous to the gamma radiation assay (see previous chapter), 2 days post L4-larval stage worms were exposed to 5000 rad (50 Grey) and dissected 120 min post irradiation.

6.6. Fluorescence in-situ hybridization (performed by Cornelia Habacher)

Fluorescent in-situ hybridization (FISH) was performed using a PCR generated probe against pairing center region of chromosome I according to protocol in (Penkner et al. 2007).

Nick translation:

2µg cosmid DNA (F56C11)

5µl dNTPs (GCA 2mM/l)

1,5µl dUTP (dig,CY3,FITC)

5µl NT-buffer (10x: 0,5M Tris pH=8,50mM MgCl2, 0,5mg/ml BSA)

1,5µl β-mercaptoethanol (0,28M)

2µl DNase I (1mg/l)

1µl Polymerase I (**Biolabs**)

ddH2O to 50µl

Hybridization:

The mixture is incubated 2 hrs on 16°C and the reaction is ended by addition of 1µl 0,5M EDTA for 10 minutes on 65°C.

Released gonad were fixed in 7,4% formaldehyde, incubated for 5 min at room temperature and frozen in liquid nitrogen. Samples were permeabilized in methanol, acetone/methanol (1:1) and acetone for 5 min, washed three times for 5 min in PBS-T and incubated 10 min on 78°C with 50µl of NaSCN under a plastic foil. Samples were washed three times with PBS-T and dehydrated in sequential ethanol dilutions (30%, 50%, 70%, 96%) for five minutes each and air-dried over night at room temperature.

3µl probe and 1µl salmon sperm DNA were dried in a vacuum centrifuge for 15 min at 45°C and dissolved in 7µl hybridization mix and 7µl formamide for 2hrs at room temperature. The mixture is applied to the samples fixed with fixogum, samples were denaturated on 70°C for

seven minutes and incubated overnight in a humid camber (37°C). Samples were rehydrated in successive SCC dilutions (2xSSC, 1xSSC, 0,2xSSC, 0,1xSSC) at 42°C in a water bath for 5 min each. Samples were washed three times in PBS-T for 5 min, blocked in blocking buffer for 10 min on room temperature and incubated in a humid chamber with the appropriate primary antibody. Samples were washed three times 5 min in PBS-T, mounted with Vectashield (Vector Laboratories®) containing 4',6-diamidin-2-phenylindol (DAPI, 2 µg/ml), covered with a coverslip and fixed with nail polish.

1xSSC

3 M NaCl, 0.3 M sodium citrate, pH 7

6.7. Time-lapse microscopy (performed by Antoine Baudrimont)

Hermaphrodites gonads were immobilized in 10 mM Levamisol and transferred onto an agarose pad (2% agarose). Mobile SUN-1::GFP aggregates were documented via a Delta Vision® deconvolution microscopy system (Applied Precision®). Specimen covered with a coverslip and sealed with Vaseline. Z-stacks were deconvolved and projected using Softworx software suite (Applied Precision®) and analysed with ImageJ® software (available from http://rsb.info.nih.gov, National Institutes of Health, USA). For detailed information see (Baudrimont et al. 2010).

6.8. RNA interference

RNA interference was performed following the protocol described in (Kamath et al. 2001). To knockdown RPA-1, we used clone II-5B18 of the Ahringer RNAi library (**Geneservice, Ltd.**) transformed into the RNase-deficient *E. coli* strain HT115. L4 larvae were transferred to *rpa-1 RNAi* feeding plates and incubated for 2 days at 20°C followed by dissection of the worm. To knockdown SYP-1 protein, clone V-10P20 of the Ahringer RNAi library (**Geneservice, Ltd.**) was transformed into the RNase-deficient *E. coli* strain HT115. 1 day old worms were transferred onto *syp-1 RNAi* feeding plates and incubated at 20° for 24 hrs. Noteworthy, age dependent characteristics of the *him-19* mutant phenotype necessitated pre-selection of L4 larvae and incubation of the worms at 20°C for 24 hrs.

We used a different protocol to target expression of endogenous CHK-1 protein, feeding *C. elegans* worms HT115 bacteria transformed with Ahringer RNAi library clone targeting CHK-1 (ORF Y39H10A.7) did not result in a detectable phenotype, for instance embryonic sterility after exposure to gamma radiation. *In vitro* transcription of dsRNA for *chk-1* RNAi was performed with T7 Megascript (**Ambion**) according to the protocol. *C. elegans* cDNA was used as template for amplification and the reaction was performed at 37°C for 4 hrs (for primers, see below). RNA was purified by phenol–chloroform extraction, resuspended in ddH2O and quantified in a NanoDrop spectrophotometer (**Thermoscientific**). L4 stage *C. elegans* larvae were incubated overnight at 20°C in M9 buffer containing the dsRNA diluted to a concentration of 1 µg/µl. Worms were then transferred to a NGM plate and recovered for 24 hrs at 20°C.

Primers for CHK-1 *in vitro* transcription

VJ1077 **TAATACGACTCACTATAGGG**ACTCAACAAGCCGAATGCTC

VJ1078 **TAATACGACTCACTATAGGG**CGAGTGCTCCACATTGACTC

Amplified fragment size 778bp, T7 promoter sequence in bold.

Following treatment protocol was used to knock down CHK-1 in a *him-19* mutant background:

Day 1	Selection of L4 larvae, incubation 48h / 16°C
Day 3	Soaking of worms in M9 buffer (1µg/µl RNAi), incubation 24 / 20°C
Day 4	Transfer on NGM plates, regeneration 1h / 20°
	Irradiation (5000rad), incubation 2hrs / 20° C

6.9. Real-Time PCR

RNA of 2 days post L4 larval stage *him-19(tm3538); fem-3(e1996)* and *fem-3(e1996)* worms was extracted with peqGOLD TriFast (**PEQLAB Biotechnologie GmbH)** according to the protocol and the RNA pellet was resuspended in 14 µl ddH2O. Putative contamination of the sample with DNA was prevented by treatment with DNAse I (**Thermoscientific**, RNAse free) according to the protocol. Reverse transcription of mRNA was performed using SMARTer™ Pico PCR cDNA Synthesis Kit (Clontech Laboratories Inc., Takara Bio Company). 3µl Smart7T27 primer (12µM) and 3µl SmartIIA primer (12µM) were added to the RNA and incubated at 65°C for 2 min, temperature was reduced to 42°C and 8µl First-Strand Buffer, 4µl 20mM DDT, 4µl 10mM dNTP, 2µl RNAse Inhibitor (40U/µl) and 2µl Powerscript Reverse Transcriptase were added to the reaction. Reverse transcription was terminated after 90 min by addition of 2µl 0.5 EDTA. cDNA was purified via Wizard® SV Gel and PCR Clean-Up system (**Promega GmbH**) and eluted in 75µl ddH2O. Real-time reaction was performed in a Thermal Cycler with a Multicolor Real-Time PCR Detection System (iQ 5 iCycler RTPCR, **BioRad**) and analysed with the iQ™ Optical System Software package (**BioRad**). Template dilutions were evaluated in quadruples from 2 biological cDNA replicates and reliability of the real-time reaction was assessed via melting curve of the PCR product.

Real-time PCR Master Mix

GoTaq® qPCR Master Mix, 2X (**Promega**)	12.5µl
Template (cDNA sample diluted 1:10, 1:100 and 1:1000 in ddH20)	1µl
PCR primers (13ng/µl, 1/75 dilution of 1µg/µl stock solution)	2µl
ddH20	fill up to 25µl

Real-time PCR Settings

Annealing temperature	55°C
Elongation time	45 sec

Target transcript amplified, primer combination used for RT PCR experiment

spo-11

VJ779	GAGATTTGCACTGTCTTCACCAAG
VJ780	CGCGTCCACAAGAGAGAATG

rad-51

VJ781	GGCAGTATCACTGAGGTTTACGG
VJ782	TCGTTCGGGTCGAAAAGTGG

chk-2

VJ783	TTGACAGGCCGCCTAATCTTCC
VJ784	GCAGTACGACAATCCGCACA

syp-2

VJ785	CGGAGAGTCAGCTTCGCATC
VJ786	ATCGGCCACATCATGAGCAG

pgl-1

VJ787	ATCGGCCACATCATGAGCAG
VJ788	GAGGAATCAGTGGAACGGGC

atm-1

VJ1383	AGAAGGACGATGCCACGTTT

VJ1384 TACACCATTCCACGCGTTCA

chk-1

VJ1385 GTTCTCCCAGCCGACAAAGA

VJ1386 GCTCCACATTGACTCCACCA

mre-11

VJ1387 AGTGGCAAACGCAGTGGATA

VJ1388 AACTTGTCCCATCTCGTCGG

6.10. Antibodies (source animal, dilution Immunochemistry)

anti-SUN-1 phospho-serine 43 (rat,1:1000) (antisera were produced against the following phospho-peptide: CVT RRD S(PO3H2)QP G)

anti-SUN-1 phospho-serine 12 (guinea pig, 1:1500), (Penkner et al. 2009)

anti-RAD-51 (rabbit , 1:100), (Colaiacovo et al. 2003)

anti-SYP-1 (rabbit , 1:250), (MacQueen et al. 2002)

anti-GFP (mouse, 1:500) (Roche Diagnostics®)

anti HIM-8 (rabbit, 1:5000) (Novus®)

anti HIM-8 (1:500, guinea pig) (Phillips, Wong et al. 2005)

anti-ZIM-3 (1:100, guinea pig) (Phillips et al. 2006)

anti-SUN-1 phospho-serine 8 (guinea pig, 1:700) (Penkner et al. 2009)

anti HTP-3 (guinea pig, 1:500) (Goodyer et al. 2008)

anti-rabbit Alexa Fluor® 568 (goat, 1:400) (Invitrogen®)

anti-rabbit Alexa Fluor® 488 (goat, 1:400) (Invitrogen®)

anti-guinea pig Alexa Fluor® 568 (1:400, goat) (Invitrogen®)

anti-guinea pig Alexa Fluor® 488 (1:400, goat) (Invitrogen®)

anti-mouse Alexa Fluor® 488 (goat, 1:400) (Invitrogen®)

rabbit anti-Chk1 (S345Pi) (1:100) (Cell Signaling®)

7. Discussion

A fundamental aspect of meiosis is the coordination of morphological changes of chromosomes with meiotic progression, a prerequisite in the production of viable gametes. One of the most pressing aspects regarding this topic is how DNA repair processes are synchronized with meiotic progression (for review see (MacQueen et al. 2011)). In this work, we addressed this question by establishing the aged *him-19* deficient background and phosphorylation of SUN-1 at serine 8 as a tool to investigate how artificially induced DNA lesions activate downstream, CHK-2 dependent, meiotic processes and which genes are involved in the respective signaling pathways. We could show that DNA damage activates CHK-2 in aged *him-19* germline cells dependent on the sensor kinases ATM-1 and ATL-1 and the checkpoint kinase CHK-1. Furthermore, defects in the meiotic axis concurrent with abrogated DNA damage signaling result in incomplete CHK-2 dependent phosphorylation of SUN-1 S8 at the onset of meiosis. While we have to speculate the sequential order on how DNA damage activates the respective kinases, for the first time, signaling pathways involving components of the DNA damage response resulting in modifications of the inner nuclear membrane could been shown in context of the *C. elegans* germline.

7.1. Dynamics of the DSB response in the *C. elegans* germline

Expanding the findings of (Penkner et al. 2009; Tang et al. 2010), I could characterize the kinetics of SUN-1 S8 phospho-modification in an irradiated, aged *him-19(tm3538)* worm strain. During the course of my thesis work I used SUN-1 S8-Pi as a sensitive read-out for CHK-2 activation. SUN-1 S8-Pi phosphorylation, concurrent with the formation of mobile SUN-1 aggregates and polarization of germline chromatin, could be shown to be a rapid and transient response to artificial DNA lesions, with first SUN-1 S8-Pi positive nuclei emerging 30 minutes after irradiation and reaching a maximum 120 min after exposure to gamma radiation. This result is especially revealing when evaluated in the light of previous publications on this topic. For instance, in *Xenopus* egg extracts activation of the sensor kinases ATM and ATR and subsequent phosphorylation of histone H2AX in response to injection of fragmented DNA was detectable after 5 minutes and robust phosphorylation of histone H2AX was achieved 30 minutes after DNA injection (Costanzo et al. 2004). Likewise,

in response to exposure to gamma radiation of 10000 rad, human fibroblast cells induce phosphorylation of ATM protein within a timeframe of 30 min (Bakkenist et al. 2003). Taken together, we could establish that meiotic DNA damage signaling in the nematode germline follows analogous dynamics to previously described DNA damage signaling pathways in various other model systems. Intriguingly, we could show the onset of meiotic SUN-1 phosphorylation at the TZ coincides with the zone in the C. elegans germline where robust homologous paring is rapidly established (see chapter 5.2).

7.2. DNA damage activates CHK-2 dependent on the sensor kinases ATM-1 and ATL-1 in aged *him-19* germline cells

In most examined biological model organisms, DNA damage signaling was shown to rely on the two highly conserved and related kinases, ATM and ATR (Harrison et al. 2006; Lovejoy et al. 2009). Interestingly, the two sensor kinases have similar functions in the DNA damage response in mitosis and meiosis, suggesting that the same signaling pathways are activated in both meiotic and mitotic cells (Burgoyne et al. 2007; Carballo and Cha 2007). However, this is a topic still under scientific investigation. For instance, previous publications indicate that exogenous DSBs might activate distinct checkpoint signaling pathways than endogenous SPO-11-dependent DNA DSBs. Phosphorylation and activation of Rad53, the yeast homologue of CHK2 protein, was shown to be a response to radiation induced DSBs but was absent in response to Spo11-induced DNA breaks during meiosis (Carballo et al. 2007). In yeast, Spo11-induced DSBs are required for crossover recombination and assembly of the SC. However, introduction of artificial DSBs in *spo11* yeast strains restores crossover recombination in spo11 mutants but not the formation of the SC (Thorne and Byers 1993; Malkova et al. 2000; Zickler 2006). These results allow two possible interpretations; Spo11, which gets covalently bound to the DSBs after performing the cut (Keeney and Neale 2006), might function in the damage signaling originating from the endogenous breaks and thereby modulating the cellular response to endogenous DSBs in meiosis. Conversely, differences in damage signaling response to artificial DNA lesions in contrast to endogenous, SPO-11-dependent breaks could arise from the fact that exogenous, gamma radiation mediated DNA DSBs induce a far greater number of DNA lesions compared to SPO-11-mediated DNA DSBs. Ionizing radiation induces DNA breaks at the sugar phosphate backbone by either direct

radical production on the DNA molecule or by formation of radicals through water radiolysis in the vicinity of the DNA. DNA DSBs form when two DNA nicks are present set apart at a distance of one or two helical turns. Therefore, the number of SSBs produced by ionising radiation by far exceeds to number of generated DSBs, most recent studies estimate a ratio between generated SSBs and DSBs of 25:1 to 1:400 (reviewed in (Barnard et al. 2013).Therefore, in addition to the formation of DNA DSBs, gamma radiation generates a great number of single-strand lesions at the used radiation dosages, an observation that could account for the variations reported in the signaling response to artificial DSBs and SPO-11-induced DSBs.

As mentioned above, most organisms detect meiotic DSBs by ATM and ATR (Harrison et al. 2006; Lovejoy et al. 2009). Interestingly, previous publications on this topic in the *C. elegans* germline show that protein function of the two phosphatidylinositol 3-kinase related proteins ATM and ATR is not essential in the coordination of meiotic DSBs with downstream meiotic effector proteins such as CHK-2. For instance, a worm strain deficient for both *atm-1* and *atl-1* does not show defects with regard to chromosomal clustering, formation of mobile SUN-1 aggregates and meiotic phosphorylation of SUN-1, all processes under the control of CHK-2 checkpoint kinase (Figure 1, (Penkner et al. 2009). These results are in accordance with the finding that chromosomal clustering and formation of SUN-1 aggregates are independent of SPO-11 protein function and, in consequence, independent on a putative meiotic DNA damage checkpoint (Dernburg et al. 1998; Penkner et al. 2009). Conversely, activation of ATM and ATR are reported to be a near universal feature in meiosis (reviewed in (MacQueen et al. 2011). Hence, we wanted to address the question whether ATM-1 and ATL-1 are able to perform analogous signaling roles in the *C. elegans* meiotic model system under challenging conditions.

In this work, I used the *him-19* deficient worm strain to demonstrate that damage signaling via ATM-1 and ATL-1 can indeed activate the checkpoint kinase CHK-2 in the *C. elegans* germline. ATM-1 and ATL-1-dependent damage signaling induced numerous CHK-2-dependent meiotic processes, such as SUN-1 aggregate formation, chromosomal clustering, and PC protein loading in aged *him-19* mutants (figure, (Penkner et al. 2009; Tang et al. 2010). I could show that restoration of CHK-2 dependent meiotic processes in the worm germline in response to DSBs was completely abrogated in aged *him-19(m3538) atm-*

1(gk186); atl-1(tm853) triple mutants. Irradiated aged *him-19(tm3538) atm-1(gk186); atl-1(tm853)* gonads showed a meiotic phenotype mirroring the *chk-2* mutant. Hence, DNA damage signaling via activation of the sensor kinases ATM-1 and ATL-1 at prophase of meiosis I might represent a cryptic, DSB damage-dependent signaling pathway in the wild type where other ways of CHK-2 activation might operate in parallel. Intriguingly, our model of ATM/ATR dependent activation of CHK-2 in response to DNA damage can help in the interpretation of the meiotic phenotypes observed in other meiotic mutants and the wild type under challenging conditions. For instance, it has been reported that both erroneous recombinational repair and synaptic defects correlate with persistent meiotic SUN-1 phosphorylation (Woglar et al. 2013). Woglar et al. could demonstrate that SUN-1 phosphorylation marks and TZ-like chromatin clustering were prolonged in a *rad-51* mutant germline, a genetic background where unrepaired DNA DSBs persist (Alpi et al. 2003; Woglar et al. 2013). In the wild type, introduction of a large amount of artificial DNA lesions via gamma radiation prolonged the zone where SUN-1 protein is phosphorylated (Woglar et al. 2013). Those respective meiotic phenotypes could be attributed to a sustained activation of CHK-2 via the sensor kinases ATM-1 and ATL-1 in the presence of unrepaired DNA lesions.

7.3. DNA damage signaling in the TZ is dependent on the sensor kinase ATM-1

Analysis of an aged *him-19 atm-1* double mutant worm strain revealed that CHK-2 activation in response to DNA DSBs in the TZ is mediated by the sensor kinase ATM-1. This result is especially intriguing, as mechanisms by which ATM is activated are subject of intensive scientific investigation (Harper and Elledge 2007; Czornak et al. 2008). In many organisms, ATM and its homologues were shown to be the initial factor detecting unprocessed DSBs in the meiotic damage response (Harrison et al. 2006; Lovejoy et al. 2009). Our data could establish the presence of an analogous, ATM-1 dependent damage signaling pathway in *C. elegans* prophase nuclei. An initial role for *C. elegans* ATM-1 in detecting DNA damage is in accordance with the literature, as ATM was reported to be activated by DSBs with blunt ends or short single-strand overhangs, both molecular substrates generated by ionizing radiation (Shiotani and Zou 2009; Barnard et al. 2013).

Our data suggests that ATM-1 can be activated at leptotene/zygotene not only by ionizing radiation, but also by spontaneous DNA breaks generated in unstable genetic backgrounds.

For instance, appearance of spontaneous DNA lesions was reported in *brc-2* and *atl-1* deficient genetic backgrounds (Garcia-Muse et al. 2005; Ko et al. 2008). In consequence, aged *him-19; brc-2* and *him-19; atl-1* double mutant worm phosphorylated SUN-1 S8 at the TZ independent of introduction of artificial DSBs. Notably, the inability to repair DNA damage in the *him-19* deficient background led to sustained activation of CHK-2 in C. elegans germline cells. For instance, a *rad-51* deficient genetic background is unable to correctly process DNA breaks and accordingly aged *him-19; rad-51* double mutants displayed hyperphosphorylation of SUN-1 S8 in response to gamma radiation.

7.4. MRE-11 and COM-1 protein are dispensable for the activation of ATM-1 in response to artificial DSBs in the *him-19* mutant

Our results indicate that strand resection mediated by MRE-11 and COM-1 is not essential for radiation-induced activation of CHK-2 via ATM-1, as aged *him-19; mre-11* and *him-19; com-1* double mutant germline cells restored SUN-1 S8-Pi and DNA polarization after induction of artificial DNA breaks. It was previously shown that the Mre11-containing MRN complex operates as a double-strand break sensor and recruits ATM to DNA lesions (Lee et al. 2005; Joyce et al. 2011), therefore our results regarding MRE-11 function open the question how ATM-1 is activated in *mre-11* deficient leptotene/zygotene nuclei. Work on *Xenopus* egg extracts did establish that high doses of DNA fragments activate ATM and downstream checkpoints independent on Mre11 function. Furthermore, histone H2AX phosphorylation was shown to be partially Mre11 independent (Costanzo et al. 2001; Costanzo et al. 2004). Ataxia-telangiectasia-like disease (ATLD) is a genetic disease characterize by mutations in the human Mre11 protein. Intriguingly, ATM can be activated in mammalian ATLD cells under challenging conditions (Jazayeri et al. 2006). Therefore, MRE-11-independent activation of the *C. elegans* ATM homologue ATM-1 could constitute a conserved mechanism of the DNA damage response. An alternative mode of ATM activation, independent of direct physical binding to the DNA strand breaks, was documented in mammalian cells and could contribute to the observed signaling response. In this instance, ATM is activated by DNA break-induced changes in chromatin structure (Bakkenist et al. 2003). Conceivably, ATM-1 protein could be activated by a similar mechanism in gamma-radiated worm germlines. We observed comparable phenotypes in both strand resection

deficient mutant strains, nevertheless, we cannot exclude the possibility that maternal contribution of MRE-11 protein, shown in the *mre-11* background, could account for the fact that we could observe SUN-1 S8-Pi restoration after irradiation in *him-19; mre-11* mutants (Chin et al. 2001).

7.5. ATM-1 and ATL-1 show a biphasic response to artificial DNA damage in *him-19 C. elegans* prophase I

In this work, we could demonstrate that artificial DNA lesions activate CHK-2 in the late-pachytene region in aged *him-19* dependent on ATL-1 protein function. It has been reported that progressive resection of DNA DSBs results in an attenuation of ATM activation and a simultaneous increase in ATR activation (Shiotani et al. 2009). This feature, termed ATM-to-ATR switch, was shown to be mediated by both ATM and the nucleases participating in DSB resection. Our data suggests that we could identify an analogous, biphasic checkpoint response in the nematode germline involving the sensor kinases ATM-1 and ATL-1. ATM-1 protein function was demonstrated to be essential for the restoration of CHK-2 dependent SUN-1 phosphorylation events in the leptotene/zygotene region of the gonad, whereas ATL-1 activate CHK-2 in the late-pachytene region in response to induced DNA lesions in *him-19*. A primary role for ATM in meiotic DSB detection is known in other meiotic model organism. For instance, ATM is primarily required for the meiotic DSB repair response in the fruit fly (Joyce et al. 2011). Notably, undisturbed meiotic progression in the *him-19* genetic background is important for the analysis of the ATM-1 and ATL-1 signaling pathways. In this respect, it was shown that the meiotic pathway is initiated normally in the *him-19* mutant (Tang et al. 2010). Furthermore, we made the observation that that gamma radiation in aged *him-19* worms induces polarization of germline chromatin, SUN-1 aggregate formation and recruitment of pairing center proteins onto the chromosomal ends at a zone similar to the wildtype.

One possible explanation of the underlying mechanism of the discrete signaling responses in aged *him-19 atm-1* and *him-19; atl-1* worms is provided by work on RAD-50 (Hayashi et al. 2007). *rad-50* encodes for the *C. elegans* orthologue of bacterial SbcC and eukaryotic Rad50 and shares structural features with the SMC domain of condensin and cohesin complexes. Work on *rad-50* could demonstrate that germline cells switch between distinct modes of

DSB repair in the course of meiotic progression. From the onset of the meiotic prophase until cells reach mid-pachytene to late pachytene stage of meiosis I, meiotic DSB repair was shown to be dependent on RAD-50 protein function to efficiently accumulate RAD-51 protein at the sites of the DNA break (Hayashi et al. 2007). Furthermore, this zone is characterized by the competence to convert DNA DSBs into interhomologue crossovers, resulting in the formation of the meiotic chiasma. Cells that have migrated past the mid-pachytene to late pachytene transition loose the capability to convert DNA DSBs into interhomologue COs (Hayashi et al. 2007). This switch in repair pathways was termed mid-pachytene to late pachytene transition and is characterized by an abrupt release from the meiotic DSB repair pathway and by a subsequent reversion to RAD-50-independent loading of RAD-51 (Hayashi et al. 2007).

We could show that DNA lesions activate CHK-2 proximal to the mid-pachytene to late pachytene transition dependent on ATL-1 protein function. Studies show that ATL-1 is recruited to DSB sites by the presence of resected, RPA-coated ssDNA and that studies confirmed a controlling role for the MRN-complex over the ATR kinase, allowing several interpretations of our data (Zhong et al. 2005; Cimprich and Cortez 2008). RAD-50-dependent resection of DNA lesions at leptotene/zygotene and early pachytene and subsequent initiation of homologous recombination may impede ATL-1 localization or activation, whereas ATM-1 is competent to activate CHK-2 in this situation. Alternatively, ATL-1 could be activated in cells proximal to the mid-pachytene to late pachytene transition mediated via RAD-50-independent strand resection that generates long ssDNA overhangs, a known activator of ATL-1 protein (Garcia-Muse et al. 2005). The fact that we could identify activation of CHK-2 via ATL-1 in irradiated aged *him-19 atm-1* in nuclei in the late pachytene region is in agreement with this model. Chromosomes partially synapse non-homologously in an aged *him-19* deficient background. Consequently, aged *him-19 atm-1* worms cannot initiate homologous recombination for DNA repair and have to rely on RAD-50-independent DSB repair of DNA lesions (Tang et al. 2010).

The switch to RAD-50 independent repair at the mid-pachytene to late pachytene transition occurs following a transient activation of MAP kinase, required for the meiotic progression from mid-pachytene to late pachytene. Activated MAP kinase can be visualized as a transient increase in the activated, diphosphorylated form of MAP kinase in cytology, therefore it

could be worthwhile to investigate if the zone of activated MAP kinase corresponds to the SUN-1 S8-Pi positive zone observed in irradiated aged *him-19 atm-1* double mutant germlines (Church et al. 1995).

7.6. Knockdown of CHK-1 abrogates DNA damage-dependent activation of CHK-2 in the *C. elegans* germline

C. elegans CHK-1 is essential for IR-induced increase in apoptosis at late pachytene stages of meiosis I (Jaramillo-Lambert et al. 2010). Here, we could demonstrate that knockdown of CHK-1 by RNA interference prevents damage dependent phosphorylation of SUN-1 in aged *him-19* animals. Irradiated *him-19; rrf-3 chk-1(RNAi*) gonads are completely devoid of phosphorylation of SUN-1 protein at serine 8 and do not restore DNA clustering in response to artificial DSBs, comparable to an aged *him-19 atm-1; atl-1* triple mutant background. This result supports previous publications in the worm, CHK-1 phosphorylation was shown to depend on ATM-1 and ATL-1 protein and activated CHK-1 protein overlapped with phosphorylated SUN-1 in *C. elegans* germline cells and was undetectable in the aged *atm-1; atl-1* double mutant (Woglar et al. 2013).

For example, cross-talk between Chk1 and Chk2 was reported in thymocytes (Zaugg et al. 2007). Loss of Chk1 activated both Chk2 and the tumor suppressor p53, additionally Chk1 was shown to be critical for the survival of proliferating cells. Initial reports demonstrated that CHK1 phosphorylation depended mainly on ATR protein, whereas CHK2 is activated via ATM. In contrast, recent studies indicate a more substantial crosstalk between CHK1 and CHK2 (Hirao et al. 2002; Sorensen et al. 2003). Interaction between the sensor kinases ATM-1 and ATL-1 and the checkpoint kinases CHK1 and CHK2 constitutes a heavily researched topic, as genomic instability is a shared characteristic of many forms of human cancer (Smith et al. 2010). Hence, factors of the DNA damage signaling response are promising target proteins for therapeutic purposes. For instance, activation of ATM and Chk1 by the chemotherapeutic agent curcumin induces cell cycle arrest and subsequent apoptosis in human pancreatic cancer cells (Sahu et al. 2009; Toledo et al. 2011; Huntoon et al. 2013). Our results extend our knowledge about how sensor and checkpoint kinases cooperate in damage signaling pathways, indicating that CHK-1 is an essential factor in the activation of CHK-2 protein in response to artificial DSBs in the worm germline. Notably, we did observe

pronounced morphological defects in the nematode germline after knockdown of CHK-1 via RNAi. This finding supports publications demonstrating an essential role for CHK-1 in somatic cells. For instance, deletion of Chk1 was shown to be highly lethal in proliferating tissues (Zaugg et al. 2007).

7.7. DNA damage dependent activation of CHK-2 is decreased in p53 homologue CEP-1 deficient *C. elegans* gonads

In this work, we show that artificial DNA DSBs did not restore CHK-2 dependent SUN-1 phosphorylation in the leptotene zygotene region in aged *him-19 cep-1* double mutant worms. This dependency on CEP-1 function in the DNA damage response was surprising, as the p53 homologue CEP-1 was primarily implicated in induction of apoptosis in late-stage pachytene germline nuclei in response to meiotic recombination failure and DNA damage (Rutkowski et al. 2011). A function for p53 in damage signaling was recently shown in human ovarian cancer cell lines, where p53 knockdown by specific siRNA greatly reduced Chk2 phosphorylation in response to cisplatin stimulation (Liang et al. 2011). However, underlying mechanisms how CEP-1 activates meiotic DNA damage signaling remains elusive. Comparative studies on the p53 protein family revealed that the *C. elegans* genome encodes for a single p53 homologues, whereas the human genome codes for 3 related proteins, p53, p63 and p73, respectively (Belyi and Levine 2009). While CEP-1 is characterized as the worm homologue to p53 (Schumacher et al. 2001), CEP-1 protein sequence and domain structure favors the interpretation that CEP-1 is more closely related to p63, the most ancient member of the p53 family (Allocati et al. 2012). It was shown in mice that while p53 is mainly involved in monitoring the genome of somatic cells, p63 is expressed constitutively in female germ cells during meiotic arrest. p63 was shown to be phosphorylated in response to DNA lesion, furthermore, p63 is essential in a DNA damage-induced oocyte death independent on p53 (Suh et al. 2006). Intriguingly, DNA repair factors, such as Braca2, Rad51 and Mre11, are direct transcriptional targets of p63 and cells deficient for p63 are reported to be impaired in DNA repair (Lin et al. 2009). Further studies in a *cep-1* deficient background could extend our understanding of CEP-1 function in meiotic, for instance RT PCR analysis to study if candidate genes involved in the DNA damage response are mis-regulation in *cep-1* worms. Taken together, our data indicates that *C. elegans* CEP-1 protein is more closely related to the most

ancient member of the p53 protein family, p63, and is able to perform analogous functions to p63 in protecting the germline from DNA damage during meiosis.

7.8. The meiotic axis and activation of DNA damage signaling are required for robust phosphorylation of the nuclear envelope protein SUN-1

The inner nuclear membrane has been shown to be phosphorylated at the onset of meiosis in the *C. elegans* germline, modifications act as a surveillance mechanism coordinating synapsis, recombination and chromosome movement (Penkner et al. 2009; Woglar et al. 2013). Our work demonstrates that formation of a meiotic chromosome axis together with induction and processing of meiotic DNA DSBs are essential for establishing wild-type SUN-1 phosphorylation levels in zygotene/leptotene germline nuclei. A mutant genetic background deficient for HIM-3 (implicated in axis morphogenesis, synapsis, chiasma formation and chromosome segregation) and MRE-11 (required for DNA repair, induction of meiotic DSBs and recombination) shows reduced SUN-1 phosphorylation. A similar observation was made in *htp-3* deficient worms, a genotype that affects DSB formation and localization of the meiotic axis proteins, for example HIM-3. One interesting question is why we do see an incomplete phenotype, with reduced numbers of SUN-1 S8-Pi positive cells, in both respective genetic backgrounds (see chapter 5.8). A mosaic phenotype can be explained by continuous activation of DNA damage signaling in both genotypes, a hypothesis that is supported by recent publications and by data from this work. As mentioned above, F1 generation *mre-11* worms were shown to displayed maternal contribution of MRE-11, F2 generation *mre-11* worms could not be assessed due to strongly reduced broodsize and embryonal lethality (Chin et al. 2001). Therefore, maternal contribution of MRE-11 protein could account for the fact that we did observe SUN-1 S8-Pi positive nuclei in *him-3; mre-11*. Secondly, genetic backgrounds that generate endogenous breaks or are failing to repair mitotic breaks activate DNA damage signaling him *him-19* worms independent of meiotic break induction via SPO-11, examples for this are *atl-1, brc-2* and *rpa-2* mutants (see chapter 5.7). Analogous, *him-19 htp-3* double mutant worms phosphorylate SUN-1 at the onset of meiosis without introduction of artificial DNA DSBs, indicating an excess of unrepaired DNA breaks (see chapter 5.8.2). Thus, persistent activation of DNA damage signaling in a fraction of *htp-3* germline nuclei can explain the partial SUN-1 phosphorylations pattern observed in

htp-3 mutants. Two independent observations led us to examine the role of the PC proteins in the coordination of modifying the nuclear at the onset of meiosis. First, the kinase PLK-2 was shown to be recruited to the pairing centers of the autosomes phosphorylating SUN-1 (Woglar et al. 2013). Furthermore, the pairing center protein ZIM-3 was shown to localize to the chromosomal ends at leptotene / zygotene in response to artificial DNA damage in aged *him-19* worms, coinciding with phosphorylation of SUN-1 and formation of motile SUN-1 aggregates (see results, chapter 5.1). Therefore, we tested for the possibility that pairing center proteins, recruited to the chromosomal ends, play a role in phosphorylation of SUN-1 S8. However, our results indicate that the ZIM proteins and/or recruitment of the ZIM proteins to the pairing centers are not required to activate CHK-2 dependent meiotic signaling pathways (see results, chapter 5.6.6). Further study of the role of DNA damage signaling and the meiotic axis in activating CHK-2 dependent SUN-1 phosphorylation could be performed in a *him-3* deficient background with absent meiotic DNA DSB induction, for instance, analysis of SUN-1 phosphorylation in a *him-3, spo-11* double mutant background. Besides, additional experiments could address which components of the meiotic axis, besides HIM-3, are involved in activating CHK-2 at the onset of meiosis. Taken together, our results in several meiotic mutant strains indicate that disruption of meiotic chromosome axis concurrent with defective processing of meiotic DNA DSBs restricts SUN-1 S8-Pi in *C. elegans* germline cells.

7.9. Aged him-19 worms correctly express meiotic candidate proteins

Worms deficient for HIM-19 display defects in multiple processes in meiosis, including SPO-11 dependent DNA strand break induction, polarization of germline chromatin, homologous paring and synapsis (see this work and (Tang et al. 2010). To gain a better insight into the role and function of HIM-19, we were interested whether this multi-faceted phenotype is the result of mis-regulation of meiotic gene expression in aged *him-19* worms. In *C. elegans*, spatial and temporal regulation of gene expression is regulated by transcription factors (Reinke et al. 2013). Many protein domains can bind DNA but can also serve other functions, including RNA binding or protein-protein interactions. This is of particular interest, as metastructure comparison did reveal similarities between HIM-19 and RNA helicases (Tang et al. 2010). Our analysis demonstrates that meiotic genes, implicated in the meiotic

processes affected in the *him-19* genotype, showed comparable expression levels in aged *him-19* adult worms compared to the wild type (see chapter 5.9). While this candidate based approach cannot rule out the possibility that genes deregulated in the *him-19* background are not included in this study, our analysis suggest that the diverse phenotype observed in aged *him-19* hermaphrodites is not a consequence of altered transcription or mRNA stability of meiotic genes. Further insight in the HIM-19 protein function could be obtained by examining cellular localization and protein-protein interactions of HIM-19. During the course of this study, biochemical tagged HIM-19 was integrated into the worm genome utilizing biolistic transformation (Wilm et al. 1999). While genomic integration of the tagged protein was successful, no specific signal against the fusion protein could be obtained in the respective strains by immunofluorescence and Western blot analysis. Future projects could use novel CrispR technology to insert a biochemically tag into the endogenous ORF to ensure correct expression of modified HIM-19 protein.

8. Appendix

8.1. Abbreviations

DSB(s) …… Double Strand Break(s)

SSB(s) …… Single Strand Break(s)

ORF …… Open Reading Frame

RPA …… Replication Protein A

ssDNA …… single stranded DNA

dNTP …… deoxynucleotide triphosphate

CO …… cross-over

PC …… pairing centers

SC …… synaptonemal complex

hrs …… hours

min …… minutes

µm …… micrometers

nm …… nanometers

TZ …… transition zone

NE …… nuclear envelope

ddH_2O …… double-distilled water

8.2. Wissenschaftlicher Lebenslauf Thomas Machacek

SCHUL- UND BERUFSBILDUNG

09/1988 - 06/1992	Volksschule Hetzendorf, Wien (Österreich)
09/1992 - 06/2000	Matura am GRG 23, Wien (Österreich)
10/2000 - 05/2001	Wehrdienst
10/2001 - 02/2008	Diplomstudium Molekulare Biologie, Universität Wien, Wien (Österreich)
09/2004 - 03/2005	Erasmus Aufenthalt im Labor von Dr. Carmen Aragón, Universidad Autónoma de Madrid, Madrd (Spanien)
06/2006 - 09/2007	Diplomarbeit im Labor von Dr. Christian Seiser, Max F. Perutz Laboratories, Universität Wien, Wien (Österreich)
03/2009 - Heute	Dr.-Studium der Naturwissenschaften Molekulare Biologie im Labor von Dr. Verena Jantsch, Max F. Perutz Laboratories, Universität Wien, Wien (Österreich)

9. Bibliography

Ahmed, S. and J. Hodgkin (2000). "MRT-2 checkpoint protein is required for germline immortality and telomere replication in C. elegans." Nature **403**(6766): 159-164.

Ahringer, J. and J. Kimble (1991). "Control of the sperm-oocyte switch in Caenorhabditis elegans hermaphrodites by the fem-3 3' untranslated region." Nature **349**(6307): 346-348.

Allocati, N., C. Di Ilio, et al. (2012). "p63/p73 in the control of cell cycle and cell death." Exp Cell Res **318**(11): 1285-1290.

Alpi, A., P. Pasierbek, et al. (2003). "Genetic and cytological characterization of the recombination protein RAD-51 in Caenorhabditis elegans." Chromosoma **112**(1): 6-16.

Archambault, V. and D. M. Glover (2009). "Polo-like kinases: conservation and divergence in their functions and regulation." Nat Rev Mol Cell Biol **10**(4): 265-275.

Bakkenist, C. J. and M. B. Kastan (2003). "DNA damage activates ATM through intermolecular autophosphorylation and dimer dissociation." Nature **421**(6922): 499-506.

Barnard, S., S. Bouffler, et al. (2013). "The shape of the radiation dose response for DNA double-strand break induction and repair." Genome Integr **4**(1): 1.

Baudrimont, A., A. Penkner, et al. (2010). "Leptotene/zygotene chromosome movement via the SUN/KASH protein bridge in Caenorhabditis elegans." PLoS Genet **6**(11): e1001219.

Belyi, V. A. and A. J. Levine (2009). "One billion years of p53/p63/p73 evolution." Proc Natl Acad Sci U S A **106**(42): 17609-17610.

Bernstein, H., H. C. Byerly, et al. (1985). "Genetic damage, mutation, and the evolution of sex." Science **229**(4719): 1277-1281.

Bhalla, N. and A. F. Dernburg (2005). "A conserved checkpoint monitors meiotic chromosome synapsis in Caenorhabditis elegans." Science **310**(5754): 1683-1686.

Blat, Y., R. U. Protacio, et al. (2002). "Physical and functional interactions among basic chromosome organizational features govern early steps of meiotic chiasma formation." Cell **111**(6): 791-802.

Boulton, S. J., A. Gartner, et al. (2002). "Combined functional genomic maps of the C. elegans DNA damage response." Science **295**(5552): 127-131.

Braun, K. A., Y. Lao, et al. (1997). "Role of protein-protein interactions in the function of replication protein A (RPA): RPA modulates the activity of DNA polymerase alpha by multiple mechanisms." Biochemistry **36**(28): 8443-8454.

Brenner, S. (1974). "The genetics of Caenorhabditis elegans." Genetics **77**(1): 71-94.

Burgoyne, P. S., S. K. Mahadevaiah, et al. (2007). "The management of DNA double-strand breaks in mitotic G2, and in mammalian meiosis viewed from a mitotic G2 perspective." Bioessays **29**(10): 974-986.

Carballo, J. A. and R. S. Cha (2007). "Meiotic roles of Mec1, a budding yeast homolog of mammalian ATR/ATM." Chromosome Res **15**(5): 539-550.

Chikashige, Y., C. Tsutsumi, et al. (2006). "Meiotic proteins bqt1 and bqt2 tether telomeres to form the bouquet arrangement of chromosomes." Cell **125**(1): 59-69.

Chin, G. M. and A. M. Villeneuve (2001). "C. elegans mre-11 is required for meiotic recombination and DNA repair but is dispensable for the meiotic G(2) DNA damage checkpoint." Genes Dev **15**(5): 522-534.

Chua, P. R. and G. S. Roeder (1998). "Zip2, a meiosis-specific protein required for the initiation of chromosome synapsis." Cell **93**(3): 349-359.

Church, D. L., K. L. Guan, et al. (1995). "Three genes of the MAP kinase cascade, mek-2, mpk-1/sur-1 and let-60 ras, are required for meiotic cell cycle progression in Caenorhabditis elegans." Development **121**(8): 2525-2535.

Cimprich, K. A. and D. Cortez (2008). "ATR: an essential regulator of genome integrity." Nat Rev Mol Cell Biol **9**(8): 616-627.

Cliby, W. A., C. J. Roberts, et al. (1998). "Overexpression of a kinase-inactive ATR protein causes sensitivity to DNA-damaging agents and defects in cell cycle checkpoints." EMBO J **17**(1): 159-169.

Colaiacovo, M. P. (2006). "The many facets of SC function during C. elegans meiosis." Chromosoma **115**(3): 195-211.

Colaiacovo, M. P., A. J. MacQueen, et al. (2003). "Synaptonemal complex assembly in C. elegans is dispensable for loading strand-exchange proteins but critical for proper completion of recombination." Dev Cell **5**(3): 463-474.

Costanzo, V., T. Paull, et al. (2004). "Mre11 assembles linear DNA fragments into DNA damage signaling complexes." PLoS Biol **2**(5): E110.

Costanzo, V., K. Robertson, et al. (2001). "Mre11 protein complex prevents double-strand break accumulation during chromosomal DNA replication." Mol Cell **8**(1): 137-147.

Couteau, F., K. Nabeshima, et al. (2004). "A component of C. elegans meiotic chromosome axes at the interface of homolog alignment, synapsis, nuclear reorganization, and recombination." Curr Biol **14**(7): 585-592.

Couteau, F. and M. Zetka (2005). "HTP-1 coordinates synaptonemal complex assembly with homolog alignment during meiosis in C. elegans." Genes Dev **19**(22): 2744-2756.

Crittenden, S. L., K. A. Leonhard, et al. (2006). "Cellular analyses of the mitotic region in the Caenorhabditis elegans adult germ line." Mol Biol Cell **17**(7): 3051-3061.

Czornak, K., S. Chughtai, et al. (2008). "Mystery of DNA repair: the role of the MRN complex and ATM kinase in DNA damage repair." J Appl Genet **49**(4): 383-396.

Dernburg, A. F., K. McDonald, et al. (1998). "Meiotic recombination in C. elegans initiates by a conserved mechanism and is dispensable for homologous chromosome synapsis." Cell **94**(3): 387-398.

Derry, W. B., A. P. Putzke, et al. (2001). "Caenorhabditis elegans p53: role in apoptosis, meiosis, and stress resistance." Science **294**(5542): 591-595.

Evans, D. G., J. M. Birch, et al. (2008). "Is CHEK2 a cause of the Li-Fraumeni syndrome?" J Med Genet **45**(1): 63-64.

Fairman, M., G. Prelich, et al. (1988). "Identification of cellular components required for SV40 DNA replication in vitro." Biochim Biophys Acta **951**(2-3): 382-387.

Falck, J., J. Coates, et al. (2005). "Conserved modes of recruitment of ATM, ATR and DNA-PKcs to sites of DNA damage." Nature **434**(7033): 605-611.

Fridkin, A., E. Mills, et al. (2004). "Matefin, a Caenorhabditis elegans germ line-specific SUN-domain nuclear membrane protein, is essential for early embryonic and germ cell development." Proc Natl Acad Sci U S A **101**(18): 6987-6992.

Frokjaer-Jensen, C., M. W. Davis, et al. (2008). "Single-copy insertion of transgenes in Caenorhabditis elegans." Nat Genet **40**(11): 1375-1383.

Furnari, B., A. Blasina, et al. (1999). "Cdc25 inhibited in vivo and in vitro by checkpoint kinases Cds1 and Chk1." Mol Biol Cell **10**(4): 833-845.

Garcia-Muse, T. and S. J. Boulton (2005). "Distinct modes of ATR activation after replication stress and DNA double-strand breaks in Caenorhabditis elegans." EMBO J **24**(24): 4345-4355.

Gartner, A., S. Milstein, et al. (2000). "A conserved checkpoint pathway mediates DNA damage--induced apoptosis and cell cycle arrest in C. elegans." Mol Cell **5**(3): 435-443.

Golden, J. W. and D. L. Riddle (1984). "The Caenorhabditis elegans dauer larva: developmental effects of pheromone, food, and temperature." Dev Biol **102**(2): 368-378.

Goldstein, P. (1984). "Sterile mutants in Caenorhabditis elegans: the synaptonemal complex as an indicator of the stage-specific effect of the mutation." Cytobios **39**(154): 101-108.

Goodyer, W., S. Kaitna, et al. (2008). "HTP-3 links DSB formation with homolog pairing and crossing over during C. elegans meiosis." Dev Cell **14**(2): 263-274.

Hansen, D. and T. Schedl (2006). "The regulatory network controlling the proliferation-meiotic entry decision in the Caenorhabditis elegans germ line." Curr Top Dev Biol **76**: 185-215.

Hansen, D. and T. Schedl (2013). "Stem cell proliferation versus meiotic fate decision in Caenorhabditis elegans." Adv Exp Med Biol **757**: 71-99.

Harper, J. W. and S. J. Elledge (2007). "The DNA damage response: ten years after." Mol Cell **28**(5): 739-745.
Harper, N. C., R. Rillo, et al. (2011). "Pairing centers recruit a Polo-like kinase to orchestrate meiotic chromosome dynamics in C. elegans." Dev Cell **21**(5): 934-947.
Harrison, J. C. and J. E. Haber (2006). "Surviving the breakup: the DNA damage checkpoint." Annu Rev Genet **40**: 209-235.
Hassold, T. and P. Hunt (2001). "To err (meiotically) is human: the genesis of human aneuploidy." Nat Rev Genet **2**(4): 280-291.
Hayashi, M., G. M. Chin, et al. (2007). "C. elegans germ cells switch between distinct modes of double-strand break repair during meiotic prophase progression." PLoS Genet **3**(11): e191.
Herman, R. K. and C. K. Kari (1989). "Recombination between small X chromosome duplications and the X chromosome in Caenorhabditis elegans." Genetics **121**(4): 723-737.
Hirao, A., A. Cheung, et al. (2002). "Chk2 is a tumor suppressor that regulates apoptosis in both an ataxia telangiectasia mutated (ATM)-dependent and an ATM-independent manner." Mol Cell Biol **22**(18): 6521-6532.
Hiraoka, Y. and A. F. Dernburg (2009). "The SUN rises on meiotic chromosome dynamics." Dev Cell **17**(5): 598-605.
Hochwagen, A. and A. Amon (2006). "Checking your breaks: surveillance mechanisms of meiotic recombination." Curr Biol **16**(6): R217-228.
Hofmann, E. R., S. Milstein, et al. (2002). "Caenorhabditis elegans HUS-1 is a DNA damage checkpoint protein required for genome stability and EGL-1-mediated apoptosis." Curr Biol **12**(22): 1908-1918.
Huntoon, C. J., K. S. Flatten, et al. (2013). "ATR inhibition broadly sensitizes ovarian cancer cells to chemotherapy independent of BRCA status." Cancer Res **73**(12): 3683-3691.
Jantsch, V., P. Pasierbek, et al. (2004). "Targeted gene knockout reveals a role in meiotic recombination for ZHP-3, a Zip3-related protein in Caenorhabditis elegans." Mol Cell Biol **24**(18): 7998-8006.
Jaramillo-Lambert, A., Y. Harigaya, et al. (2010). "Meiotic errors activate checkpoints that improve gamete quality without triggering apoptosis in male germ cells." Curr Biol **20**(23): 2078-2089.
Jazayeri, A., J. Falck, et al. (2006). "ATM- and cell cycle-dependent regulation of ATR in response to DNA double-strand breaks." Nat Cell Biol **8**(1): 37-45.
Johzuka, K. and H. Ogawa (1995). "Interaction of Mre11 and Rad50: two proteins required for DNA repair and meiosis-specific double-strand break formation in Saccharomyces cerevisiae." Genetics **139**(4): 1521-1532.
Jones, M. R., J. C. Huang, et al. (2012). "The atm-1 gene is required for genome stability in Caenorhabditis elegans." Mol Genet Genomics **287**(4): 325-335.
Joyce, E. F., M. Pedersen, et al. (2011). "Drosophila ATM and ATR have distinct activities in the regulation of meiotic DNA damage and repair." J Cell Biol **195**(3): 359-367.
Kamath, R. S., M. Martinez-Campos, et al. (2001). "Effectiveness of specific RNA-mediated interference through ingested double-stranded RNA in Caenorhabditis elegans." Genome Biol **2**(1): RESEARCH0002.
Keeney, S., C. N. Giroux, et al. (1997). "Meiosis-specific DNA double-strand breaks are catalyzed by Spo11, a member of a widely conserved protein family." Cell **88**(3): 375-384.
Keeney, S. and M. J. Neale (2006). "Initiation of meiotic recombination by formation of DNA double-strand breaks: mechanism and regulation." Biochem Soc Trans **34**(Pt 4): 523-525.
Kelly, K. O., A. F. Dernburg, et al. (2000). "Caenorhabditis elegans msh-5 is required for both normal and radiation-induced meiotic crossing over but not for completion of meiosis." Genetics **156**(2): 617-630.
Kimberly Van Auken, c. c. http://www.wormbase.org.
Kimble, J. E. and J. G. White (1981). "On the control of germ cell development in Caenorhabditis elegans." Dev Biol **81**(2): 208-219.
Ko, E., J. Lee, et al. (2008). "Essential role of brc-2 in chromosome integrity of germ cells in C. elegans." Mol Cells **26**(6): 590-594.

Krejci, L., V. Altmannova, et al. (2012). "Homologous recombination and its regulation." Nucleic Acids Res **40**(13): 5795-5818.
Labella, S., A. Woglar, et al. (2011). "Polo kinases establish links between meiotic chromosomes and cytoskeletal forces essential for homolog pairing." Dev Cell **21**(5): 948-958.
Lavin, M. F. (2008). "Ataxia-telangiectasia: from a rare disorder to a paradigm for cell signalling and cancer." Nat Rev Mol Cell Biol **9**(10): 759-769.
Lee, J. H. and T. T. Paull (2005). "ATM activation by DNA double-strand breaks through the Mre11-Rad50-Nbs1 complex." Science **308**(5721): 551-554.
Lee, S. E., J. K. Moore, et al. (1998). "Saccharomyces Ku70, mre11/rad50 and RPA proteins regulate adaptation to G2/M arrest after DNA damage." Cell **94**(3): 399-409.
Lee, S. J., A. Gartner, et al. (2010). "The Caenorhabditis elegans Werner syndrome protein functions upstream of ATR and ATM in response to DNA replication inhibition and double-strand DNA breaks." PLoS Genet **6**(1): e1000801.
Lehner, B., C. Crombie, et al. (2006). "Systematic mapping of genetic interactions in Caenorhabditis elegans identifies common modifiers of diverse signaling pathways." Nat Genet **38**(8): 896-903.
Lemmens, B. B., N. M. Johnson, et al. (2013). "COM-1 promotes homologous recombination during Caenorhabditis elegans meiosis by antagonizing Ku-mediated non-homologous end joining." PLoS Genet **9**(2): e1003276.
Lemmens, B. B. and M. Tijsterman (2011). "DNA double-strand break repair in Caenorhabditis elegans." Chromosoma **120**(1): 1-21.
Liang, X., Y. Guo, et al. (2011). "The Role of Wild-Type p53 in Cisplatin-Induced Chk2 Phosphorylation and the Inhibition of Platinum Resistance with a Chk2 Inhibitor." Chemother Res Pract **2011**: 715469.
Lin, Y. L., S. Sengupta, et al. (2009). "p63 and p73 transcriptionally regulate genes involved in DNA repair." PLoS Genet **5**(10): e1000680.
Loidl, J., A. Lukaszewicz, et al. (2012). "The Tetrahymena meiotic chromosome bouquet is organized by centromeres and promotes interhomolog recombination." J Cell Sci **125**(Pt 23): 5873-5880.
Lovejoy, C. A. and D. Cortez (2009). "Common mechanisms of PIKK regulation." DNA Repair (Amst) **8**(9): 1004-1008.
MacQueen, A. J., M. P. Colaiacovo, et al. (2002). "Synapsis-dependent and -independent mechanisms stabilize homolog pairing during meiotic prophase in C. elegans." Genes Dev **16**(18): 2428-2442.
MacQueen, A. J. and A. Hochwagen (2011). "Checkpoint mechanisms: the puppet masters of meiotic prophase." Trends Cell Biol **21**(7): 393-400.
MacQueen, A. J., C. M. Phillips, et al. (2005). "Chromosome sites play dual roles to establish homologous synapsis during meiosis in C. elegans." Cell **123**(6): 1037-1050.
MacQueen, A. J. and A. M. Villeneuve (2001). "Nuclear reorganization and homologous chromosome pairing during meiotic prophase require C. elegans chk-2." Genes Dev **15**(13): 1674-1687.
Maguire, M. P. (1986). "The pattern of pairing that is effective for crossing over in complex B-A chromosome rearrangements in maize. III. Possible evidence for pairing centers." Chromosoma **94**(1): 71-85.
Malkova, A., F. Klein, et al. (2000). "HO endonuclease-induced recombination in yeast meiosis resembles Spo11-induced events." Proc Natl Acad Sci U S A **97**(26): 14500-14505.
Marcon, E. and P. B. Moens (2005). "The evolution of meiosis: recruitment and modification of somatic DNA-repair proteins." Bioessays **27**(8): 795-808.
Martin, J. S., N. Winkelmann, et al. (2005). "RAD-51-dependent and -independent roles of a Caenorhabditis elegans BRCA2-related protein during DNA double-strand break repair." Mol Cell Biol **25**(8): 3127-3139.
Martinez-Perez, E. and A. M. Villeneuve (2005). "HTP-1-dependent constraints coordinate homolog pairing and synapsis and promote chiasma formation during C. elegans meiosis." Genes Dev **19**(22): 2727-2743.

McKim, K. S., A. M. Howell, et al. (1988). "The effects of translocations on recombination frequency in Caenorhabditis elegans." Genetics **120**(4): 987-1001.

Menon, V. and L. Povirk (2014). "Involvement of p53 in the repair of DNA double strand breaks: multifaceted Roles of p53 in homologous recombination repair (HRR) and non-homologous end joining (NHEJ)." Subcell Biochem **85**: 321-336.

Minn, I. L., M. M. Rolls, et al. (2009). "SUN-1 and ZYG-12, mediators of centrosome-nucleus attachment, are a functional SUN/KASH pair in Caenorhabditis elegans." Mol Biol Cell **20**(21): 4586-4595.

Moreau, S., J. R. Ferguson, et al. (1999). "The nuclease activity of Mre11 is required for meiosis but not for mating type switching, end joining, or telomere maintenance." Mol Cell Biol **19**(1): 556-566.

Morimoto, A., H. Shibuya, et al. (2012). "A conserved KASH domain protein associates with telomeres, SUN1, and dynactin during mammalian meiosis." J Cell Biol **198**(2): 165-172.

Nabeshima, K., S. Mlynarczyk-Evans, et al. (2011). "Chromosome painting reveals asynaptic full alignment of homologs and HIM-8-dependent remodeling of X chromosome territories during Caenorhabditis elegans meiosis." PLoS Genet **7**(8): e1002231.

Nabeshima, K., A. M. Villeneuve, et al. (2005). "Crossing over is coupled to late meiotic prophase bivalent differentiation through asymmetric disassembly of the SC." J Cell Biol **168**(5): 683-689.

Nagaoka, S. I., T. J. Hassold, et al. (2012). "Human aneuploidy: mechanisms and new insights into an age-old problem." Nat Rev Genet **13**(7): 493-504.

Nishi, Y., E. Rogers, et al. (2008). "Polo kinases regulate C. elegans embryonic polarity via binding to DYRK2-primed MEX-5 and MEX-6." Development **135**(4): 687-697.

Oliveira, R. A. and K. Nasmyth (2010). "Getting through anaphase: splitting the sisters and beyond." Biochem Soc Trans **38**(6): 1639-1644.

Page, S. L. and R. S. Hawley (2003). "Chromosome choreography: the meiotic ballet." Science **301**(5634): 785-789.

Pasierbek, P., M. Jantsch, et al. (2001). "A Caenorhabditis elegans cohesion protein with functions in meiotic chromosome pairing and disjunction." Genes Dev **15**(11): 1349-1360.

Pazdernik, N. and T. Schedl (2013). "Introduction to germ cell development in Caenorhabditis elegans." Adv Exp Med Biol **757**: 1-16.

Penkner, A., Z. Portik-Dobos, et al. (2007). "A conserved function for a Caenorhabditis elegans Com1/Sae2/CtIP protein homolog in meiotic recombination." EMBO J **26**(24): 5071-5082.

Penkner, A., L. Tang, et al. (2007). "The nuclear envelope protein Matefin/SUN-1 is required for homologous pairing in C. elegans meiosis." Dev Cell **12**(6): 873-885.

Penkner, A. M., A. Fridkin, et al. (2009). "Meiotic chromosome homology search involves modifications of the nuclear envelope protein Matefin/SUN-1." Cell **139**(5): 920-933.

Petronczki, M., M. F. Siomos, et al. (2003). "Un menage a quatre: the molecular biology of chromosome segregation in meiosis." Cell **112**(4): 423-440.

Phillips, C. M. and A. F. Dernburg (2006). "A family of zinc-finger proteins is required for chromosome-specific pairing and synapsis during meiosis in C. elegans." Dev Cell **11**(6): 817-829.

Reinke, V., M. Krause, et al. (2013). "Transcriptional regulation of gene expression in C. elegans." WormBook: 1-34.

reported by Williams, A. B., & Michael, W. M. . . (2011). "The role of the protein kinase CHK-1 in early germ line development in C. elegans (presented in International Worm Meeting)."

Rinaldo, C., P. Bazzicalupo, et al. (2002). "Roles for Caenorhabditis elegans rad-51 in meiosis and in resistance to ionizing radiation during development." Genetics **160**(2): 471-479.

Rinaldo, C., S. Ederle, et al. (1998). "The Caenorhabditis elegans RAD51 homolog is transcribed into two alternative mRNAs potentially encoding proteins of different sizes." Mol Gen Genet **260**(2-3): 289-294.

Roeder, G. S. and J. M. Bailis (2000). "The pachytene checkpoint." Trends Genet **16**(9): 395-403.

Rose, A. M., D. L. Baillie, et al. (1984). "Meiotic pairing behavior of two free duplications of linkage group I in Caenorhabditis elegans." Mol Gen Genet **195**(1-2): 52-56.
Rosenbluth, R. E. and D. L. Baillie (1981). "The genetic analysis of a reciprocal translocation, eT1(III; V), in Caenorhabditis elegans." Genetics **99**(3-4): 415-428.
Ruijs, M. W., A. Broeks, et al. (2009). "The contribution of CHEK2 to the TP53-negative Li-Fraumeni phenotype." Hered Cancer Clin Pract **7**(1): 4.
Rutkowski, R., R. Dickinson, et al. (2011). "Regulation of Caenorhabditis elegans p53/CEP-1-dependent germ cell apoptosis by Ras/MAPK signaling." PLoS Genet **7**(8): e1002238.
Sahu, R. P., S. Batra, et al. (2009). "Activation of ATM/Chk1 by curcumin causes cell cycle arrest and apoptosis in human pancreatic cancer cells." Br J Cancer **100**(9): 1425-1433.
Sato, A., B. Isaac, et al. (2009). "Cytoskeletal forces span the nuclear envelope to coordinate meiotic chromosome pairing and synapsis." Cell **139**(5): 907-919.
Sauvageau, S., A. Z. Stasiak, et al. (2005). "Fission yeast rad51 and dmc1, two efficient DNA recombinases forming helical nucleoprotein filaments." Mol Cell Biol **25**(11): 4377-4387.
Scherthan, H. (2001). "A bouquet makes ends meet." Nat Rev Mol Cell Biol **2**(8): 621-627.
Schild-Prufert, K., T. T. Saito, et al. (2011). "Organization of the synaptonemal complex during meiosis in Caenorhabditis elegans." Genetics **189**(2): 411-421.
Schumacher, B., K. Hofmann, et al. (2001). "The C. elegans homolog of the p53 tumor suppressor is required for DNA damage-induced apoptosis." Curr Biol **11**(21): 1722-1727.
Severson, A. F., L. Ling, et al. (2009). "The axial element protein HTP-3 promotes cohesin loading and meiotic axis assembly in C. elegans to implement the meiotic program of chromosome segregation." Genes Dev **23**(15): 1763-1778.
Shakes, D. C., J. C. Wu, et al. (2009). "Spermatogenesis-specific features of the meiotic program in Caenorhabditis elegans." PLoS Genet **5**(8): e1000611.
Sherizen, D., J. K. Jang, et al. (2005). "Meiotic recombination in Drosophila females depends on chromosome continuity between genetically defined boundaries." Genetics **169**(2): 767-781.
Shiotani, B. and L. Zou (2009). "Single-stranded DNA orchestrates an ATM-to-ATR switch at DNA breaks." Mol Cell **33**(5): 547-558.
Simmer, F., M. Tijsterman, et al. (2002). "Loss of the putative RNA-directed RNA polymerase RRF-3 makes C. elegans hypersensitive to RNAi." Curr Biol **12**(15): 1317-1319.
Smith, J., L. M. Tho, et al. (2010). "The ATM-Chk2 and ATR-Chk1 pathways in DNA damage signaling and cancer." Adv Cancer Res **108**: 73-112.
Smolikov, S., K. Schild-Prufert, et al. (2009). "A yeast two-hybrid screen for SYP-3 interactors identifies SYP-4, a component required for synaptonemal complex assembly and chiasma formation in Caenorhabditis elegans meiosis." PLoS Genet **5**(10): e1000669.
Sorensen, C. S., R. G. Syljuasen, et al. (2003). "Chk1 regulates the S phase checkpoint by coupling the physiological turnover and ionizing radiation-induced accelerated proteolysis of Cdc25A." Cancer Cell **3**(3): 247-258.
Sourirajan, A. and M. Lichten (2008). "Polo-like kinase Cdc5 drives exit from pachytene during budding yeast meiosis." Genes Dev **22**(19): 2627-2632.
Stauffer, M. E. and W. J. Chazin (2004). "Physical interaction between replication protein A and Rad51 promotes exchange on single-stranded DNA." J Biol Chem **279**(24): 25638-25645.
Stergiou, L., K. Doukoumetzidis, et al. (2007). "The nucleotide excision repair pathway is required for UV-C-induced apoptosis in Caenorhabditis elegans." Cell Death Differ **14**(6): 1129-1138.
Stracker, T. H. and J. H. Petrini (2011). "The MRE11 complex: starting from the ends." Nat Rev Mol Cell Biol **12**(2): 90-103.
Suh, E. K., A. Yang, et al. (2006). "p63 protects the female germ line during meiotic arrest." Nature **444**(7119): 624-628.
Tang, L., T. Machacek, et al. (2010). "Mutations in Caenorhabditis elegans him-19 show meiotic defects that worsen with age." Mol Biol Cell **21**(6): 885-896.
Thorne, L. W. and B. Byers (1993). "Stage-specific effects of X-irradiation on yeast meiosis." Genetics **134**(1): 29-42.

Toledo, L. I., M. Murga, et al. (2011). "Targeting ATR and Chk1 kinases for cancer treatment: a new model for new (and old) drugs." Mol Oncol **5**(4): 368-373.
Tomita, K. and J. P. Cooper (2006). "The meiotic chromosomal bouquet: SUN collects flowers." Cell **125**(1): 19-21.
Tsai, J. H. and B. D. McKee (2011). "Homologous pairing and the role of pairing centers in meiosis." J Cell Sci **124**(Pt 12): 1955-1963.
Tsubouchi, H. and H. Ogawa (1998). "A novel mre11 mutation impairs processing of double-strand breaks of DNA during both mitosis and meiosis." Mol Cell Biol **18**(1): 260-268.
Villeneuve, A. M. (1994). "A cis-acting locus that promotes crossing over between X chromosomes in Caenorhabditis elegans." Genetics **136**(3): 887-902.
Vlatkovic, N., M. T. Boyd, et al. (2013). "Nucleolar control of p53: a cellular Achilles' heel and a target for cancer therapy." Cell Mol Life Sci.
von Wettstein, D., S. W. Rasmussen, et al. (1984). "The synaptonemal complex in genetic segregation." Annu Rev Genet **18**: 331-413.
Ward, J. D., D. M. Muzzini, et al. (2010). "Overlapping mechanisms promote postsynaptic RAD-51 filament disassembly during meiotic double-strand break repair." Mol Cell **37**(2): 259-272.
Wilkins, A. S. and R. Holliday (2009). "The evolution of meiosis from mitosis." Genetics **181**(1): 3-12.
Wilm, T., P. Demel, et al. (1999). "Ballistic transformation of Caenorhabditis elegans." Gene **229**(1-2): 31-35.
Woglar, A., A. Daryabeigi, et al. (2013). "Matefin/SUN-1 phosphorylation is part of a surveillance mechanism to coordinate chromosome synapsis and recombination with meiotic progression and chromosome movement." PLoS Genet **9**(3): e1003335.
Wright, J. A., K. S. Keegan, et al. (1998). "Protein kinase mutants of human ATR increase sensitivity to UV and ionizing radiation and abrogate cell cycle checkpoint control." Proc Natl Acad Sci U S A **95**(13): 7445-7450.
Wu, H. Y., H. C. Ho, et al. (2010). "Mek1 kinase governs outcomes of meiotic recombination and the checkpoint response." Curr Biol **20**(19): 1707-1716.
Yin, Y. and S. Smolikove (2013). "Impaired resection of meiotic double-strand breaks channels repair to nonhomologous end joining in Caenorhabditis elegans." Mol Cell Biol **33**(14): 2732-2747.
Zaugg, K., Y. W. Su, et al. (2007). "Cross-talk between Chk1 and Chk2 in double-mutant thymocytes." Proc Natl Acad Sci U S A **104**(10): 3805-3810.
Zetka, M. C., I. Kawasaki, et al. (1999). "Synapsis and chiasma formation in Caenorhabditis elegans require HIM-3, a meiotic chromosome core component that functions in chromosome segregation." Genes Dev **13**(17): 2258-2270.
Zhang, W., N. Miley, et al. (2012). "HAL-2 promotes homologous pairing during Caenorhabditis elegans meiosis by antagonizing inhibitory effects of synaptonemal complex precursors." PLoS Genet **8**(8): e1002880.
Zheng, H., L. Chen, et al. (2013). "p53 promotes repair of heterochromatin DNA by regulating JMJD2b and SUV39H1 expression." Oncogene.
Zhong, H., A. Bryson, et al. (2005). "Rad50 depletion impacts upon ATR-dependent DNA damage responses." Hum Mol Genet **14**(18): 2685-2693.
Zickler, D. (1977). "Development of the synaptonemal complex and the "recombination nodules" during meiotic prophase in the seven bivalents of the fungus Sordaria macrospora Auersw." Chromosoma **61**(4): 289-316.
Zickler, D. (2006). "From early homologue recognition to synaptonemal complex formation." Chromosoma **115**(3): 158-174.
Zickler, D. and N. Kleckner (1999). "Meiotic chromosomes: integrating structure and function." Annu Rev Genet **33**: 603-754.